Vebjørn Kjerstad

Modelling of Iceberg Impact Interaction with Floating Structures

Master's thesis in Marine Technology
Supervisor: Prof. Jørgen Amdahl/Post. Doc. Zhaolong Yu
January 2019

Master's thesis

NTNU
Norwegian University of Science and Technology
Faculty of Engineering
Department of Marine Technology

NTNU
Norwegian University of
Science and Technology

Vebjørn Kjerstad

Modelling of Iceberg Impact Interaction with Floating Structures

Master's thesis in Marine Technology
Supervisor: Prof. Jørgen Amdahl/Post. Doc. Zhaolong Yu
January 2019

Norwegian University of Science and Technology
Faculty of Engineering
Department of Marine Technology

NTNU
Kunnskap for en bedre verden

Abstract

Due to the increased activities in the ice-infested Arctic areas, it is desirable to gain insight into the possible consequences ice-structure impacts may bring to structural integrity. The main objective of the present master thesis is to increase the understanding of ice mechanics and the effect various material data has on the performance of the modelled glacial ice in impact interaction with floating marine structures. The work comprises literature review of relevant subjects, comparisons of existing ice material models, development of a new material model implementation based on the work by Liu (2011), calibration of the new implementation and integrated analyses of ice-structure impacts.

The investigations and comparison of existing ice material models lead to an understanding of the optimal way to perform the intended mathematical operators. Thus, this is adopted in the newly developed implementation. Numerical simulations show that the new code behaves as desired with respect to the plastic flow, failure occurrence and erosion. However, some shortcomings are revealed as well. Problems arise in numerical analyses when the cut-off pressure is located within the yield surface. Hence, it is recommended to use ice material constants so the cut-off-pressure is located outside the yield surface, e.g. by the constants proposed by Kierkegaard (1993). The amount of hourglass energy is another subject that needs further investigation since the attempt to reduce it to acceptable levels is not completely successful.

The calibration of the implementation is evaluated to be successfully performed against Polar Class 3 in the Unified Requirements for Polar ships by IACS, even though an undesired initial peak is present in the crushing resistance. The calibration is performed by manipulating the failure criterion.

Both coupled and uncoupled integrated analyses of ice-structure impacts are performed and compared in two impact scenarios. However, the ice does not dissipate any substantial amount of energy and the two methods yield similar results. Hence, no significant coupling effects are discovered. Possible explanations of the lack of energy dissipation in the ice may be increased confinement of the ice or the initial peak in the calibration. It is noteworthy that the structure is not ice-strengthened and the ice is only deformed when hitting areas of particular stiffness, such as bulkheads or frames. Hence, it would be interesting to do analysis with a stiffer structure. However, in coupled analysis with weaker ice it still only contributes by a fraction of the shared energy dissipation and less than other preceding uncoupled studies have estimated, such as the ST19 report (Lu et al., 2018). Consequently, further investigation and validation must be performed to build proper confidence in coupled analysis with glacial ice.

Sammendrag

På grunn av økt aktivitet i de is-infiserte arktiske områdene er det ønskelig med økt innsikt i de mulige konsekvensene av støt mellom is og konstruksjon og hvordan det kan påvirke den strukturelle integriteten. Hovedmålet med denne masteroppgaven er å øke forståelsen av ismekanikk og effekten ulike materialdata har på ytelsen til det modellerte isfjellet i støt mellom isfjell og offshore konstruksjoner. Arbeidet inkluderer litteraturstudier av relevante emner, sammenlikninger av eksisterende materialmodeller av is, utvikling av en ny implementasjon av materialmodell basert på arbeidet av Liu (2011), kalibrering av den nye implementasjonen, samt integrerte analyser av støt mellom isfjell og offshore konstruksjoner.

Undersøkelser og sammenligninger av eksisterende implementerte materialmodeller av is førte til en forståelse for den beste måten å utføre de ønskede matematiske operasjoner. Dette er adoptert i den nyutviklete koden. Numeriske simuleringer viser at den nye implementasjonen oppfører seg som ønsket når det gjelder plastisk flytning, brudd og erosjon. Imidlertid er det også påvist noen mangler. Problemer oppstår i numeriske analyser når avskjæringstrykket befinner seg innenfor flyteflaten. Det er derfor anbefalt å bruke konstanter i flytefunksjonen slik at avskjæringstrykket ligger utenfor flyteflaten, slik som konstantene foreslått av Kierkegaard (1993). Mengden av timeglassenergi er et annet emne som må utforskes videre da forsøket på å redusere det til akseptable nivåer ikke er fullstendig tilfredsstillende.

Kalibreringen av implementasjonen er vurdert til å være vellykket for Polarklasse 3 i «Unified Requirements for Polar ships» av IACS, selv om en uønsket topp er tilstede i knusningsmostanden til isen. Kalibreringen ble utført ved å manipulere bruddkriteriet. Både koblede og ikke-koblede integrerte analyser av støt mellom isfjell og en offshore plattform er utført og sammenliknet for to ulike støt-scenarier. Isen opptar nesten ikke noe energi, og de to metodene gir tilsvarende resultater. Dette gjelder for begge scenariene og det er derfor ikke oppdaget noen signifikante koblingseffekter. Mulige forklaringer på manglende energiopptak i isen kan skyldes innsetting av isen eller på grunn av den første toppen i kalibreringen. Det er verdt å nevne at strukturen ikke er is-forsterket og isen blir bare deformert når den treffer områder med høy stivhet, som for eksempel ved skott eller rammer. Det vil derfor være interessant å gjøre analyser med en stivere struktur. Likevel, også i koblede analyser med svakere is bidrar den bare med en brøkdel av den delte energifordelingen og betydelig mindre enn andre ikke-koblede studier har estimert, for eksempel ST19-rapporten (Lu et al., 2018). Følgelig så må videre undersøkelser og validering utføres for å ha stor tillit til koblede analyser med is.

NTNU
Norges teknisk-naturvitenskapelige universitet
Institutt for marin teknikk

MASTER THESIS 2018

For

Stud. Vebjørn Kjerstad

Modelling of iceberg impact interaction with floating structures

Modellering av interaksjon ved støt mellom isfjell og offshore konstruksjoner

Background

With the increased activities in the artic area, operators and designers are challenged to design structures which can safely operate in iceberg infested waters. On the other hand, the aim is to optimize as much as possible the steel work reducing the new building cost without compromising on the overall safety. As part of this process, the modelling of iceberg interaction with floating structures has an important role. An industrial consensus on how the design iceberg load and response are determined for ice-structure interaction scenarios shall be determined and applied for design purposes.

According to NORSOK, an offshore installation is designed to sustain iceberg impact loads according to three different strategies. These are *Ductility design, Strength design and Shared-energy design*.
In the first case, all the available energy is dissipated by the deformation of the structure; the iceberg is modelled as rigid and do not contribute to the energy dissipation. This simplify the analysis as the analyst does not have to deal with the uncertainties related to the strength of the iceberg. However, the penetration model for the iceberg (i.e. its shape) needs to be assumed.
In a *Strength design* the structure is assumed rigid and can crush the ice, i.e. can resist the maximum pressure that the ice can deliver. The ability of structure to sustain iceberg load is evaluated using pressure-area (ISO 19906) model to describe the iceberg resistance, preferably with an associated penetration-area model.
In the third case, both the iceberg and the structure are explicitly modelled and contributing to the energy dissipation. In a simple manner, this can be achieved by combining the cases above, bearing in mind that severe limitations may appear, especially with the onset of large deformations.

Rigorously speaking, *Shared-energy design* approach is the most challenging as the iceberg deformation as well as the structural deformation of installation depend on each other. With the developing deformation, their stiffness will also change, thus changing the pressure that the ice can deliver to the structure and that the structure can sustain.
An integrated analysis with both objects explicitly modelled, is capable of accounting for all relevant effects for assessing the structural damages with the highest precision. This includes the progressive changes in the contact surface as well as the relative strength changes during the impact. The main challenge is however to have a consistent constitutive model for the iceberg with suitable material and crushing failure properties.

Objective

In 2015, DNV GL (Maritime Advisory) implemented in cooperation with the master student Nicole Ferrari (University of Genoa) a material model for glacial ice material response in the Abaqus FE

software, the constitutive model was presented by Liu et al, 2010. However, due to time and resources, the performance of the developed continuum model was not fully investigated.

The objective is to increase the understating of ice mechanics and effect of different material data and shape on the performance of the modelled iceberg. As part of the presented master thesis, it is proposed to perform a benchmark study and implement modifications to the existing code to reproduce published results. Perform parametric studies varying material properties, investigate the effects on the iceberg-structure interaction by performing non-linear integrated analysis for selected scenarios and iceberg geometries.

Method

The approach used for solving the overall task will constitute a combination of review of existing literature as well as tests, analytical work and numerical analyses using non-linear FE tool.

The following topics should be addressed:

1) Give a brief overview of the physics behind the various failure modes of ice, with special emphasis on crushing of icebergs/growlers and level ice. Describe the explicit or inherent assumption regarding force versus contact area or pressure versus contact area relationships that are adopted in various code formulations.

2) Further investigate the source to the deviation in the results obtained with ABAQUS (DNV GL version), ABAQUS (Woongshik Nam version) and LS-DYNA. As far as possible describe the mathematical models that are adopted, notably with respect to the plasticity formulations, plastic flow theory, the influence of confinement, the return algorithms, failure modeling and the erosion techniques adopted. By numerical analysis document how the various approaches behaves w.r.t. plastic flow, failure occurrence and erosion. Document the amount of hourglass energy, how tit may influence the results and investigate methods/parameters to reduce the hourglass energy to acceptable levels. It is recommended to start with analysis of single volume element subjected to crushing , before advancing to larger ice features.

   If possible, this part of the investigation should end with recommendations for the best approach to perform the intended mathematical operations.

3) Simulate ice crushing against a rigid wall and compare the results with respect to the pressure distribution, force and energy dissipation during crushing. Perform calibration of the selected "best" ice model against relevant force-area or pressure-area curves as deemed most relevant. The calibration may be made against code formulations or test results. Describe the motivation for using the selected curve.

4) Develop ice models with different local shapes and simulate crushing against realistic stiffened panels. Try to determine the "worst" shape that the panel is not able to crush in the early stages and thus smoothen the contact.

5) Perform simulation of impacts with a bergy bit against a ships side model. The bergy bit may hit in the ice-strengthened region, but it will also be interesting to investigate impacts above this region due to relative motion between ship and waves. Analysis should be

carried out for both transverse impact and impact in the longitudinal direction in the bow area. It would be interesting to realize large damage, e.g. up to the inner hull.

6) To the extent possible perform calculations of the damage by means of simplified method, and compare with the results obtained with ABAQUS.

7) Conclusion and recommendation for further work in the master thesis project.

Literature studies of specific topics relevant to the thesis work may be included.

The work scope may prove to be larger than initially anticipated. Subject to approval from the supervisor, topics may be deleted from the list above or reduced in extent.

In the thesis the candidate shall present his personal contribution to the resolution of problems within the scope of the thesis work.

Theories and conclusions should be based on mathematical derivations and/or logic reasoning identifying the various steps in the deduction.

The candidate should utilize the existing possibilities for obtaining relevant literature.

The thesis should be organized in a rational manner to give a clear exposition of results, assessments, and conclusions. The text should be brief and to the point, with a clear language. Telegraphic language should be avoided.

The thesis shall contain the following elements: A text defining the scope, preface, list of contents, summary, main body of thesis, conclusions with recommendations for further work, list of symbols and acronyms, references and (optional) appendices. All figures, tables and equations shall be numerated.

The supervisor may require that the candidate, in an early stage of the work, presents a written plan for the completion of the work. The plan should include a budget for the use of computer and laboratory resources which will be charged to the department. Overruns shall be reported to the supervisor.

The original contribution of the candidate and material taken from other sources shall be clearly defined. Work from other sources shall be properly referenced using an acknowledged referencing system.

The report shall be submitted in two copies:
- Signed by the candidate
- The text defining the scope included
- In bound volume(s)
- Drawings and/or computer prints which cannot be bound should be organised in a separate folder.

Supervisor:
Prof. Jørgen Amdahl /Post Doc Zhaolong Yu

Contact person at DNV GL
Gabriele Notaro/Ole Jakob Hareide

Deadline: June 11 , 2019

Trondheim, January15, 2019

Jørgen Amdahl

Preface

The present report contains the master thesis of Stud. Vebjørn Kjerstad at the Norwegian University of Science and Technology(NTNU) in the spring of 2019. It is a continuation of the project thesis in the fall of 2018. The work is a concluding part of a Master of Science degree in Marine Structural Engineering at NTNU. The task was proposed by DNV GL and the work has been performed at the Institute of Marine Technology. The main supervisor has been Professor Jørgen Amdahl, with Postdoctoral fellow Zhaolong Yu as co-supervisor. Ole Jakob Hareide and Gabriele Notaro have been the contact persons at DNV GL(Maritime Advisory).

The work has been challenging, yet rewarding. Most of the topics included were new to me before the thesis, including the Finite Element Analysis software Abaqus. I have obtained a lot of new knowledge, not only for the special problem in hand but also regarding general non-linear finite element analyses and how academic work shall be performed.

Readers of the thesis should preferably have knowledge of structural mechanics and Finite Element Analysis, both linear and non-linear. Knowledge within the field of ice mechanics is also beneficial. However, theory required to apprehend this subject is presented in the thesis.

Vebjørn Kjerstad
Trondheim, June 11, 2019

Acknowledgements

First of all, I would like to thank my supervisor Prof. Jørgen Amdahl for all the help during the master thesis and for always being available for discussions. I would also like to thank my co-supervisor Postdoctoral fellow Zhaolong Yu for guidance and for running analyses in LS-DYNA. Gabriele Notaro and Ole Jakob Hareide at DNV GL has been very helpful and always sharing their perspective and possible solutions to problems along the way. Their expertise in Abaqus has been crucial for the progress. I would also like to thank PhD. candidate Woongshik Nam at NTNU, Professor Mihkel Kõrgesaar at Tallinn University of Technology and Doctoral candidate Li Fang at Aalto University for letting me use their implemented material models to compare against. In addition, the knowledge about ice physics and calibration of Associate Professor Ekaterina Kim has been a valuable contribution to this thesis.

Nomenclature

Abbreviations

AF Hull Area Factor

ALIE Abnormal-Level Ice Event

ALS Accidental Limit State

AR Aspect Ratio

BWH Bressan-William-Hill instability criterion

ELIE Extreme-Level Ice Event

FE Finite Element

FEA Finite Element Analysis

FLS Fatigue Limit State

IACS International Association of Classification Societies

ISO International Organization for Standardization

NLFEA Non-Linear Finite Element Analysis

NORSOK Norsk Sokkels Konkuranseposisjon

PC Polar Class

PPF Peak Pressure Factor

SLS Serviceability Limit State

ULS Ultimate Limit State

WMO World Meteorological Organization

Symbols

ϵ_0	Initial failure strain
ϵ_f	Fracture strain
ϵ_{eq}^p	Equivalent plastic strain
ϵ_{ij}^p	Equivalent plastic strain tensor component
ϕ	Radial return scaling factor
σ_Y	Yield stress
$\sigma_{allowable}$	Allowable yield stress
σ_{eq}	von Mises stress
σ_{ij}^{trial}	Deviatoric trial stress component
τ	Octahedral shear stress
τ	Shear stress
A	Area
a_0	Ice material constant
a_1	Ice material constant
a_2	Ice material constant
$d\lambda$	Plastic multiplier
D^e	Constitutive matrix
E_A	Artificial Strain Energy
E_I	Internal Work
E_P	Inelastic dissipated Energy
E_S	Strain Energy
E_W	External Work
E_{FD}	Frictional Energy Dissipated
f	Yield function
J_2	Second deviatoric invariant

k	Calibration factor in the yield surface
k_a	Aspect ratio factor
k_w	Influencing factor for patch load
M	Calibration parameter in the failure criterion
m	Mass
N	Calibration parameter in the failure criterion
p	Hydrostatic pressure
p	Pressure
p_2	Second root of the yield function
s	Stiffener spacing
s_{ij}	Deviatoric stress tensor component
t	thickness
v	Velocity
Z	Elastic section modulus
Z_P	Plastic section modulus
Z_{Pfl}	Plastic section modulus for flanges
Z_{Pweb}	Plastic section modulus for web

Contents

List of Figures

List of Tables

Chapter 1

Introduction

1.1 Background

Throughout history, the Arctic has been a more or less uncharted territory due to the hostile environment that habits these areas. This part of the world hasn't been very accessible, until recent decades. The acceleration of melting of ice and technological developments have made the Arctic more accessible and new areas can now be explored in a way that hasn't been possible before. As a consequence of this, the focus on oil and gas explorations has increased. In addition, new possible sailing roots are becoming available. An example of this is the Northwest Passage. This sailing route was until recent years unavailable for shipping traffic most of the year. As the ice melting is accelerated, the passage is more navigable and has great value as a shipping route between Asia and Europe.

With an increased amount of operations in these ice-infested areas, the possibility of floating marine structures colliding with icebergs increases. Glacial ice features may cause a great threat to marine structures as an impact can affect structural integrity. Figure 1.1 illustrates that there might be enormous forces associated with ice collisions and the corresponding damages may be critical for structural integrity. Glacial ice larger than 15 m in waterline length, often referred to as icebergs, are relatively easy to detect with modern radar and satellite technology. However, smaller ice features, such as Growlers (less than 5 m in waterline length) and Bergy bits (5 m - 15 m in waterline length), are harder to detect and represent a potential threat. This challenges the operators and designers of marine structures which are to operate in ice-infested areas. They have to design structures that can operate in this harsh environment in a safe manner, but at the same time must the structures be optimized in order to reduce the cost. Therefore, the modelling of impact interaction with floating structures and glacial ice plays a very important role in the design.

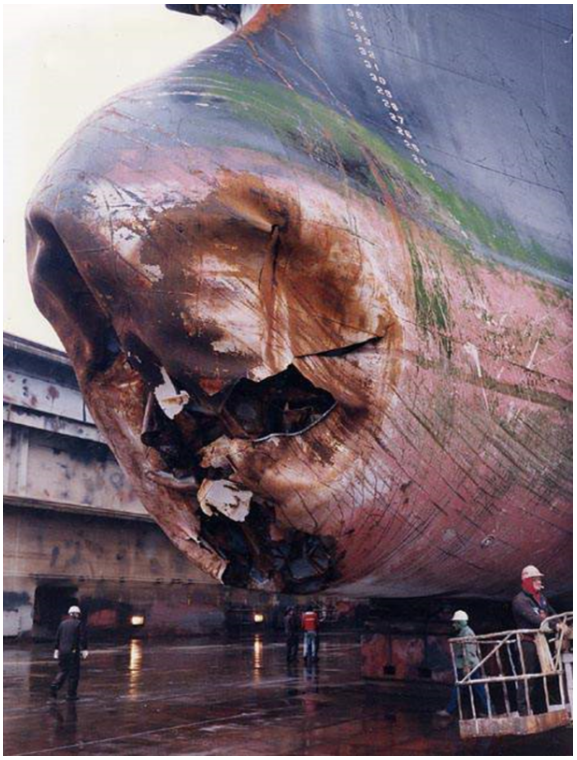

Figure 1.1: Bow damage of Overseas Ohio due front collision with iceberg (Hill, 2006).

Offshore structures are designed to withstand the impact load by three different design methods; the *Ductile design method*, the *Strength design method* and the *Shared-energy design method*. In ductile design, the structure dissipates all the energy and the ice is assumed rigid, while in the strength design it is opposite, i.e. the structure is assumed rigid and the ice is crushed. In the shared-energy design method, both the structure and the ice are deformable and contributing to the energy dissipation. This is a desirable approach as it represents reality well. However, this is the most challenging approach as the deformation of the glacial ice and the structure are dependent on each other. In addition, the relative strength between the bodies changes as the stiffness changes with the deformations. However, the greatest challenge introduced in this approach with respect to impact with glacial ice is to have a consistent constitutive model of the iceberg and crushing failure properties.

1.2 Problem Description

The constitutive material model proposed by Liu (2011) was implemented in Abaqus FE software by DNV GL in cooperation with the master student Nicole

Ferrari at the University of Genoa. The implementation is not fully investigated due to limited time and resources. The main objective of this master thesis is to increase the understanding of ice mechanics and the effect various material data has on the performance of the modelled iceberg. The existing implementation is to be investigated and modified, or a new code may be developed from scratch. Parametric studies are to be performed by varying the material properties and the effects on the iceberg-structure interaction by non-linear integrated analysis for selected scenarios and iceberg geometries shall be performed. The work will include a review of existing literature and tests, analytical work and numerical analyses sing non-linear FE software.

The present master thesis addresses the following topics:

1. Brief review of the physics behind failure modes of ice and the assumptions regarding force-area/pressure-area relationships that are adopted in various code formulations.

2. Description of the material model proposed by Liu (2011) with an investigation of the implemented material models in non-linear FE software by Ferrari (2014)(Abaqus), Woongshik Nam(Abaqus) and Liu (2011)(LS-DYNA).

3. A new implementation is developed in Abaqus FE software with the approach that is found to be most suitable to perform the intended mathematical operations.

4. The various implementations are subjected to numerical analyses and their behaviour with respect to plastic flow, failure occurrence, erosion and hourglass energy are documented.

5. Simulation of ice crushing against a rigid wall is performed in order to calibrate the new material model with respect to the pressure distribution, force and energy dissipation during crushing.

6. Integrated shared-energy analysis, both coupled and uncoupled, of glacial ice impact interaction with a column of an offshore platform.

The work scope has changed some during the thesis. For instance, it was proposed to implement modifications to the existing code developed by DNV GL and Ferrari (2014). However, some drawbacks in this code were revealed and a new implementation is developed from scratch instead. This was a time-consuming process which lead to less focus on other areas in the thesis proposal, such as the role the geometry of the ice plays in the impact. The amount of hourglass energy and the study of this is another topic that was more comprehensive than first anticipated. It was decided to perform integrated

impact analyses with a bergy bit against a semi-submersible column instead of a ship side model. All work scope changes are made in agreement with supervisor Prof. Jørgen Amdahl.

Chapter 2

Principles of Structural Design

NORSOK N-003 (NORSOK, 2016) specifies that the presence of icebergs cannot be neglected for any structure that is to operate in the Barent Sea and that the probability of impacts between structures and icebergs must be taken into account in the design. Even the effect of small pieces of ice should be assessed since they may be thrown onto the deck of facilities. If the annual probability of iceberg impact is more than 10^{-4}, impact shall be taken into account in the design. It should be considered that it is a larger probability for impacts with large icebergs than for smaller ones. In addition, there is a larger probability that the icebergs that are moving faster have a higher probability of impact with structures due to the larger areas that are covered by more movement. Probabilistic approaches should be applied to identify actions that have a probability of occurring larger than 10^{-4}. These actions are dealt with in the form of limit states. Figure 2.1 shows the probability zones that shall be used at the Norwegian Continental Shelf if site-specific impact probabilities aren't calculated. Between the dashed line and the solid line in the figure, only ALS actions are relevant as the annual probability of occurrence is between 10^{-4} and 10^{-2}(corresponding to a return period of 100 years and 1000 years, respectively)

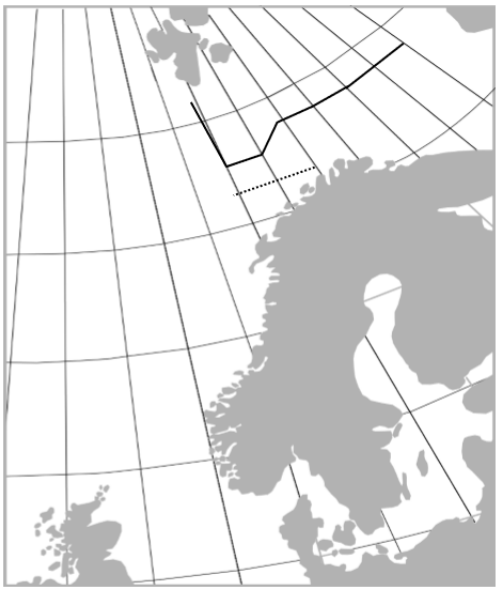

Figure 2.1: Probability of collision with iceberg at the Norwegian Continental Shelf. Solid line and dotted line indicates probability of exceeding of 10^{-4} and 10^{-2}, respectively(NORSOK, 2016).

2.1 The Ultimate Limit State

In the Ultimate Limit State(ULS) the design principles are such that the structure should not undergo excessive plastic deformations and the structural analysis should be carried out as linear elastic, simplified rigid–plastic, or elastic-plastic analyses, according to NORSOK N-004 (NORSOK, 2017). In this limit state the structure is designed to withstand loads that have an annual probability of exceeding of a certain level, typically 10^{-2} (corresponding to a return period of 100 years). Ships and offshore structures are often designed according to ULS methods and checked with Accidental Limit State(ALS) methods.

2.2 The Accidental Limit State

In ALS the structure shall be checked for all design actions that are defined in the risk analysis. These actions typically have an annual probability of exceeding 10^{-4}. Contrary to in the ULS, the structure may undergo buckling, yielding and significant permanent deformations in the ALS. This makes it necessary to evaluate the structure using non-linear analysis. However, even though the structure may be effected in a more severe way in ALS, the integrity of the structure should not be inhibited. The ALS consists of two parts:

1. Resistance of the structure against design accidental actions.

2. Post accident resistance of the structure against environmental actions. It should only be checked if the resistance is reduced by structural damage caused by the design accidental actions.

Collisions of floating structures, such as between a ship and an iceberg, can be described in terms of kinetic energy, which is governed by the mass, hydrodynamic effects and impact speed. The part of this kinetic energy which does not remain as kinetic energy after the collision must be dissipated as strain energy. In ALS, NORSOK N-004 distinguish between three different design principles in terms of distributed strain energy; *Strength design*, *Ductile design* and *Shared-energy design*, see Figure 2.2.

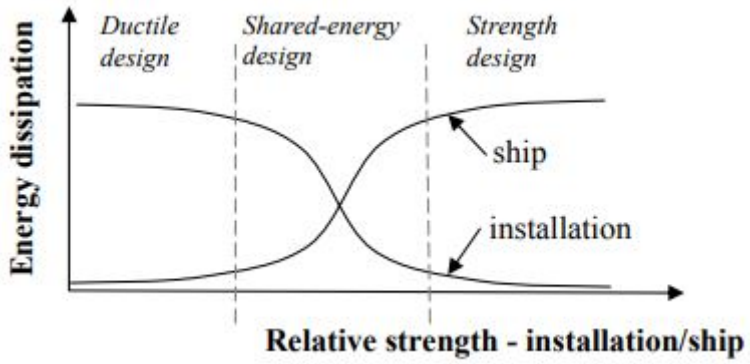

Figure 2.2: Energy dissipation for strength, ductile and shared-energy design. In the present case, the iceberg is represented by the curve of ship. Figure from NORSOK N-004.

In the strength design principle, the structure is strong enough to crush the iceberg with minimal deformation. This means that the structure must be able to resist the maximum pressure resulting from the ice interaction contact area. This design strategy is very similar to the ULS design approach and may result in a too conservative design and unnecessarily expensive structures. However, it may be relevant in some cases, e.g. where it is too much cost connected to downtime while the structure is repaired. In Figure 2.2 the curve for the ship corresponds to the iceberg in the present case in this master thesis. As one can see from the figure, using the strength design principle it is the iceberg that will dissipate almost all of the energy. A strength design where the body has no dissipation of energy is not possible in reality. Thus, a strength design should be used with a damage limit that is acceptable.

The ductile design principle is the opposite of the strength design; the iceberg is viewed as rigid and undamaged, while the structure dissipates the major part of the strain energy from the interaction and undergoes large plastic deformations. This is often an adopted approach but may result in overly large dimensions and

costly structures. On the other hand, this approach simplifies the calculations of the damage of the structure (Storheim, 2016).

The shared-energy design is a combination of the design methods above, i.e. both the structure and the iceberg deform and share the dissipated strain energy. This method is very challenging since the deformations of both the iceberg and the structure depend on each others behaviour (Liu et al., 2010). I.e. the resistance of the structure depends on the loading from the iceberg and the other way around. The weakest of the structure and the iceberg is the one that will deform, but the relative strength of the materials changes during the deformation caused by the impact. In order to be able to use this shared-energy design approach in collision analysis with ice, it is necessary to have a continuum mechanics model of the ice. The shared-energy design is desirable since it leads to the possibility of optimizing the structure with respect to strength and weight.

Due to limited trust in existing continuum mechanics models of glacial ice, the shared-energy design approach in NORSOK N-004 Appendix A (NORSOK, 2017) has been adopted in ice-structure impact studies so far. This approach determines the energy dissipation of the glacial ice and the installation separately and then combines the two. This approach doesn't take coupling effects of the interaction into account. An example of a coupling effect is that with deformation of one body the contact area increases. Consequently, the resistance of the other body increases.

2.3 Collision Mechanics

Evaluations and calculations of collisions is a very complex coupled process. A common approach is to decouple the problem into external and internal mechanics. Internal mechanics describes the local deformations and how the strain energy is dissipated, while the external mechanics deals with rigid body motions and describes the kinetic energy, both initial and final, that gives the global response of the system. The mechanisms are connected to each other through the demand for energy dissipation. Internal mechanics are assessed with plasticity theory or Non-Linear Finite Element Analysis(NLFEA).

In the methods of external mechanics, it is normal to assume that the impact duration is short enough so it isn't any change of force direction in the collision and inertia and collision forces predominate. Other forces are usually neglected due to the magnitude of the impact force, and the deformation of the colliding bodies is limited to the contact surface. Simple calculation methods exist to evaluate the external mechanics with respect to principles of conservation of

momentum and conservation energy. It is distinguished between floating and fixed structures. Floating structures are free to move. Thus, the energy is dependent on the mass and velocity of the impacted structure.

$$E_s = \frac{1}{2}(m_a + a_a)v_a^2 \frac{(1 - \frac{v_b}{v_a})^2}{1 + \frac{m_a + a_a}{m_b + a_b}} \tag{2.1}$$

where v_a and v_b are the velocities of the colliding bodies, a_a and a_b are the added mass of the colliding bodies and m_a and m_b are the masses of the colliding bodies.

The simple methods to evaluate external mechanics assumes that the collision is head on, which only requires a one-degree of freedom system and it will give conservative results. In order to describe the external mechanics more accurately, it is necessary to do a multi-degree-of-freedom analysis. Liu (2011) proposed a three-dimensional impact theory in order to analyze iceberg-ship collisions, which is based on Stronge's 3D impact theory (Stronge, 2000). This method uses two local coordinate systems for each of the colliding bodies. Numerical simulations with this 3D method gave good agreement with 2D methods when the vertical eccentricity was neglected. However, when the vertical eccentricity was included the results show that it was significantly influenced by this factor. This indicates that 2D theory may overestimate the impact energy due to the neglected vertical eccentricity.

The input to the internal mechanics evaluation is the required energy dissipation from the external mechanics considerations. The ultimate goal of internal mechanics assessments is to investigate the energy dissipation and damage caused by the bodies involved in the collision. Presently, this is preferably solved by NLFEA. However, plastic analysis is widely used as it is very efficient with respect to cost versus accuracy and the possibility of making mistakes in the calculations are limited. It is several different simplified methods for the evaluation of internal mechanics. Some of the most central methods are described in closer detail in the Ph.D. thesis by Storheim (2016).

Chapter 3

Polar Codes for Marine Structures

Several codes, rules and requirements exist for the design of marine structures to operate in the Arctic areas. Some of these will be briefly reviewed here.

3.1 Polar Classes

Both the International Association of Classification Societies(IACS) and DNV GL have developed polar classes. In this section, these rules and the principles behind the rules are discussed, with emphasis on the structural requirements.

3.1.1 DNV GL Polar Class

The Polar Class notation by DNV GL is a set of rules for ships with steel hulls which are to operate in waters that are ice-infested. These rules are equivalent to the unified rules for polar vessels developed by IACS, but they are generally based on different principles with respect to the structural requirements.

It is possible to review the structural capacity by means of either elastic or plastic theory. The rules in the DNV GL Polar class are based on elastic methods. Due to symmetry may the boundary conditions of a plate subjected to uniform loading be regarded as clamped. The DNV GL rules evaluate the bending stress at the midspan of a plate strip, not the boundaries, see Figure 3.1. This is to account for the increased plate resistance due to membrane stresses that develop under finite deformations. The derived plate thickness requirement with this elastic analysis method is in Equation 3.1. The plate strip analogy is reasonable if the aspect ratio is large enough (Amdahl, 2007).

$$t = \frac{1}{2} s \sqrt{\frac{p}{\sigma_Y}} \tag{3.1}$$

where p is the pressure, s is the stiffener spacing and σ_Y is the yield stress.

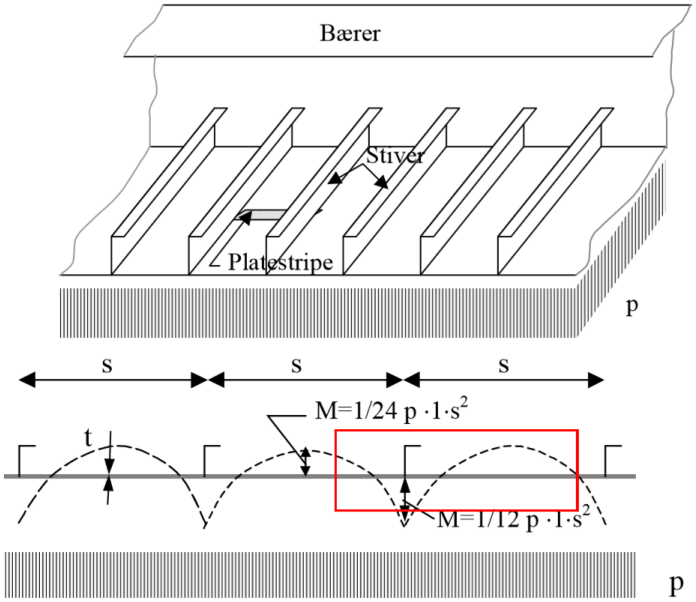

Figure 3.1: Plate strip for elastic analysis (Amdahl, 2007).

According to Amdahl (2007), the plate resistance in the DNV GL rules may be expressed as:

$$r = \frac{4(\frac{\sigma_Y}{1.36})t^2}{s^2}\frac{1}{k_w}\frac{1}{k_a^2} \tag{3.2}$$

where t is the plate thickness, k_a is aspect ratio factor and k_w is an influencing factor for patch load when the ice pressure is not acting on the entire height.

The required elastic section modulus stiffeners in the DNV GL rules are:

$$Z = \frac{psl^2}{12\sigma_{allowable}} \tag{3.3}$$

where $\sigma_{allowable}$ is dependent on the location of the stiffener.

3.1.2 IACS Unified Requirements for Polar Ships

The International Association of Classification Societies(IACS) have developed a set of seven Polar Classes, see Table 3.1. These rules are for ships with steel hulls which are intended to independently navigate in ice-covered polar waters. Ships are assigned a Polar Class notation such that they can operate independently at continuously speed at the ice conditions corresponding to the Polar Class. If the

ships are not designed to operate independently in these areas, the intent of the operation shall be stated in the Certificate of Classification (IACS, 2016).

Table 3.1: Polar classes IACS.

Polar Class	**General description**
Polar Class 1	Year round operation in all Polar Waters
Polar Class 2	Year round operation in moderate multi-year ice conditions
Polar Class 3	Year round operation in second-year ice with old ice inclusions
Polar Class 4	Year round operation in thick first-year ice which may contain old ice inclusions
Polar Class 5	Year round operation in medium first-year ice with old ice intrusions
Polar Class 6	Summer/autumn operation in medium first-year ice with old ice inclusions
Polar Class 7	Summer/autumn operation in thin first-year ice with old ice inclusions

The hull of Polar Class ships are divided into four main parts which reflect the magnitude of load that they are expected to be subjected to; the bow, bow intermediate, mid-body and the stern, as shown in Figure 3.2. The design ice loads are dependent on the average pressure P_{avg}, patch height, b, and width, w. These are again dependent on the shape coefficient, total glancing impact force, line load and pressure for the bow area for all ships and within the bow intermediate area for PC 6 and 7 ships. Thus, all of these must be found to determine the design ice loads. In the other hull areas the load parameters, P_{avg}, w and b are not dependent on the hull shape, but they are based on a fixed load patch aspect ratio, $AR = 3.6$.

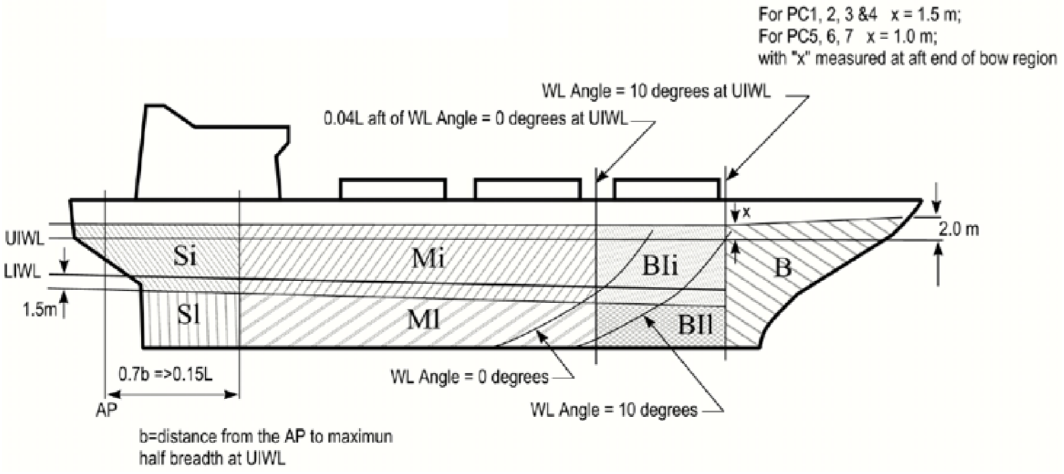

Figure 3.2: Divided hull areas (IACS, 2016).

The shell plating elements are stiffened panels that are to be designed in order to handle the ice load actions. The thickness required to withstand the ice loading is dependent on the orientation of the framing, i.e. the angle between the chord of the waterline and the line of the first level framing, see Figure 3.3. In addition, the plate thickness is dependent on the Peak Pressure Factor(PPF) and the Hull Area Factor(AF) (which can be found from tables in IACS (2016)).

The longitudinal and transverse frames, stringers and web frames in the areas of the hull that are exposed to ice loading are referred to as framing members. The longitudinal and transverse frames are on the sides of the ship structure and should have enough plastic capacity to withstand the effect of both shear and bending stress combined. The midspan load that causes the development of plastic mechanism determines the plastic capacity. The load carrying stringers and web frames shall be designed by applying the load patch at areas where the combined bending and shear capacity is minimized for the members.

(a) (b)

Figure 3.3: Shell framing angle (IACS, 2016).

The unified rules for polar vessels developed by IACS are based on plastic

methods of analysis. Plastic methods are suitable for actions that occur in a few extremes, i.e. the actions are not repetitive. The shell plating resistance is capable of redistributing the action effects and ductility, due to the resulting increased plate resistance with finite deformations and membrane stresses. The in-plane membrane stresses occur in plates with large deformations and boundaries that are free to move in but remains straight. These boundary conditions are often used for plates that are in a continuous plate field and in post-buckling analyses of plates. The large deformations in the middle of the plate want to "pull-in" the plate at the long edge boundaries. This results in transverse tensile stresses that develop at the midspan, which is counteracted by the transverse compressive stress at the shortest edges of the plate. Even though plastic and elastic analysis methods are based on different principles, they give fairly similar results (Amdahl, 2007).

Such as for the elastic analysis, the plate strip assumption may also be used for plastic analysis. In this case is the hinge mechanism in Figure 3.4 used. However, this yields the same results as for the elastic analysis for the plate thickness, i.e. Equation 3.1.

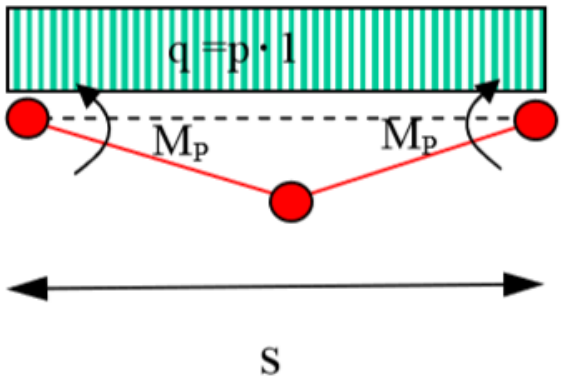

Figure 3.4: Hinge mechanism in plastic plate strip analysis (Amdahl, 2007).

The unified rules for polar vessels by IACS are based on a yield line model for plates with patch loading, as shown in Figure 3.5. The yield line is formed as a so-called "roof-type" and is assumed to lay on the boundary of the load patch, but in reality, it is located outside the load boundary area. Hence, the assumption is non-conservative. This is corrected by using a simplified expression for the collapse resistance.

$$r = 4(1 + \frac{0.5}{b/s})^2 = \frac{4\sigma_y t^2}{s^2}(1 + 0.5\frac{s}{l})^2 \tag{3.4}$$

where the last equality holds if the plate is loaded over the entire length. The

second term is the plate aspect ratio effect.

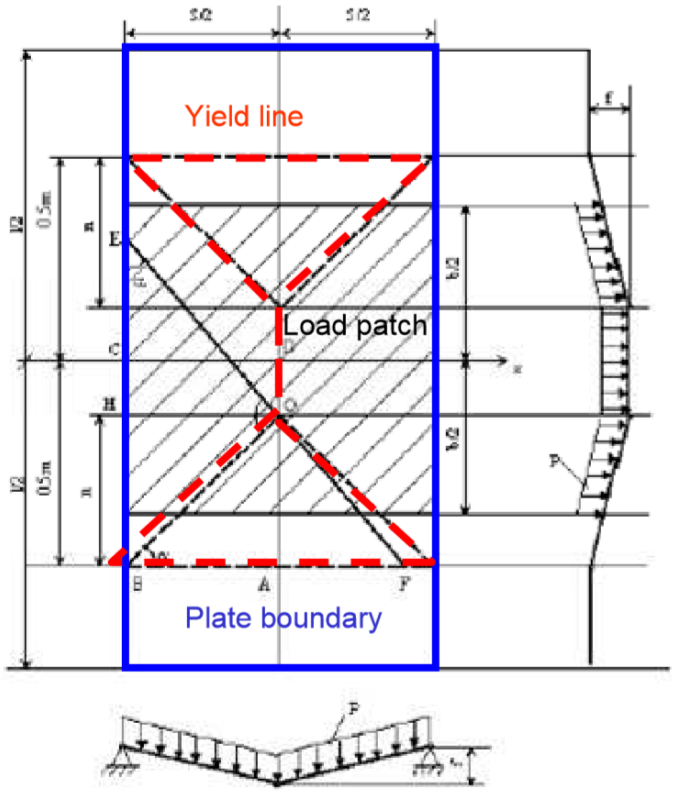

Figure 3.5: Yield line model with patch loading (Amdahl, 2007).

In Figure 3.6 the aspect factor for the DNV GL rules, IACS rules and plastic analysis are compared. This show that the DNV GL rules are conservative for all aspect ratios and the difference from the plastic analysis for small aspect ratios is significant. The reason for this is that the redistribution effect after yielding is underestimated. IACS rules are closer to the plastic analysis, but still conservative for low aspect ratios.

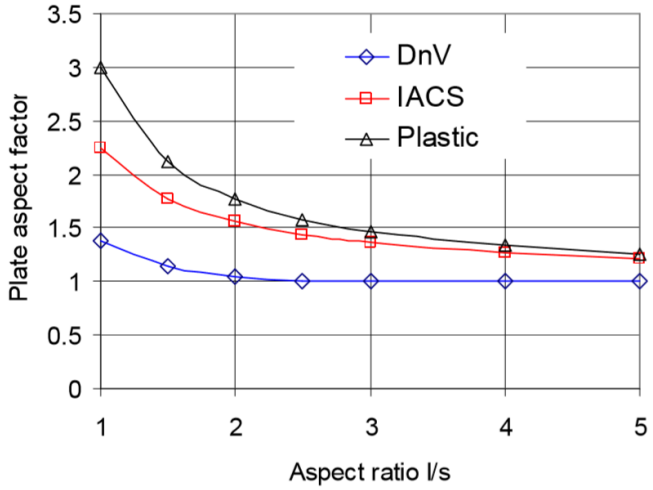

Figure 3.6: Aspect factor for plates(Amdahl, 2007).

IACS distinguish between two types of load conditions of stiffeners; centrally loaded ice pressure(symmetric) and end loaded ice pressure(asymmetric). In the centrally loaded pressure condition, a three-hinge mechanism is used(Figure 3.4). In the middle, it is a full plastic bending moment, while at the support are the plastic moment interacted with shear forces, which have a reductive effect. For the symmetric case, Equation 3.5 is valid for the resistance.

$$r = \frac{4}{l^2}\frac{1}{1-\frac{b}{2l}}\frac{\sigma_Y}{bs}(Z_P + Z_{Pfl} + Z_{Pweb}(1-(\frac{\tau}{\tau_Y})^2),\ \frac{\tau}{\tau_Y} < 1 \tag{3.5}$$

where Z_P is the plastic section modulus, Z_{Pfl} is the plastic section modulus for the flanges, Z_{Pweb} is the plastic section modulus for the web and τ is the shear stress.

For the asymmetric load case, the same three hinge model is used, but it is only developed a fully plastic hinge at one end. At the hinge at the other end is the shear force at maximum. Thus, the web fails here by shear yielding. The resulting collapse resistance is described as:

$$r = \frac{4}{l^2}\frac{1}{1-\frac{b}{2l}}\frac{\sigma_Y}{bs}(Z_P\frac{1}{l-a} + Z_{fl}[\frac{2}{a} - \frac{1}{l-a}] + \frac{A_w}{\sqrt{3}}) \tag{3.6}$$

3.2 ISO 19906

The International Organization for Standardization(ISO) developed *ISO 19906 Petroleum and natural gas industries - Arctic offshore structures*. This uses the limit

state design methodology. It states that the structure shall be designed for ULS requirements and that the ULS design condition for ice shall be the extreme-level ice event(ELIE) and both local and global actions shall be considered. The structure shall also be checked for ALS in order to ensure that it has sufficient reserve capacity and energy capability. The Serviceability Limit State(SLS) and Fatigue Limit State(FLS) considerations shall of course also be taken into account (ISO, 2007).

To check for ALS, this includes checking for so-called Abnormal-Level Ice Events(ALIE) in ISO 19906. The iceberg impacts of significant damage that have an annual probability of occurrence between 10^{-3} to 10^{-5} are recommended to be considered as ALIE. Non-linear methods(i.e. NLFEA) may be used to evaluate such actions and some structural damage is allowed in ALS. Almost all the field data in ISO 19906 are from relatively small ice-featured experiments with either flat or convex surfaces. In these tests, the structure in question wasn't particularly damaged. Consequently, these data are unreliable for problems containing damaged structures due to ice actions. The results from an iceberg impact analysis depend on assumptions made, e.g. iceberg shape and orientation. However, there are no recommendations with respect to the iceberg shape in ISO 19906. On the other hand, the contact area shall be based on local structural configurations in order to ensure that the most critical cases are covered (Kim, 2014).

Pressure-Area Curve

Research has indicated that pressure and the contact area are of great importance when it comes to iceberg impact problems (Bøhlerengen, 2013). The pressure is inversely proportional to the contact area, i.e. with increasing contact area decreases the pressure. In ISO 19906 the pressure-area relation in Equation 3.7 is proposed.

$$p = 7.4A^{-0.7} \tag{3.7}$$

where p is the pressure and A is the contact area. The pressure versus contact area is plotted in Figure 3.7, together with experimental data from several different experiments that the relationship in Equation 3.7 is based on.

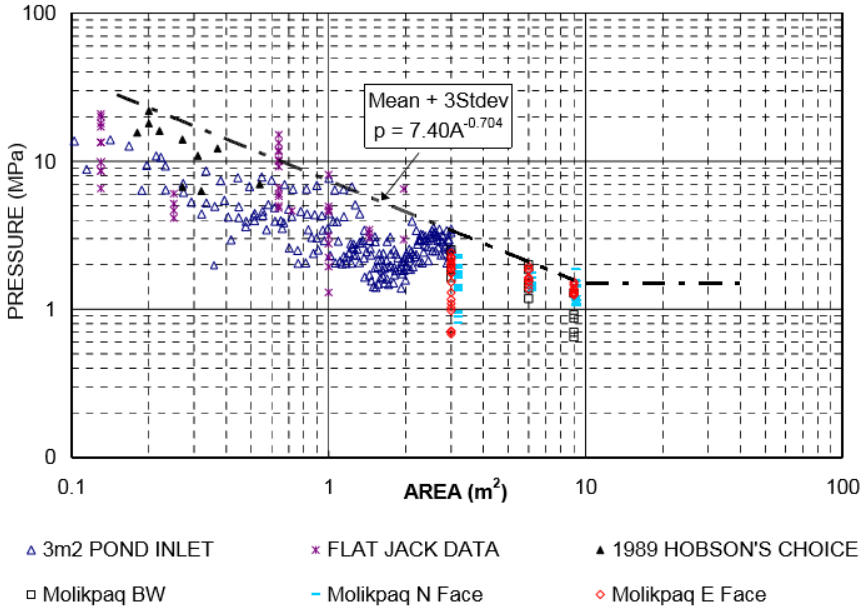

Figure 3.7: Pressure area curve with data measures (ISO, 2007).

3.3 Ice Crushing Considerations

The ice crushing properties may be considered with pressure-area curves, as in ISO 19906. These are evaluated in terms of local and global actions. As described above, the characterization of the ice crushing process is affected by the chosen limit state. The requirements in ULS is that the structure cannot obtain significant deformations. Consequently, the high local pressure can develop in the contact area and dominate the local design. In ALS, the structure is allowed to deform. Hence, it is the overall crushing process that governs the contact force, and localized high peaks are not of great interest. For this reason, the pressure-area curve proposed by ISO 19906 is deemed too conservative by Lu et al. (2018). In the report, it is suggested to instead use a curve of $P = P_0 A^{-0.1}$.

Chapter 4

Ice Physics and Ice Material Modelling

4.1 Characteristics of Ice

4.1.1 Classification of Ice

Floating ice exists in several forms and environments and is often classified thereafter. The World Meteorological Organization (WMO) divides floating ice in four categories, according to Høyland (2017);

1. Sea ice - Formed by the freezing of seawater.
2. Ice from land - Ice formed on land or in an ice shelf.
3. Lake ice - Formed on lakes.
4. River ice - Formed on rivers.

Glacial ice, which is subjected to this study, is under the category of ice from land. There is also other ways to classify ice, such as by age, feature type or position. Glacial ice is categorized after the waterline length and the height above water, see Table 4.1. Larger icebergs are fairly easy to detect and do therefore not introduce too much risk. However, smaller features of glacial ice, such as Bergy bit and Growlers, are harder to detect. Icebergs of this size may also have larger velocity than larger ones and can cause significant damage to structures. Hence, it is absolutely crucial to evaluate the damage an impact with glacial ice may bring if one is to operate in ice-infested waters.

Table 4.1: Categories of glacial ice.

Category	Waterline length [m]	Height above water [m]
Growler	< 5	< 1
Bergy bit	5 - 15	1 - 5
Small iceberg	15 - 60	5 - 15
Medium iceberg	61 - 120	15 - 45
Large iceberg	121 - 200	46 - 75
Very large iceberg	> 200	> 75

4.1.2 Properties

Glacial ice exists in temperatures which are close to their melting temperature and have several special properties that make it challenging to represent in mathematical models. A reasonable assumption for the properties is that they are isotropic. This is not the case for sea ice which is considered as an anisotropic material. Some of the properties of icebergs that are important to consider in ice-structure impact interaction are briefly discussed in this section.

Size Effects of Ice properties

Ice can experience different kinds of failure depending on the size of the ice(Palmer and Croasdale, 2013). This is often referred to as *size effect*. For small-scale ice, it is observed a ductile behaviour, while in larger scales the failure is of brittle nature. These features become important to consider during an impact between a marine structure and glacial ice. The reason is that when this happens, the ice will not fail in the whole area at the same time. Some parts of the area will experience a higher load and will fail first, which influences the parts that haven't been broken yet. This will cause the unbroken parts to fail more easily. Design codes take this size effect into account by pressure-area curves to determine ice strength.

Strain-Rate Dependency

As discussed in (Liu et al., 2010), the strength of icebergs increases with increasing strain rates, but only up to some point. Derradji-Aouat (2000) concluded that the yield envelope of the iceberg increases to a maximum value and then decreases again, i.e. the strength of the iceberg decreases for high strain rates. This turning point is believed to be around $10^{-3}s^{-1}$. The strain-rate dependency of ice has been verified by Kim (2014) by tests on granular ice. At low strain rates, the mechanical behaviour of ice is ductile, while for high strain rates brittle failure is dominant, as illustrated in Figure 4.1. Ductile materials

will undergo plastic deformation and thus increase its hardness, while a brittle material will fail without any significant plastic deformation.

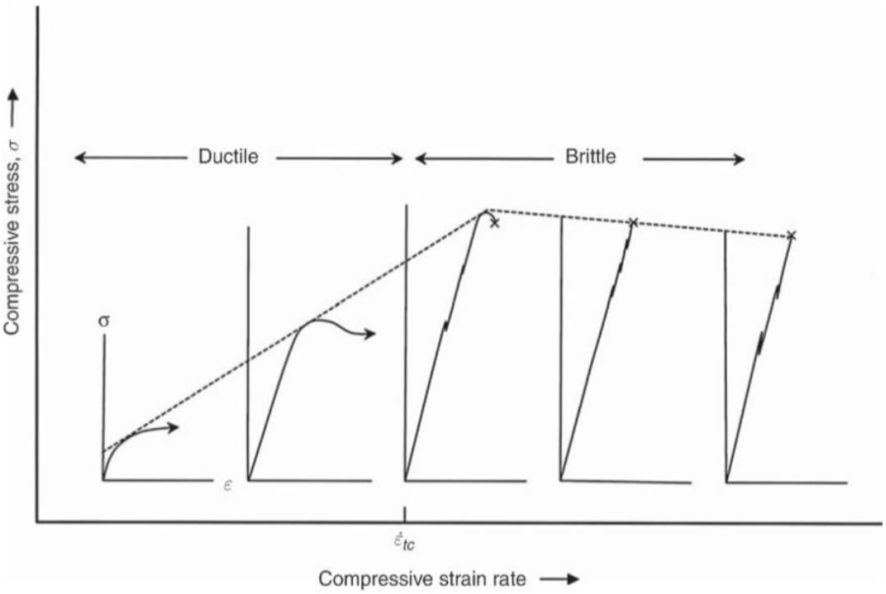

Figure 4.1: Stress-strain curves for different strain rates(Schulson and Duval, 2009).

Liu et al. (2010) argued on the basis of numerical simulations in LS-DYNA that ship and iceberg impacts involves high strain rates, higher than $10^{-3}s^{-1}$, and thus the ice is in brittle failure mode. In order to implement strain rate behaviour in a material model, it is necessary to have a sufficient amount of experimental data, which is not the case here. Hence, a yield envelope representing high strain rates is used in many numerical simulations.

Temperature Dependency

According to studies performed on the temperature profile of glacial ice, the submerged part is subjected to a steep temperature gradient and the core temperature is reached approximately 3 m from the surface (Løset, 1993). The strength of ice is opposite proportional to the temperature. The temperature dependency is adopted in some material models of ice, such as in the work of Liu (2011), where the yield surface can be adjusted to take the temperature dependency into account.

Pressure Dependency

Equivalent hydrostatic pressure has a nonlinear effect on the behaviour of ice, and the deviatoric stress that it can withstand is dependent on the equivalent hydrostatic pressure, i.e. ice is stronger in compression than in tension. This difference in strength is reviewed to be between 2-10 times in favour of compressive strength. In addition, there are some suggestions that the phase changes due to hydrostatic pressure (Kim, 2014). The pressure dependency is reflected in the Tsai-Wu yield surface, which will be described in more detail later in the chapter.

4.2 Mathematical Model

Ice is a very complex material which appears in various conditions, and to develop a material model that describes the behaviour in all conditions mathematically is not realistic. However, Liu (2011) developed a material model of ice in his Ph.D. thesis which is to represent the physical behaviour of ice in collision analyses. In the following, the mathematical model is described in more detail with respect to the plasticity formulations, plastic flow theory, the influence of confinement, the return algorithms, failure modelling and the erosion techniques adopted.

4.2.1 Yield Surface

Ice may experience large compression and confinement within the contact area during collisions with structures. Areas with high pressures arise and spall and extrusions may occur. This makes it possible for ice to change phase. Hence, the magnitude of the deviatoric stress that the ice can handle is dependent on the hydrostatic pressure. The von Mises yield criterion is the most widely used criterion used for steel under impact problems. However, it is not suitable for ice since it is independent of the hydrostatic pressure. Other popular yield criteria, such as the Drucker-Prager and the Mohr-Coulomb yield criterion, are unsuitable to use for ice due to the same inability to model the pressure-dependency.

Derradji-Aouat (2000) proposed the elliptical yield envelope for icebergs shown in Equation 4.1:

$$(\frac{\tau - \eta}{\tau_{max}})^2 + (\frac{p - \lambda}{p_c})^2 = 1 \tag{4.1}$$

where p is the hydrostatic pressure, τ is the octahedral shear stress, and η, λ, τ_{max} and p_c are constants.

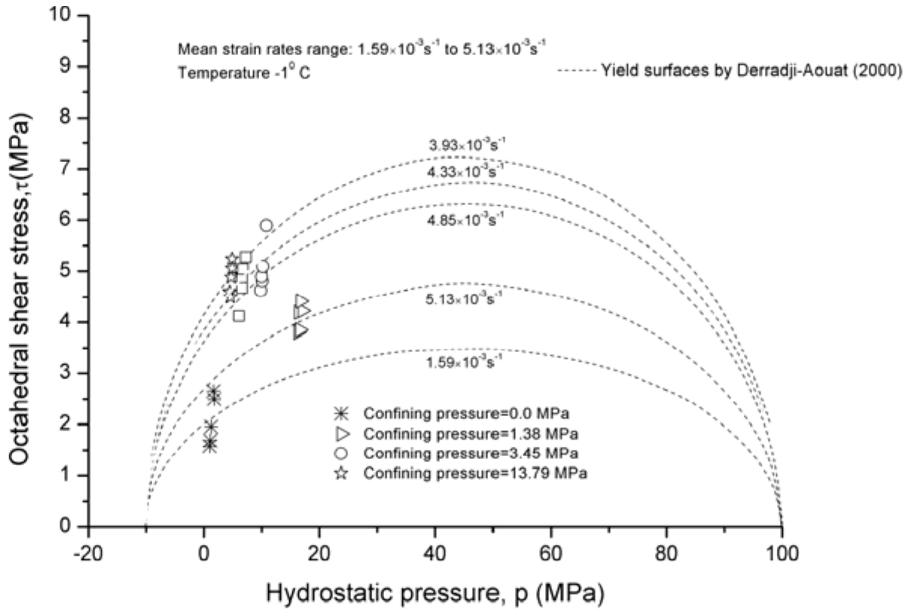

Figure 4.2: Yield surface proposed by Derradji-Aouat (2000). Figure from Liu (2011).

In Figure 4.2 the yield surface from Derradji-Aouat (2000) is plotted. It shows the octahedral shear stress versus the hydrostatic pressure for a temperature at -1°C. This yield surface is the same as the *Tsai-Wu yield surface* when the constant $\eta = 0$. The material model for icebergs that Liu (2011) proposed is based on the Tsai-Wu yield surface, which can be expressed with the yield function in Equation 4.2:

$$f(p, J_2) = J_2 - (a_0 + a_1 p + a_2 p^2), \qquad f(p, J_2) \leq 0 \tag{4.2}$$

where J_2 is the second invariant variable for the deviatoric stress(Equation 4.2.1), a_0, a_1 and a_2 are constants found from triaxial experiments, p is the hydrostatic pressure.

$$J_2 = \frac{1}{2} s_{ij} : s_{ij} \tag{4.3}$$

$$p = \frac{\sigma_{kk}}{3} \tag{4.4}$$

The yield function is defined such that if it has a negative value there is no loading, and $f(p, J_2) = 0$ is the elastic limit, i.e. when the yield function lies on

this limit plasticity occurs. $f(p, J_2) > 0$ is inadmissible, and in order to lay on this elastic limit the yield surface must change in shape and/or position during plasticity.

The values of the parameters, a_0, a_1 and a_2 in the Tsai-Wu yield surface have been investigated and proposed by several researchers, see Table 4.2. The yield function is plotted in Figure 4.3 in the $p - J_2$ space to show how the ice material constants affects the shape of the surface.

Table 4.2: Proposed material constants.

Researcher	a_0 $[MPa^2]$	a_1 [MPa]	a_2 [-]
Derradji-Aouat (2000)	22.93	2.06	-0.023
Kierkgaard (1993)	2.588	8.63	-0.163
Riska and Frederking Data set 1 (1987)	1.60	4.26	-0.62
Riska and Frederking Data set 2 (1987)	3.10	9.20	-0.83

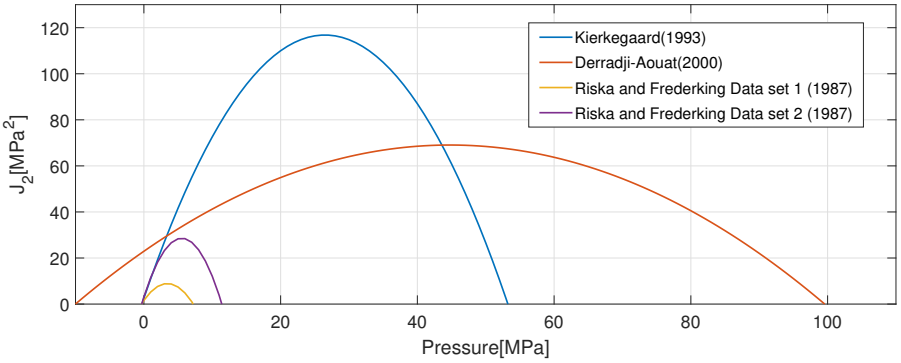

Figure 4.3: Tsai-Wu Yield function in $p - J2$ space with various proposed ice constants.

4.2.2 Flow Rule

Liu (2011) proposed to describe the plastic material model by the the associated flow rule. This means that the plastic strain increment is normal to the yield surface and the yield function is used as the plastic potential. To use the yield criterion to derive the plastic strains is often referred to as the normality rule. The plastic strain increment, $d\epsilon^p$, is then determined by:

$$d\epsilon^p = d\lambda \frac{\partial f}{\partial \sigma} = d\lambda \nabla f \tag{4.5}$$

where f is the yield function and $d\lambda$ is the plastic multiplier that determines the magnitude of the plastic strain increment in the direction normal to the yield surface.

4.2.3 Failure Modelling

The failure modelling is based on the stress state and the equivalent plastic strain. Impact with icebergs are well confined and the hydrostatic pressure is an important variable in this action. The hydrostatic pressure and the friction in the impact may lead to different failure mechanisms, such as frictional or non-frictional, Coulombic or plastic failure (Schulson and Duval, 2009). At low confinement pressure Coulombic failure can occur due to shear forces, while plastic fault occurs when the confinement pressure is so large that the frictional gliding in the material is suppressed. Figure 4.4 shows a sketch of the Coulombic and the plastic faults.

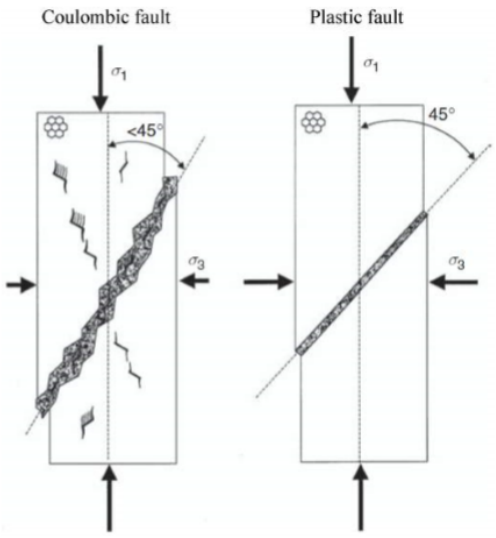

Figure 4.4: Coulombic and Plastic shear fault. Figure from Schulson and Duval (2009).

In the case of Coulombic faults in icebergs, the ice will experience shear forces in the beginning. In a numerical analysis, these elements are kept in this state until they reach a certain level of shear force and then removed from the analysis using erosion technique. This makes it fairly easy to satisfy the failure criterion as the pressure increases. The case of plastic faults makes it more difficult to reach the failure criterion since the ice will have increased stiffness due to increasing pressure. Liu (2011) proposed a U-shaped failure criterion in terms of equivalent plastic strain and pressure, as seen in Figure 4.5. The failure criterion

is based on empirical data and can be described by Equation 4.6 and 4.7. If the equivalent plastic strain, ϵ_{eq}^{p}, is larger than the failure strain, ϵ_f, the elements are eroded from the analysis. Erosion of elements will also occur if the pressure is larger than the cut-off pressure, p_{cut}. This cut-off pressure is introduced in order to describe the difference in strength for tensile and compression conditions and it defines the leftmost dotted line of the failure criterion with constants proposed by Derradji-Aouat (2000) in Figure 4.5.

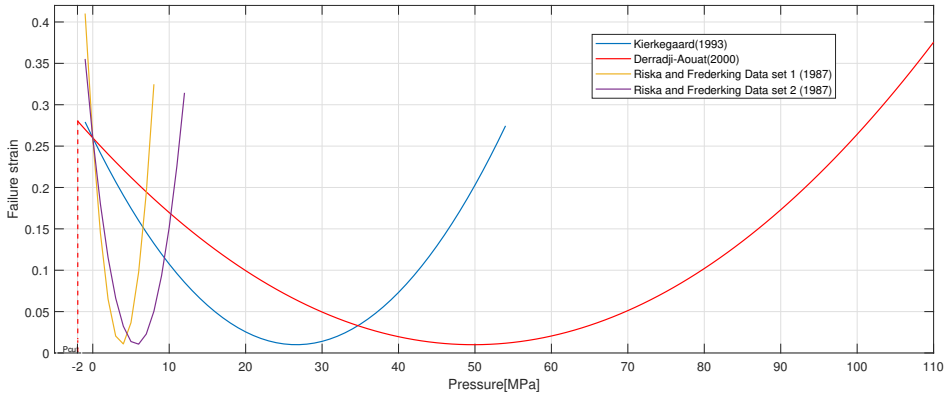

Figure 4.5: U-shaped failure criteria proposed by Liu (2011) with various proposed material constants.

$$\epsilon_{eq}^{p} = \sqrt{\frac{2}{3}\epsilon_{ij}^{p} : \epsilon_{ij}^{p}} \tag{4.6}$$

$$\epsilon_f = \epsilon_0 + (\frac{p}{p_2} - 0.5)^2 \tag{4.7}$$

where ϵ_{ij}^{p} is the equivalent plastic strain tensor component, p_2 is the second root of the yield function, ϵ_0 is the initial failure strain and ϵ_f is the current failure strain.

4.3 Ice Material Model Implementations

The mathematical model that Liu (2011) proposed has been attempted to implement as subroutines in both the FE-software LS-DYNA and Abaqus by various authors. Even though these subroutines are based on the same mathematical model, the implementations differ from each other in some areas. In this section some of the implementations will be described and compared.

4.3.1 Numerical Ice Model Implemented in LS-DYNA by Liu (2011)

Liu (2011) implemented the material model in LS-DYNA as a subroutine written in the programming language FORTRAN. The subroutine splits the deviatoric and hydrostatic pressure and describes the yield criterion in the $p - J2$ space, as shown in Equation 4.2.

When plasticity occurs, it is necessary to map the plasticity back to the yield surface. This is done with *the cutting plane return algorithm*. The procedure in this algorithm is to first calculate an elastic trial stress by integrating the elastic equations with total strain increments. The next step is to map the stress to a suitable updated yield surface in an iterative process(Huang and Griffiths, 2009). This is schematically represented in Figure 4.6.

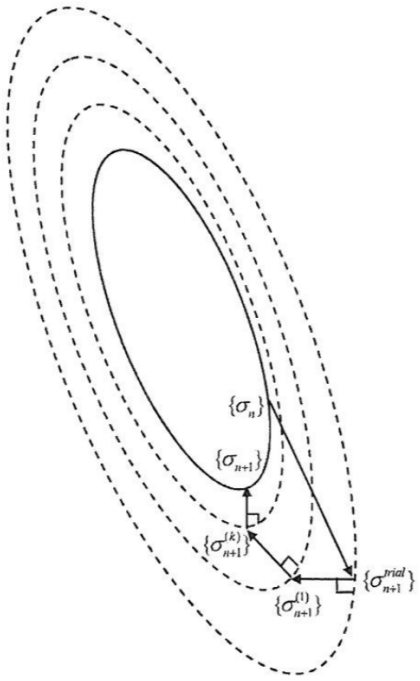

Figure 4.6: Stress return with Cutting Plane Algorithm(Huang and Griffiths, 2009).

The plasticity correction process is determined by the plastic multiplier, $\Delta\lambda^{k+1}$. Hence, during the elastic correction phase the plastic strain is fixed and in the plastic correction phase the total strain is fixed. The normality rule is applied at the beginning of each step and we get:

$$\Delta\boldsymbol{\sigma}^{(k)} = \boldsymbol{\sigma}^{(k+1)} - \boldsymbol{\sigma}^{(k)} = -\boldsymbol{D}^{e}\Delta\boldsymbol{\epsilon}^{p(k)} \tag{4.8}$$

$$\Delta \boldsymbol{\epsilon}^{\boldsymbol{p}(\boldsymbol{k})} = \Delta \lambda^{(k)} \nabla f^{(k)} \tag{4.9}$$

where k is the iteration counter in the mapping process and $\boldsymbol{D}^{\boldsymbol{e}}$ is the constitutive matrix. In every iteration, the yield function is linearized with the current stress, which yields Equation 4.10.

$$f^{k+1} = f^k + \nabla f^{(k)^T} (\boldsymbol{\sigma}^{(\boldsymbol{k+1})} - \boldsymbol{\sigma}^{(\boldsymbol{k})}) \tag{4.10}$$

By requiring that $f = 0$ the plasticity parameter that governs the plastic correction is defined as:

$$\Delta \lambda^{k+1} = \frac{f^k}{\nabla f^{(k)^T} \boldsymbol{D}^{\boldsymbol{e}} \nabla f^{(k)}} \tag{4.11}$$

Erosion technique means that when the damage in an element reaches a critical value the element is removed from the analysis. When erosion occurs in the implementation by Liu (2011), the deviatoric stresses on the element are set to zero, but not hydrostatic pressure. Due to the fact that the removal of an element is equivalent to setting the stress level to zero, this can be viewed as a rapid softening process. Since this technique is very dependent on the meshing, regularization may be necessary to improve the convergence properties(Hopperstad and Børvik, 2018).

4.3.2 Ice Material Model Implemented in Abaqus VUMAT by Woongshik Nam

Woongshik Nam implemented a user subroutine in Abaqus. This subroutine is pressure- dependent, but strain-rate and temperature independent. Similar to the implementation by Liu (2011), the yield function adopted is the Tsai-Wu yield function. However, Woongshik Nam has formulated it in the $p - \sigma_{eq}$ space:

$$f(p, \sigma_{eq}) = \sigma_{eq} - \sqrt{3(a_0 + a_1 p + a_2 p^2)}, \qquad \sigma_{eq} = \sqrt{3J_2} \tag{4.12}$$

where σ_{eq} is the von Mises stress. In this implementation the equivalent plastic strain increment is calculated and set equal to the plastic multiplier:

$$d\epsilon^p_{eq} = d\lambda \tag{4.13}$$

This relationship is valid when using the associative flow rule and yields the same results as the method of directly calculating the equivalent plastic strains

from the associative flow rule (Krabbenhøft, 2002).

Woongshik Nam has also adopted the cutting plane return algorithm and the failure criteria in Equation 4.7. During element erosion, Woongshik Nam does not explicitly set the deviatoric and hydrostatic stresses to zero, like it is done in the implementation by Liu (2011). However, this has no effect on the results as Abaqus pass zero stresses and strain increments for all deleted material points. The update of specific internal energy and update of the dissipated inelastic specific energy are calculated within the subroutine, while in LS-DYNA this is done outside the subroutine. In the implementation by Woongshik Nam(the current version when this master thesis is written), an suspected error is found in the energy update. It is not an absolute requirement to update the energy variables when implementing a material model in Abaqus VUMAT. Thus, it is uncertain how the wrong calculation of energy affects the results. Another noteworthy feature of this implementation is that the subroutine only uses the cut-off pressure when the return mapping algorithm is activated. Thus, if one uses ice material constants that creates a yield surface where the cut-off pressure is within the elastic region, the elements may not be deleted even though the cut-off pressure is exceeded.

4.3.3 Numerical Ice Model Implemented in Abaqus VUMAT by Ferrari (2014)

Ferrari (2014) adopted a material model to simulate ice behaviour in analyses of iceberg-structure impacts. This model was implemented in the FEM software Abaqus as a subroutine written in the programming language FORTRAN.
The yield function corresponds to the Tsai-Wu yield surface in Equation 4.2 and is only dependent on the deviatoric stress and the hydrostatic stress. However, Ferrari (2014) has formulated it in the $p - \sigma_{eq}$ space in the same way as Woongshik Nam did.

The subroutine is built up such that the user has to define six material properties; Young's modulus, Poisson ratio, initial plastic strain and the three constants in the Tsai-Wu yield function. The subroutine calculates the strain increment tensor by Equation 4.14 and uses a trial von Mises stress, σ_{eq}^{trial}, to check if this stress is lower than the equivalent elastic limit, σ_0, see Equation 4.15.

$$d\epsilon_{i+1}^{N} = \frac{\partial \Delta \mathbf{x}}{\partial (x_i + \frac{1}{2}\Delta \mathbf{x})} \tag{4.14}$$

where $\mathbf{x}$ is the position in time and $d\epsilon_{i+1}^{N}$ is the strain increment tensor.

$$\sigma_{eq}^{trial} = \sqrt{\frac{3}{2}\sigma_{ij}^{trial\prime} : \sigma_{ij}^{trial\prime}}, \qquad \sigma_{ij}^{trial\prime} = \sigma_{ij}^{trial} - \frac{1}{3}\delta_{ij}\sigma_{kk}^{trial} \tag{4.15}$$

$\sigma_{ij}^{trial\prime}$ is the trial deviatoric stress tensor component, which is the stress tensor minus the hydrostatic component.

If the trial von Mises stress is less than the equivalent elastic limit it will be used as the new stress state. However, if $\sigma_{ij}^{trial} > \sigma_0$, i.e. the elastic limit is exceeded, plasticity will occur and a new elastic limit is calculated by Equation 4.16.

$$\sigma_0 = (\sigma_0)_i + H'\Delta\epsilon_{eq}^{p} \tag{4.16}$$

In order to not exceed the yield surface, the stresses are mapped back onto the yielding surface by a scaling factor, ϕ, as in the *Radial return mapping algorithm*. This is the most popular algorithm for plasticity models, especially for metals. The idea behind the method is to first calculate trial stress by assuming elasticity. If the trial stress is outside the yield surface, the stress will be projected onto the point on the yield surface that is closest, as Figure 4.7 schematically shows. The method has been formulated to an arbitrary convex yield surface. Before the radial return process, the stress and equivalent plastic strain from the previous step are known, in addition to the strain increment in the current step. In the process the stress and equivalent plastic strains are updated.

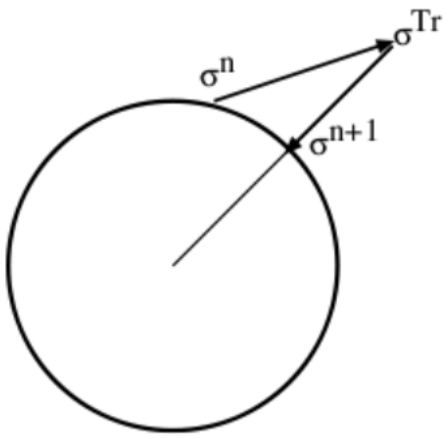

Figure 4.7: Stress return with radial return(LS-DYNA, 2005).

The closest point on the yield surface lies along the line from the centre of the yield surface and to the trial stress. Hence, the resulting deviatoric stress will be $\sigma' = \phi\sigma^{Tr}$, where ϕ is a scaling factor. The new equivalent plastic strain is calculated by the requirement that the final equivalent stress is equal to the new

yield stress. Then the scaling factor is calculated and the trial stress is mapped back onto the yield surface before the radial return procedure is ended by adding the deviatoric and mean stress (LS-DYNA, 2005).

The new equivalent von Mises stress is equal to the new equivalent elastic limit and the hydrostatic stresses are added.

$$\phi = \frac{\sigma_0}{\sigma_{eq}^{trial}}, \qquad \sigma_{ij} = \phi\sigma_{ij}^{trial\prime} + \frac{1}{3}\delta_{ij}\sigma_{kk}^{trial} \tag{4.17}$$

The total equivalent plastic strain is updated according to Equation 4.18:

$$\epsilon_{eq}^{p} = (\epsilon_{eq}^{p})_i + \Delta\epsilon_{eq}^{p} \tag{4.18}$$

The final step in the subroutine is to calculate the dissipated plastic specific energy per unit volume by the trapezoidal rule:

$$\boldsymbol{E_{pl}^{v}} = \int_0^{\epsilon_{eq}^{p}} \boldsymbol{\sigma_0(s)ds} = \boldsymbol{(E_{pl}^{v})_i + \frac{1}{2}[(\sigma_0)_i + \sigma_0]\Delta\epsilon_{eq}^{p}} \tag{4.19}$$

This procedure is repeated in an iterative process.

Comments

By investigation of the subroutine by Ferrari (2014), it is believed that it fails to correctly implement the mathematical model proposed by Liu (2011). There are two areas which are of special concern:

- It fails to implement the associative flow rule. It calculates the gradient $\nabla f(\sigma_{eq})$ instead of $\nabla f(\sigma_e, p)$. I.e. it disregards that the yield function is dependent on the pressure. Thus, it violates the condition that the total plastic strain increment is normal to the loading surface. An iterative return algorithm should be applied.

- The plastic strain increment is calculated from the solver and set equal to the strain increment, which is not correct. The plastic strain increment should be calculated from the flow rule.

Since the implementation of the mathematical model is not correct, the model by Ferrari (2014) is not further used. However, some analyses are performed with the implementation by Ferrari (2014) and the results of these can be found in the Appendix.

4.3.4 New Ice Material Model Implementation in Abaqus VUMAT

An objective of this master thesis was to further develop the implemented material model by Ferrari (2014). However, since the implementation is found to be insufficient, a new implementation of the material model by Liu (2011) has been developed from scratch in Abaqus VUMAT instead. In the development of the code, the code in LS-DYNA by Liu (2011) and in Abaqus by Woongshik Nam have been of guidance.

The new implementation is based on the same assumptions as the mathematical model by Liu (2011). It is developed with the same yield function, flow rule, failure criterion and return algorithm as Liu (2011) implemented in LS-DYNA, which is described in Section 4.2 and 4.3.1. The yield function is formulated in the $J_2 - p$ space and the equivalent plastic strain increment is calculated directly from the flow rule. The Young's modulus, Poisson ratio, ice material constants, initial failure strain and the cut off pressure are all defined as input parameters. Thus, there is no need for the user to do any changes in the subroutine when changing any of these parameters.

Chapter 5

Comparisons of Material Model Implementations with Numerical Analyses

In order to evaluate the subroutines described in Chapter 4 further, they are tested and compared by various numerical simulations in Abaqus and LS-DYNA, which are presented in this chapter.

5.1 Single Volume Element Analysis

An introductory study is performed in Abaqus on a single C3D8R 3D-cubic element to check the performance of the newly implemented material model and the implementation by Woongshik Nam. These analyses are performed in order to increase the reliability of the implementations before advancing to larger ice feature analyses. The single volume element is assigned material properties according to Table 5.1. The C3D8R element is an eight-node linear brick element with 1 integration point(reduced integration), whichis located in the centre of the element.

Table 5.1: Ice material properties.

Material property	**Value**
Young's modulus, E	9500 [MPa]
Poisson ratio, ν	0.3 [-]
a_0	2.588 $[MPa^2]$
a_1	8.630 [MPa]
a_2	-0.163 [-]
Initial failure strain, ϵ_0	0.010 [-]
Density, ρ	900 $[\frac{kg}{m^3}]$

Yield Function Test

First, the implementations are tested to see if they are able to follow the Tsai-Wu yield function with increasing hydrostatic pressure. All four nodes at one side of the cube are fixed in all degrees of freedoms, including rotational degrees of freedom, while the nodes on the other side are applied loading with displacement control. Figure 5.1a shows the setup and in Figure 5.1b shows the deformation pattern. The failure criterion is turned off in this test.

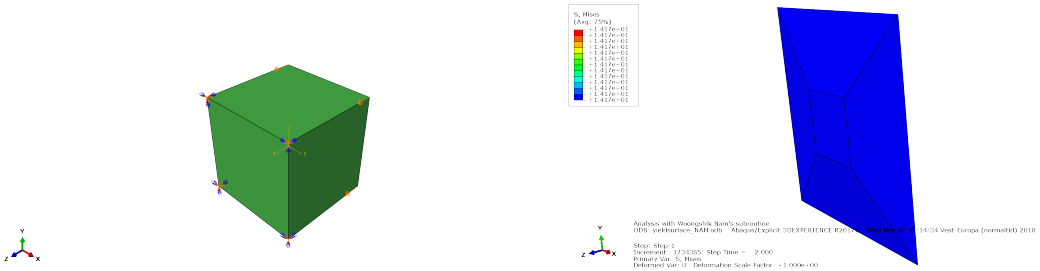

(a) Model setup. (b) Deformed cube.

Figure 5.1: Simple analysis model of a single cubic element.

As Figure 5.3 and 5.2 shows, both the implementations are able to follow the yield function once they reach the yielding limit. The yielding limit is not exceeded at any point. Thus, the implementations are able to both update the yielding limit and to stay on this limit when the pressure is increased.

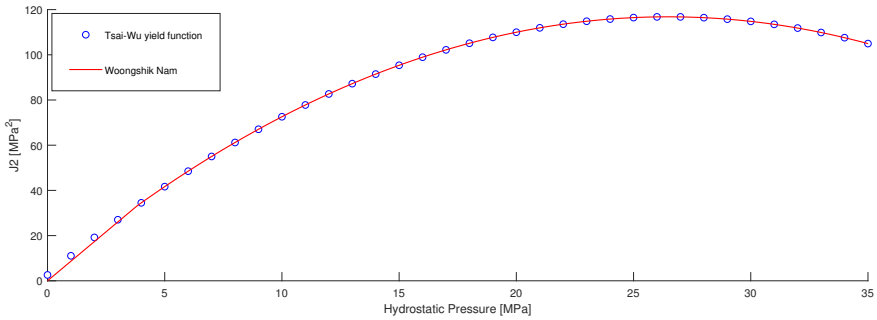

Figure 5.2: J_2 - Pressure plot of the implementation by Woongshik Nam with Kierkegaard's parameters.

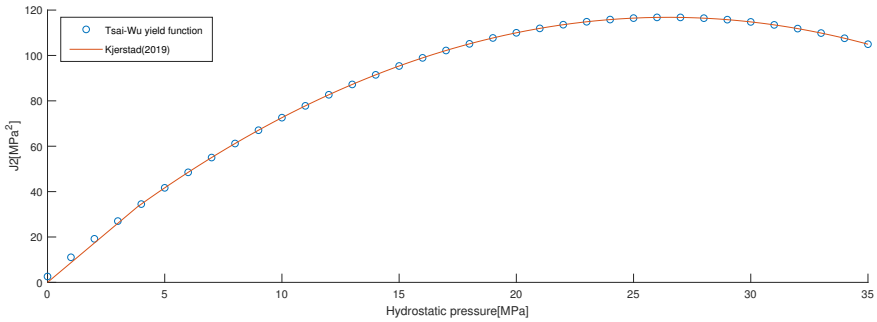

Figure 5.3: J_2 - Pressure plot of the new implementation with Kierkegaards parameters.

Reloading Test Case

The new implemented code is also tested in a model were the applied loading is unloaded then reloaded again. This test is performed in order to see how the equivalent plastic strains are calculated and to show that the subroutine is reliable when unloaded and reloaded.

The model setup consists of three cubic solid C3D8R elements, as displayed in Figure 5.4. The ice material is applied to the central cube, while the two other cubes are applied purely elastic material properties. The model is subjected to a varying uniaxial force, which is applied to the rightmost cube. The nodes to the central element are constrained to have the same displacement as the nodes of the two side-elements in the loading direction. This constraint is applied to avoid sudden change of the transverse section due to plasticity in the central element. The erosion criterion is turned off in this test.

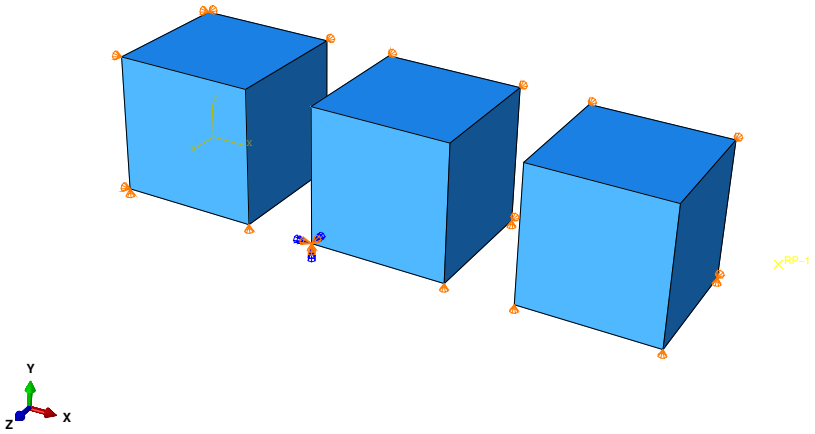

Figure 5.4: Model setup - reloading test case.

In Figure 5.5 the von Mises stress, yielding limit and the accumulation of the equivalent plastic strain in the central element are plotted. It shows that the von Mises stress varies with the varying applied loading and the implementation is able to update the yielding limit when the loading(and thus the pressure) changes. The von Mises stress never exceeds the yielding limit, but rather follows the Tsai-Wu yield function. This indicates that the return algorithm is working properly. The equivalent plastic strains are accumulated when the von Mises stress lie on the yielding limit and they are held constant when the stresses are in the elastic range. These results increase the reliability of the newly implemented material model.

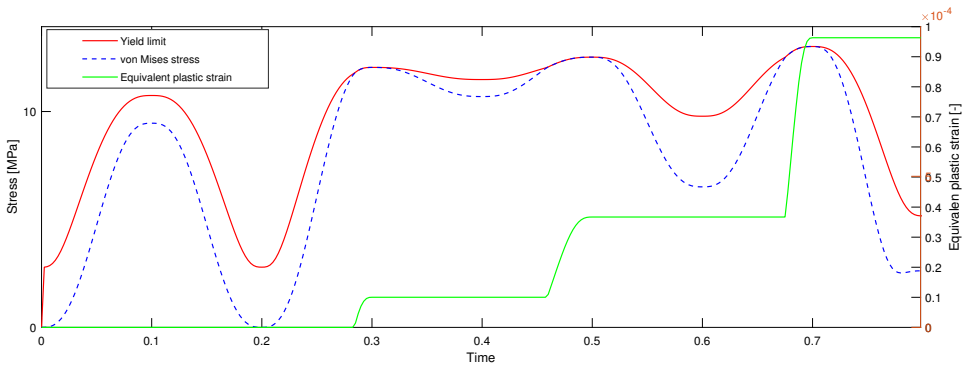

Figure 5.5: Results reloading test case in terms of yielding limit, von Mises stress and development of equivalent plastic strains.

5.2 Non-Linear Analysis of Iceberg Crushing Against a Rigid Wall

In this master thesis analyses of a half-sphere shaped iceberg is crushed against a rigid wall are performed to evaluate the performance of the subroutines. I.e. the du energy design method is used in this analysis, as described in Chapter 2.

The analysis model consists of two parts, a rigid plate and a deformable half-sphere. The rigid plate is representing the structure in the strength energy design method(such as shipboard) and the half-sphere is representing the iceberg. Initially, a model in Abaqus was developed. However, to compare the implemented material models across FEA software was it deemed necessary to establish a new model which could be exported to both Abaqus and LS-DYNA. The results from the old model setup is shown in Appendix B. The model is generated using the FEA pre- and post-processing software MSC Patran. This powerful software provides solid modelling and meshing for several solvers, including LS-DYNA and Abaqus. This ensures that the solid modelling and the mesh are identical across the two FEA software.

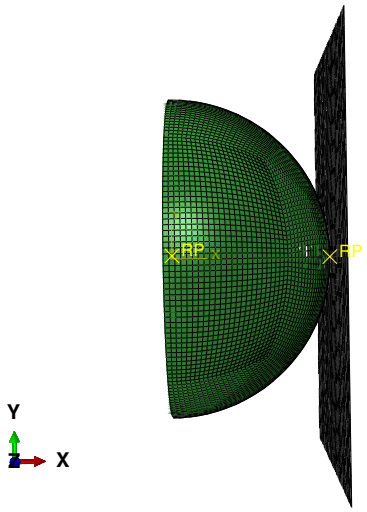

Figure 5.6: Model setup.

Iceberg

The iceberg has a radius of 1.5 m, the same sphere-size as Storheim (2016) used in his doctoral thesis. It consists of solid C3D8R elements, which is the same element used in the single element analysis. The iceberg is created in MSC Patran by the tool “Creating a Solid Sphere and Hex mesh” This tool creates a cubic box in the middle of the sphere and creates layers with cubic elements

around to make a sphere. The cubic box in the middle has a dimension of 0.75 m. This creates a fine mesh, as Figure 5.7 shows. The iceberg is meshed with cubic elements with dimensions of 50 mm.

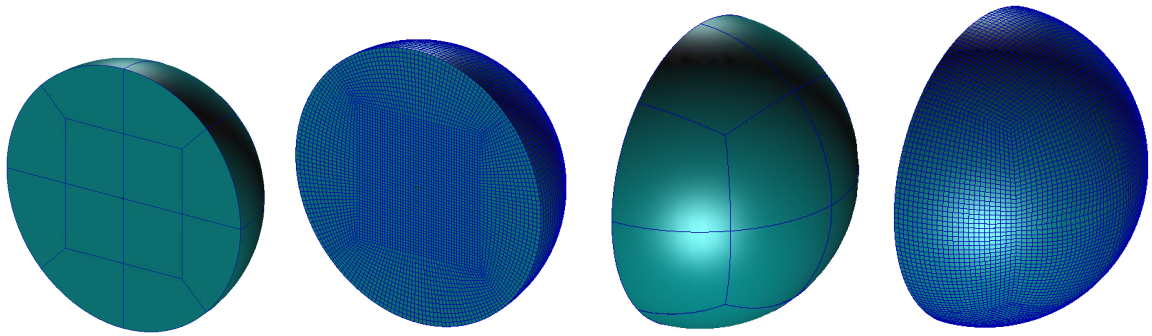

Figure 5.7: Iceberg model in ISO view.

Plate

The rigid plate is a square plate with length of 4 m. It is meshed with R3D4 elements, which is a rigid 3-dimensional 4-node element and is often used to define master surfaces in contact problems. The mesh size is 50 mm.

Boundary Conditions

The back surface of the iceberg is fixed in all degrees of freedom, while the plate is fixed in all degrees of freedom, except translations along the x-axis. A velocity of 1 m/s along the x-axis towards the iceberg is applied the plate.

Contact

The general contact option in Abaqus is used in this analysis. The contact domain is the rigid wall with the surface of the sphere, both the external and internal. The internal surfaces account for all six surfaces of the cubic elements. The contact with the interior surfaces makes it possible to erode the interior elements as well, not only the exterior. In addition, general contact is also applied on the interior surfaces with itself. For all contact, the penalty formulation is used with a friction coefficient of 0.15.

5.2.1 Comparison of Implemented Material Models in Abaqus

The material model implementation developed in this master thesis is compared to the implementation in Abaqus VUMAT by Woongshik NAM with respect to

the reaction force from the analysis with an iceberg crushing against a rigid wall. In addition, the analysis is performed with a third code in Abaqus. This is an implementation by Professor Mihkel Kõrgesaar at Tallinn University of Technology and Doctoral candidate Li Fang at Aalto University. The implementation will not be described in detail here, but it is based on the mathematical model by Liu (2011). The code is modified slightly; initially, a restriction of maximum failure strain was set to 26.9 %. This restriction is removed in this analysis and the failure strain is purely based on the failure criterion in Equation 4.7. The same model setup is run in LS-DYNA with the implementation by Liu (2011). Postdoctoral fellow Zhaolong Yu performed the LS-DYNA analysis.

In Figure 5.8 the reaction force is plotted against the crushing distance for all four implementations described in this thesis. The ice material constants proposed by Kierkegaard (1993) are used in all of the analyses. In the analyses in Abaqus, the default hourglass control is applied. The analysis in LS-DYNA yields the lowest forces, while the new implementation in Abaqus yields the highest forces. The difference is significant, the force in LS-DYNA is about one-third of the magnitude of the force in the new code. The implementations by Woongshik Nam and Kõrgesaar/Li are in between. All of the implementations have the same pattern with a more or less linear increase in force with increasing crushing distance. The forces oscillates a little, but not more than one could expect in numerical analyses like this. It should be noted that the amount of hourglass is different in the models. Hence, this might explain some of the difference in the force magnitude. This is subjected to further investigation later in the thesis.

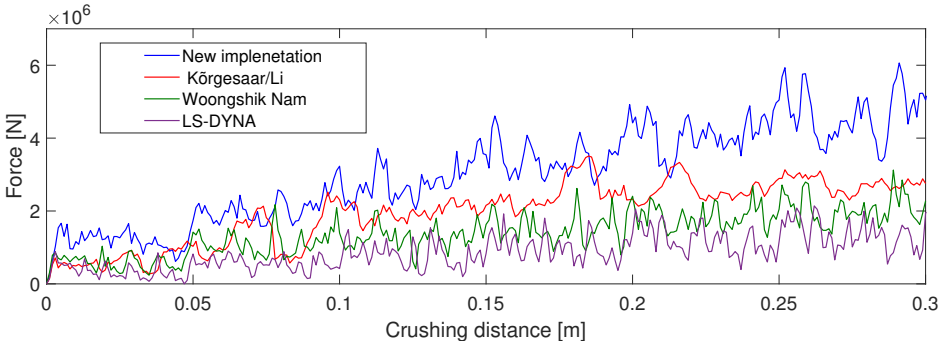

Figure 5.8: Comparison of the reaction force with the material model implementations in Abaqus with the ice constants by Kierkegaard (1993).

Figure 5.9 shows the erosion pattern of the four models at a crushing distance of 0.25 m for all four implemented codes. They all erode elements layer for layer as the crushing distance increases. The erosion pattern is similar to waves from a

dropped object in water; the erosion starts in the centre of the sphere and radiates outwards from the centre. None of the models creates any hole in the contact zone. Visually, erosion seems reasonable. It is observed that the implementation by Kõrgesaar/Li creates a less ordered pattern than the other implementations.

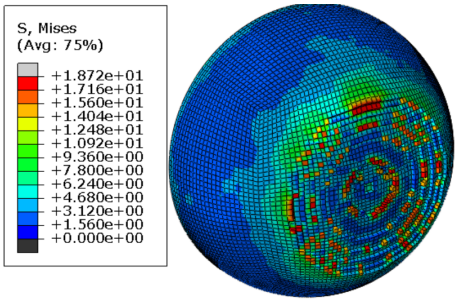

(a) New implementation

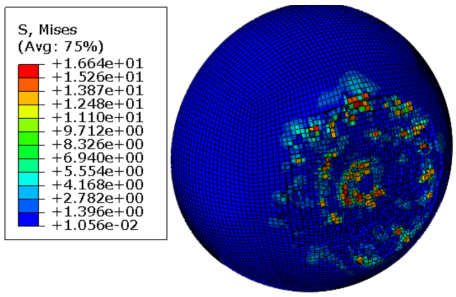

(b) Kõrgesaar/Li

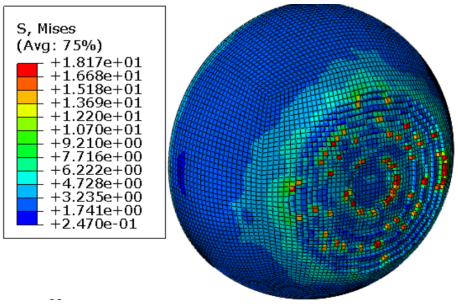

(c) Woongshik Nam

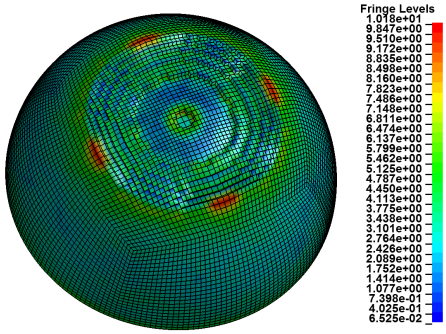

(d) LS-DYNA

Figure 5.9: Erosion pattern.

5.2.2 Ice Material Constants

Several authors have proposed material constants to be used in the Tsai-Wu yield function, i.e a_0, a_1 and a_2. Table 5.2 shows the proposed constants of Derradji-Aouat (2000) and Kierkegaard (1993). The constants affect the allowable stress in the elements, as Figure 4.3 shows. In addition, the failure criterion is dependent on the second root of the yield function(Equation 4.7). Thus, the failure strain and corresponding deletion of elements are also dependent on the ice material constants. In this section, the effect these constants have on the implementations with respect to the reaction force is investigated.

Table 5.2: Proposed material constants.

Researcher	a_0 $[MPa^2]$	a_1 $[MPa]$	a_2 [-]
Derradji-Aouat (2000)	22.93	2.06	-0.023
Kierkegaard (1993)	2.588	8.63	-0.163

In Figure 5.10 the reaction force is plotted versus the crushing distance with Woongshik Nam's subroutine. The parameters by Derradji-Aouat (2000) gives an initially higher peak and the force is slightly higher with these constants. However, the results are very similar and the implementation by Woongshik Nam yield consistent results between these to sets of proposed ice material constants.

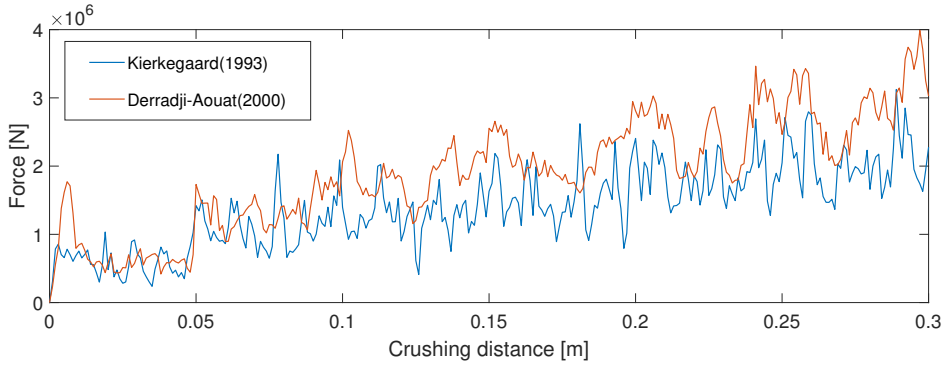

Figure 5.10: The effect of the proposed ice constants on the reaction force with Woongshik Nam's implemented subroutine.

The same analysis is performed with the newly developed subroutine. Here, the forces deviate more between the proposed material constants. With the Derradji-Aouat (2000) constants it is an initial peak up to about 3.5 MN. This peak is not present with the constants proposed by Kierkegaard (1993). The blue curve has a more steady increase in force levels, while the red curve has large variations and is eventually starting to decrease. This is not an expected behaviour. By visual investigation, it is observed that the analysis has an odd behaviour, as Figure 5.13a clearly shows. This might explain the fall in force magnitude.

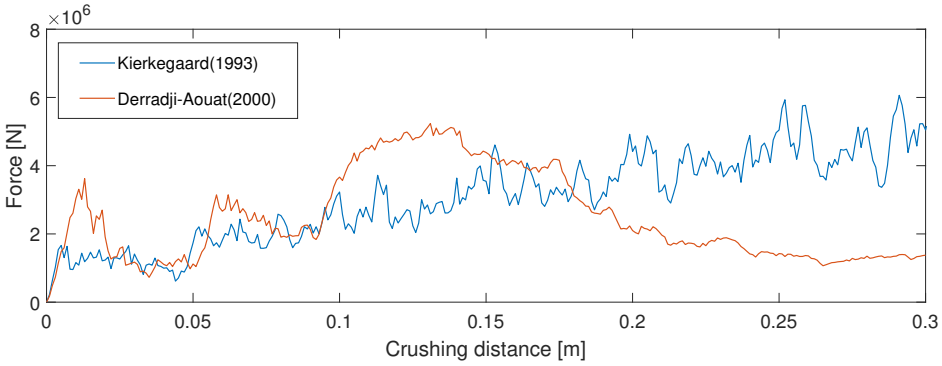

Figure 5.11: The effect of the proposed ice parameters on the reaction force with the new implemented material model.

The results from the ice material constants analysis with the implemented code by Kõrgesaar/Li has similarities with the new code. Here, the force with the Kierkegaard (1993) constants has a steady increase. The force with the Derradji-Aouat (2000) constants has larger variations and the mean value of these variations seems almost constant after about 0.1 m of crushing distance. As displayed in Figure 5.13b, also this analysis has an unexpected behaviour where the modelled ice is "exploding".

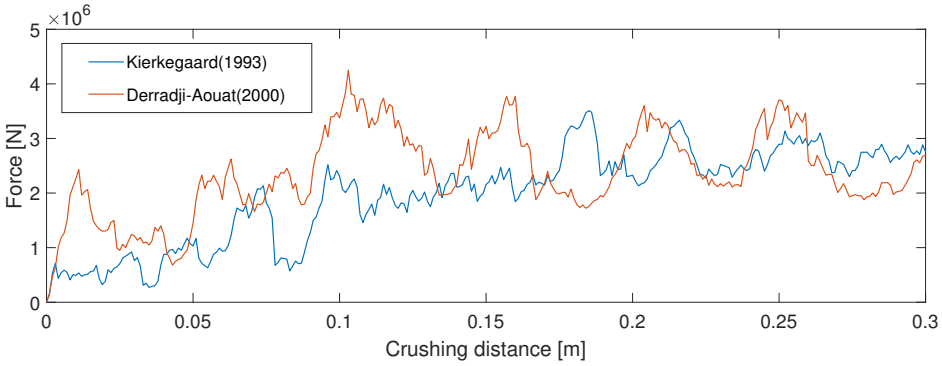

Figure 5.12: The effect of the proposed ice constants on the reaction force with the implemented subroutine by Kõrgesaar/Li.

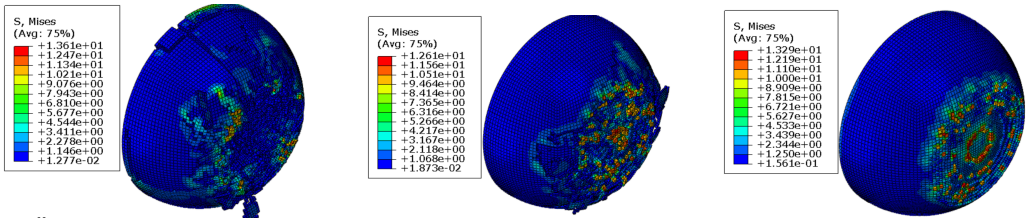

(a) New implementation (b) Kõrgesaar/Li (c) Woongshik Nam

Figure 5.13: Erosion pattern with the ice constants by Derradji-Aouat (2000).

In conclusion, with the implementation by Woongshik Nam, the results are similar between the ice material constants tested in this thesis. However, both the new implementation and by Kõrgesaar/Li gives odd results, both in terms of force-displacement curve and erosion pattern. A possible explanation of this may be that with the Derradji-Aouat (2000) material constants, the cut-off pressure plays an important role. The reasons is that the first root of the yield function is less than $-2MPa$ and the cut-off pressure is activated when the pressure goes below this value. The first root of the yield function with the Kierkegaard (1993) constants is larger than the cut-off pressure, i.e. it is located outside the yield surface. Hence, the stress state is returned back to the surface and the cut-off pressure is never reached. The activation of the cut-off pressure may be a factor causing the unexpected results with the Derradji-Aouat (2000) constants. This "explosion" in the analysis is not present in the code by Woongshik Nam. However, it is suspected that this implementation only uses the cut-off pressure when the return mapping algorithm is activated, which might be a reason why this is not occurring.

With this in mind, it is recommended to use ice material constants so the cut-off pressure lay outside the yield surface. In further analyses in this thesis, the parameters proposed by Kierkegaard (1993) will be used in order to avoid the issue concerning the cut-off pressure.

5.2.3 Hourglass Energy

The energy balance in Abaqus can be written as:

$$E_I + E_V + E_{FD} + E_{KE} - E_W = E_{total} = constant \tag{5.1}$$

where E_I is the internal energy, E_V is the viscous energy dissipated, E_{FD} is the frictional energy dissipated, E_{KE} is the kinetic energy, E_W is the work done by the externally applied loads, and E_{total} is the sum of these energy components

and should be constant and relatively small. The internal energy component is a sum of several underlying components;

$$E_I = E_E + E_P + E_{CD} + E_A \tag{5.2}$$

where E_E is the strain energy, E_P is the inelastic dissipated energy, E_{CD} is the energy dissipated by viscoelasticity and E_A is the artificial strain energy. The artificial strain energy includes energy stored in hourglass resistances and transverse shear in shell and beam elements(Abaqus, 2005b). Since the iceberg consists of solid elements, the artificial strain energy is the same as hourglass in these analyses.

This is a quasi-static analysis, meaning that the kinetic energy will be low compared to the other energy components. The energy components of significant magnitude are E_W, E_{FD} and the internal energy components E_E, E_P and E_A. For the newly implemented material model and the implementation by Woongshik Nam, the amount of hourglass and how it influences the results are subjected to investigation in this section. Analyses of the half-sphere iceberg crushing against a rigid wall are run with several different hourglass controls, see Table 5.5 and Table 5.3. From the hourglass control in Abaqus three hourglass approaches found are found suitable in this quasi-static analysis; the relax stiffness, stiffness and enhanced hourglass control. A more detailed description of the hourglass controls can be found in the Abaqus user manual (Abaqus, 2005a). In addition, the effect of the displacement scaling factor, in combinations with these hourglass controls options, on the hourglass energy is investigated. This factor is dimensionless and relates to the specific displacement degrees of freedom. The implementation in LS-DYNA is subjected to short hourglass investigation.

Implementation by Woongshik Nam

As Table 5.3 shows, the amount of energy is substantial in the numerical analyses with the implementation by Woongshik Nam. This is true for all applied hourglass controls. The runs with a displacement scaling factor of 1.0, i.e. Run 1, 3 and 4, yield similar force levels. Run 3 gives the larges oscillations. From these results, the *Stiffness* approach is the most effective with respect to reducing the hourglass energy, and by applying a displacement scaling factor of 0.2(which is the lowest recommended value of this factor) the hourglass is not far from acceptable. However, even though the hourglass energy is reduced, the force level increase when the scaling factor is below 1.0. This is also the case with the *Relax Stiffness* approach and is opposite to what one could expect. Since the goal is to decrease the amount of the artificial energy in the analysis, the

corresponding force should then decrease as well.

Table 5.3: Hourglass analyses with the implementation by Woongshik Nam.

Run	Hourglass control	Displacement scaling factor	Hourglass
1	Relax stiffness	1.0	55 %
2	Relax stiffness	0.2	51 %
3	Enhanced	-	57 %
4	Stiffness	1.0	45 %
5	Stiffness	0.2	14 %

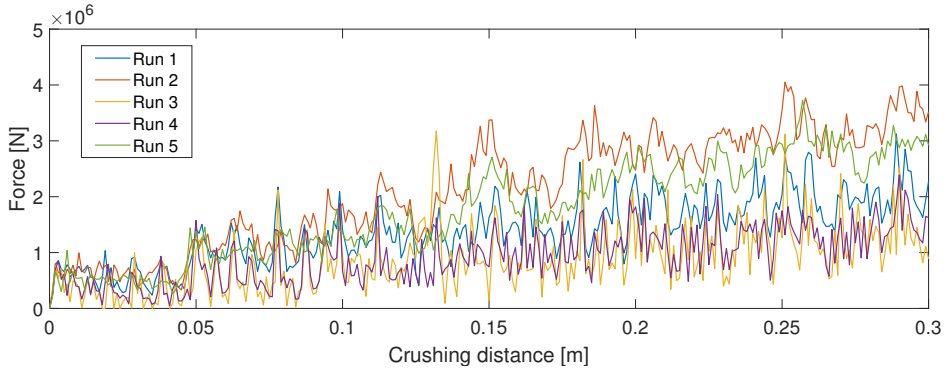

Figure 5.14: The effect of hourglass controls with the implementation by Woongshik Nam.

The energy in the analysis is the same as the area under the force-displacement curve. Since the force levels increase even though the hourglass energy is reduced, the energy must be moved from the hourglass energy component to another energy component. The energy components that are of significant magnitude are listed in Table 5.4. This table indicates that with applied displacement scaling factor less than 1.0, the frictional and the internal energy increases. The main contributor to the increase in internal energy is the strain energy component. An explanation may be that if the scale factor is reduced to less than 1.0, the elements would have to keep hourglass shape, which may lead the ice elements to have more contact with the rigid plate. Hence, it might show an increase in strain and friction energy and the force level increases.

Table 5.4: Energy components in the analyses with the implementation by Woongshik Nam.

Energy component	**Run 1**	**Run 2**	**Run 3**	**Run 4**	**Run 5**
E_W **[MNm]**	42	64	26	27	54
E_{FD} **[MNm]**	4	10	2	2	11
E_I **[MNm]**	36	53	21	22	43
E_A [MNm]	20	27	12	10	6
E_S [MNm]	15	25	7	12	35
E_P [MNm]	1	1	3	1	2

New Implementation

The newly implemented material model is subjected to analyses with the same hourglass controls. In addition, the effect of the displacement scaling factor is investigated a little further. The runs are listed in Table 5.5 and the resulting forces from the corresponding runs are displayed in Figure 5.15. In general, it is observed that the force level is higher with the new implementation than with the one by Woongshik Nam.

Also with this code, the hourglass energy is substantial. The Stiffness approach is the most effective, but the amount of hourglass energy is not severely reduced unless a scaling factor of 0.01 is applied, which is less than the recommended values for this factor. The coherence between the displacement scaling factor and the forces is not that dominating here, but the it is still present. By comparing the energy components in Table 5.6, the same trend is observed as in the analyses with Woongshik Nam's implementation, i.e. a increase in strain and friction energy the displacement scaling factor is less than 1.0.

Table 5.5: Hourglass analyses with the new implementation.

Run	**Hourglass control**	**Displacement scaling factor**	**Hourglass**
1	Relax stiffness	1.0	53 %
2	Relax stiffness	0.2	34 %
3	Enhanced	-	48 %
4	Stiffness	1.0	36 %
5	Stiffness	0.5	38 %
6	Stiffness	0.2	35 %
7	Stiffness	0.01	6 %

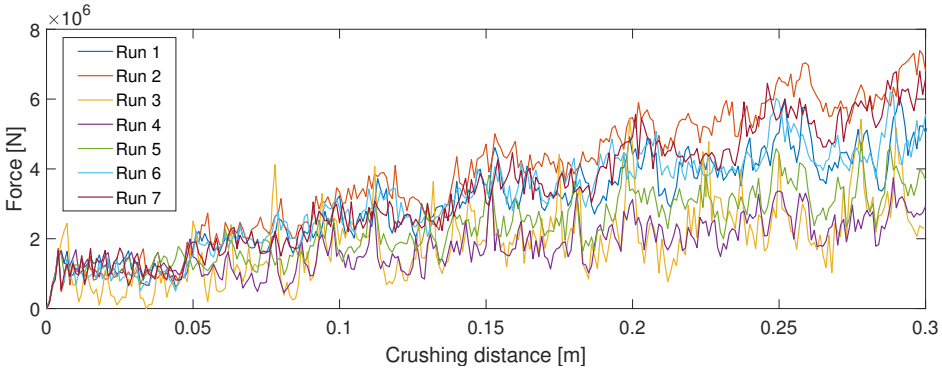

Figure 5.15: The effect of hourglass controls with the new implemented material model.

Table 5.6: Energy components in the analyses with the new implementation.

Component	**Run 1**	**Run 2**	**Run 3**	**Run 4**	**Run 5**	**Run 6**	**Run 7**
E_W **[MNm]**	91	115	57	54	70	93	100
E_{FD} **[MNm]**	9	19	4	5	7	12	20
E_I **[MNm]**	80	96	52	47	60	79	81
E_A [MNm]	42	33	25	17	23	28	5
E_S [MNm]	36	58	24	25	34	47	67
E_P [MNm]	2	3	3	4	4	4	9

In further analyses, the newly implemented material model is used with the Stiffness hourglass approach and an applied scaling factor of 1.0. This means that hourglass of above 30 % is accepted even though it is much higher than recommended(which is about 5-10 %). The reason for this is that even though it is possible to achieve lower hourglass energy, the effect of the scaling factor is uncertain. Thus, it is safer to use default hourglass control. In addition, the forces and the amount of hourglass are more similar to the analyses in LS-DYNA.

Implementation in LS-DYNA by Liu (2011)

The amount of hourglass energy is also an issue with the implementation in LS-DYNA. Figure 5.16 show the amount of hourglass in the analysis in LS-DYNA. The internal energy is in this software the sum of both the internal energy and eroded energy outputs from LS-DYNA. The results show that the amount of hourglass is about 15 %. This is above recommended values, but it is not too far off. The output of energy components and calculation of the amount of hourglass energy may be an area where it is a severe difference in the two FE software used in this thesis, i.e. Abaqus and LS-DYNA. In Abaqus, there is no eroded energy when using these subroutines and the amount of hourglass is

calculated by dividing the hourglass energy on the internal energy. LS-DYNA has this additional output of eroded energy, which makes the calculation of the amount of hourglass different. This makes it difficult to completely compare the hourglass energy across the two software.

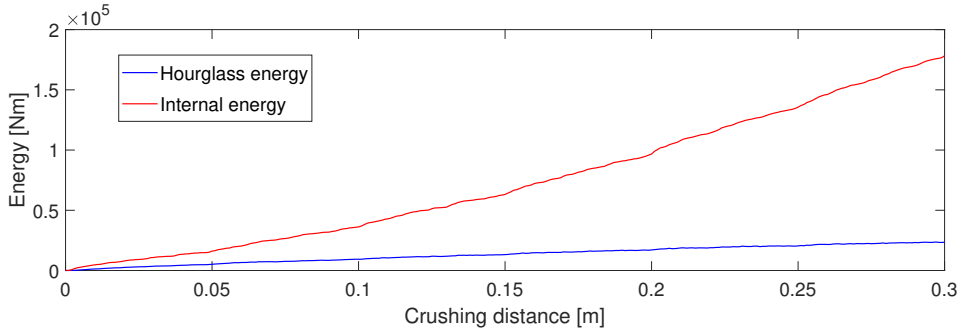

Figure 5.16: Hourglass energy in LS-DYNA.

5.3 Recommended Implementation of Intended Mathematical Operations

The various ice codes studied in this thesis have many similarities. However, they deviate on some areas and some implementations of the mathematical operations are deemed more suitable than others. With respect to the calculations of the equivalent plastic strains, it is recommended to use the flow rule. This is performed in all of the implementations, except for the one by Ferrari (2014) where the total strain increment from the Abaqus solver is used. The mathematical model proposes to use the associative flow rule, implying that the plastic strain increment shall be normal to the yield surface. In order to ensure this, it is necessary to adopt an iterative return algorithm (Krabbenhøft, 2002). Otherwise one cannot be certain to obtain a closed form solution due to the special yield surface used in modelling of ice. The cutting plane return algorithm is suitable in this manner. When the equivalent plastic strain is larger than the failure criteria proposed by Liu (2011), the elements are eroded from the analyses. In Abaqus, this involves that the material points are not removed from the analysis, but zero stresses and strain increments are passed in all deleted material points. This is found to be a suiting way to erode elements in the implementation as it is recommended by the Abaqus user manual. However, the effect deletion of one element has on adjacent elements is not fully investigated.

Both the code by Woongshik Nam and the newly implemented material model fulfil these recommendations. The code that will be used further is the one

developed in this thesis. Investigation of the implementation of the mathematical operations has not revealed any weaknesses in the newly implemented subroutine. However, it has shown some weaknesses during numerical analyses. The model does not seem to be stable when the cut-off pressure lay within the yield surface, which is the case with the ice constants proposed by Derradji-Aouat (2000). Hence, it is recommended to use ice material constants so the cut-off pressure problem is avoided. Another issue to keep in mind is the substantial amount of hourglass energy in the analyses and that it is found very difficult to find a method that reduces the amount of hourglass to acceptable values.

Chapter 6

Calibration of the New Implemented Material Model

6.1 Background

The newly implemented material model is subjected to calibration in this master thesis. This is performed in order to increase the confidence in the implementation so it can be used in design scenarios. The calibration is made against Polar Class 3 in the IACS code formulation (IACS, 2016).

The basis for the IACS Unified Requirements for Polar ships is the concept that ice loads can be linked with design scenarios. For plating and framing design, the basis of the ice loads is a glancing collision on the shoulders of the bow. The ship is assumed to have a design speed colliding into an angular ice edge. During impact, the ship penetrates the ice and rebounds away. In order to use this scenario for other hull regions than the bow and the stern of double-acting ships, loads are set as a proportion of the bow area by empirical hull area factors. In addition, bow loads are normalized by a standard set of bow angles since the loads on other hull areas are not strongly dependent on the bow angles. The load calculations are derived from the energy-based collision model where the kinetic energy is identical to the ice crushing energy. The calculations are in close agreement with several studies performed with numerical models, models tests and operational experience(Daley, 2000). Thus, the IACS code is deemed to be a good choice to calibrate against.

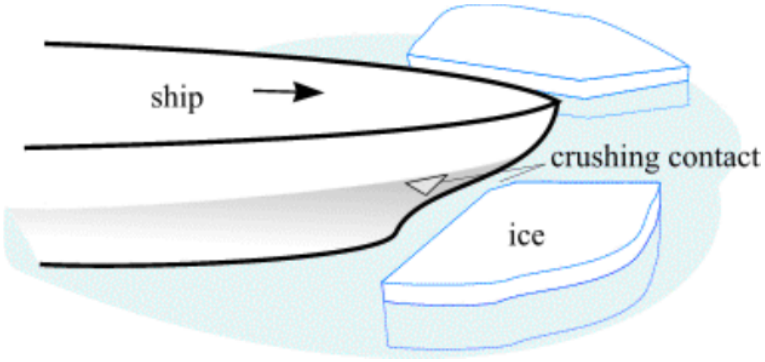

Figure 6.1: Glancing collision on shoulder of the bow (Daley, 2000).

The calibration is performed against the force-displacement curve instead of the pressure-area curve, which has been the most common approach in ISO 19906. The code specifies that ice actions shall include the total action on the structure applied over the nominal contact area(Global action) and the local actions that are applied on specific parts of the nominal contact area. The pressure distribution within the nominal contact area is not uniform. The ice at the boundaries may be broken off, reducing the actual contact area. Hence, the pressure distribution may vary quite a lot for larger ice features and local areas may experience high-pressure peaks. The local action shall, according to ISO (2007), be evaluated separately using local pressure peaks, which is relevant when the plastic deformations are small.

When large deformations are allowed, such as in the ALS, the same approach is not as straight forward. This is due to the resistance of the structure may be governed by the interface pressure. As a consequence of this, the ice will maintain its shape in areas of high pressure and the deformations will increase locally. However, at the same time, the contact area will expand and adjacent structural members will be activated to withstand the forces. Hence, in ALS design the global ice actions and the resistance to the total applied force are of most concern.

The calibration is performed with the same model setup as described in Chapter 5.2, where the nominal contact area is used to calculate the calibration curve. The average pressure area in IACS is found from the relation:

$$P = P_0 A^{ex} \tag{6.1}$$

where P is the average pressure, P_0 is the class dependent ice pressure, A is the nominal contact area and ex is the pressure area exponent. Polar class 3 are used in the calibration, meaning that $P_0 = 3.2MPa$. It is assumed that $ex = -0.1$. The force, F, to calibrate against is then formulated as:

$$F = PA = P_0 A^{-0.1} A = P_0 A^{0.9} \tag{6.2}$$

The nominal contact area is directly linked to the crushing distance. Since the ice model is formed as a half sphere, the formula for the radius of the nominal contact area, r, becomes:

$$x^2 + r^2 = R^2 \longrightarrow r = \sqrt{R^2 - x^2} \tag{6.3}$$

where R is the radius of the half sphere and x is the position of the contact area from the centre of the sphere. x is dependent on the crushing distance $x = R - d$. Combining this, the nominal contact area and the crushing distance is connected by Equation 6.4.

$$A = \pi r^2 = \pi(R^2 - x^2) = \pi(R^2 - (R - d)^2) = \pi(2Rd - d^2) \tag{6.4}$$

6.2 Calibration with the Failure Criterion

The calibration is performed by using the default hourglass control in Abaqus(relax stiffness with a scaling factor of 1.0). Initially, only the failure criterion is adjusted by the initial failure strain, ϵ_0, and the constants M and N in Equation 6.7. With $M = 1.0$ and $N = 0.5$, this is the same failure criteria as in Equation 4.7. The ice constants proposed by Kierkegaard (1993) are used in this section. The calibration method is similar to the calibration performed by Kim (2014) in her PhD thesis.

$$\epsilon_f = \epsilon_0 + (\frac{p}{Mp_2} - \frac{N}{M})^2 \tag{6.5}$$

The constants affect the failure criteria in different ways. ϵ_0 shifts the failure curve vertically, M decides how narrow or wide the curve is, while N shifts the curve in the horizontal direction.

6.2.1 Effect of the Initial Failure Strain, ϵ_0

The initial parameter that is changed in order to calibrate the implementation against Polar class 3 is the initial failure strain. In Table 6.1 the values of ϵ_0 that are tested is listed and the corresponding failure curves can be seen in Figure 6.2.

Table 6.1: Calibration analyses with adjusting ϵ_0.

Run	ϵ_0 [-]	**M [-]**	**N [-]**
1	0.010	1.00	0.50
2	0.020	1.00	0.50
3	0.050	1.00	0.50
4	0.070	1.00	0.50
5	0.075	1.00	0.50

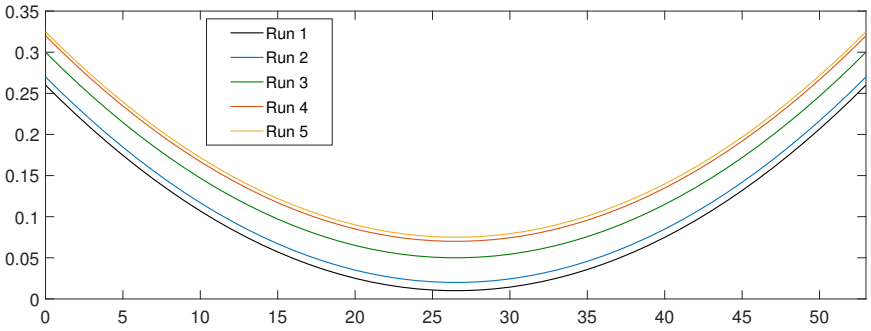

Figure 6.2: Failure curves for the calibration runs by adjusting ϵ_0.

In Figure 6.3 the reaction forces to the corresponding change of ϵ_0 are displayed. The blue curve represents the IACS PC3 that is desirable to duplicate in the numerical analyses. As expected, the force levels increase as the initial failure strain is increased. However, so does the oscillations. Run 1 and 2 clearly yield to low forces and are not sufficient. Run 3 is rather close to PC3 and has some peaks that are very high, but the mean value of the curve is lower than PC3. Run 4 and 5 are slightly above the calibration curve and could be used as a conservative parameter. This set of failure criteria parameters result in force oscillation with very large peaks, which is not desirable.

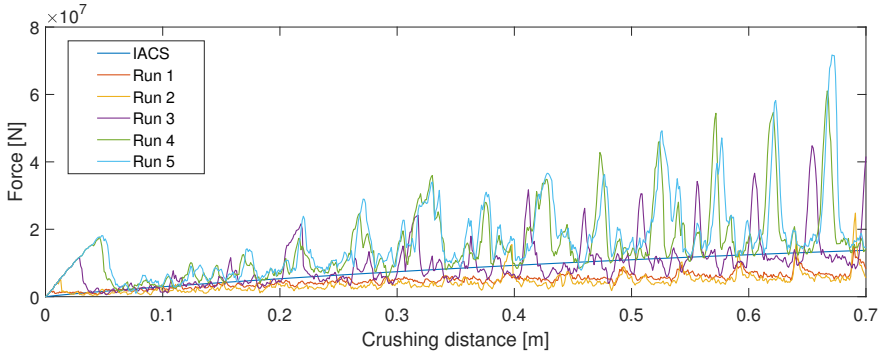

Figure 6.3: Reaction forces in the calibration runs by adjusting ϵ_0.

6.2.2 Effect of Changing the Constants M and N in the Failure Criterion.

Table 6.2: Calibration analyses by adjusting the constants M and N in the failure criteria.

Run	ϵ_0 [-]	M [-]	N [-]
1	0.010	0.60	0.50
2	0.010	0.75	0.50
3	0.010	1.00	0.60
4	0.010	1.00	0.75

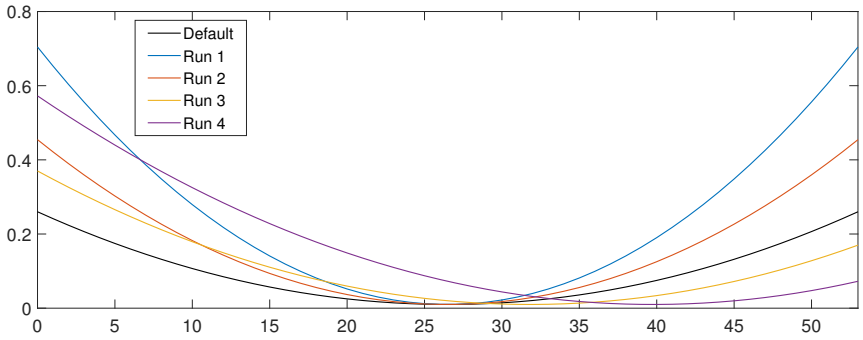

Figure 6.4: Failure curves for the calibration runs by adjusting either the M or N constant in the failure criteria.

In an attempt to reduce the peaks in the force oscillations, the implementation is tested with various values of the M and N constants in the failure criteria. Two runs are tested by decreasing the value of M, Run 1 and 2, which narrows the failure curve. This does not affect the force particularly and it is observed from Figure 6.5 that this is to low compared to PC3. A possible explanation for this may be that much of the erosion occurs around a hydrostatic pressure value of 20-25 MPa, and in this area, the failure criteria for the forces Run 1 and 2 are very similar to the original failure criteria. This can be seen in Figure 6.4. In Run 3 and 4, the value of the N-constant is decreased. This shifts the failure curve to the right. Run 3 yield similar results as Run 1 and 2 and this might be explained in the same manner. However, when N is increased to 0.75(Run 4), the forces increase quite a lot. Now the failure curve has a larger value than the original criteria until the hydrostatic pressure is about 32 MPa, which in reality might be rarely reached. Run 4 oscillates around a mean value corresponding approximately to PC3. Hence, this set of parameters may be a reasonable choice. The force oscillations are present, but they are less severe than when the initial failure strain is increased.

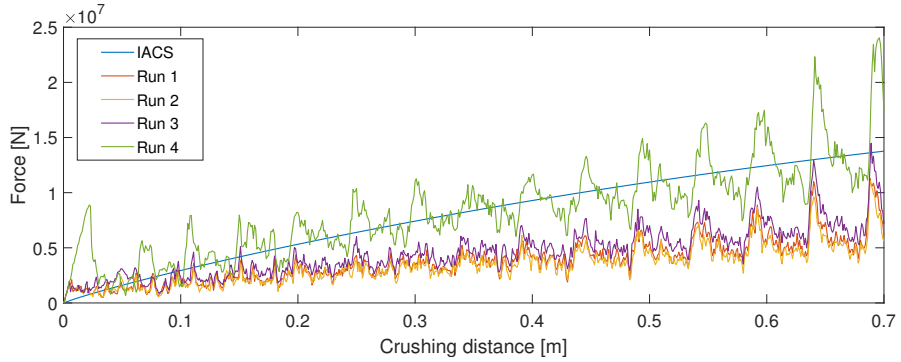

Figure 6.5: Reaction forces in the calibration runs by adjusting either the M or N constant in the failure criteria.

In Figure 6.6 the hydrostatic pressure is plotted in the sphere in Run 4 just before erosion. From this figure, one see that the high-pressure zone the hydrostatic pressure is around 25 MPa. Thus, it might explain that Run 4 yields higher forces since it allows larger equivalent plastic strains before erosion at this pressure level.

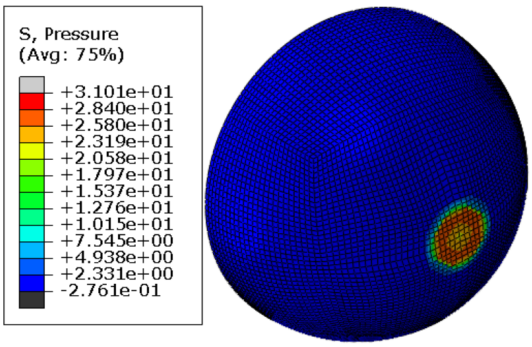

Figure 6.6: Hydrostatic pressure plot right before erosion in Run 4.

6.2.3 Calibration by Changing Two Parameters Simultaneously.

Table 6.3: Calibration analyses by changing two constants simultaneously.

Run	ϵ_0 [-]	**M [-]**	**N [-]**
1	0.050	1.00	0.60
2	0.050	1.25	0.50
3	0.010	2.00	0.90
4	0.010	2.00	1.00

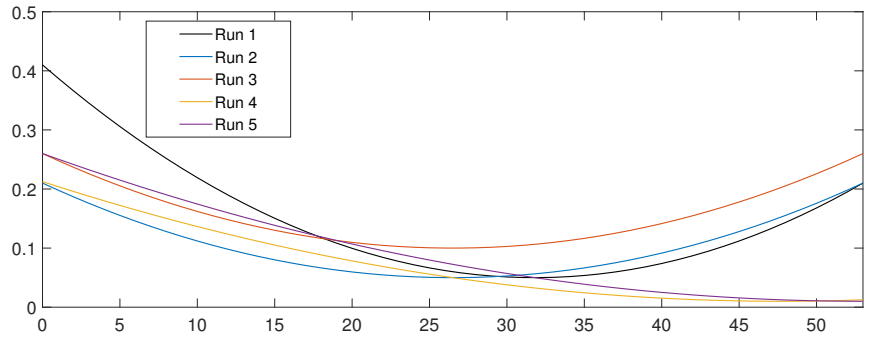

Figure 6.7: Failure curves for the calibration runs by adjusting two parameters simultaneously.

The effect of varying two parameters in the failure criteria simultaneously is also investigated briefly. The tested parameter combination are in Table 6.3 and the corresponding failure curves and forces are in Figure 6.7 and Figure 6.8. These parameters combinations are selected on the basis of the failure criteria and especially for the value of the failure curve at around 20-30 MPa. The runs are able to have a mean value pretty close to the IACS PC3 curve. However, none of the runs are able to minimize the force peaks any more than Run 4 in Table 6.2.

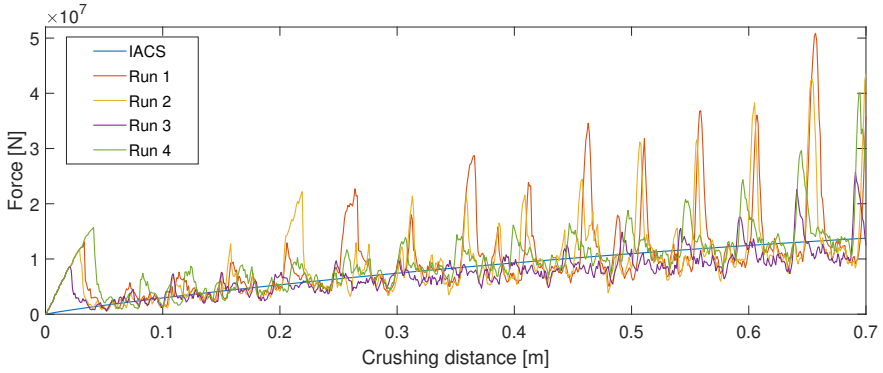

Figure 6.8: Reaction forces in the calibration runs by adjusting two parameters simultaneously.

6.3 Calibration by Adjusting the Yield Surface

An alternative method to calibrate against IACS Polar class 3 is also tested. This method is to adjust the yield surface by the ice material constants, a_0, a_1 and a_2. To do this efficiently, the ice material constants proposed by Kierkegaard (1993) are used as a basis. The proposed ice material constants are applied a factor, k, to

be able to change the radius in the Tsai-Wu yield surface, see Table 6.4, Figure 6.9 and Equation 6.6. This makes it possible to keep the same roots in the yield function as with the original constants. Hence, the failure criterion is unaffected since it only depends on the second root of the yield function. In addition, the issue with the cut-off pressure is avoided since it is located outside the yield surface.

$$f(p, J_2) = J_2 - k(a_0 + a_1 p + a_2 p^2) \tag{6.6}$$

Table 6.4: Calibration analyses by adjusting the yield surface.

k	a_0 $[MPa^2]$	a_1 $[MPa]$	a_2 **[-]**
1.0	2.588	8.630	-0.163
1.5	3.882	12.945	-0.245
2.0	5.176	17.260	-0.326

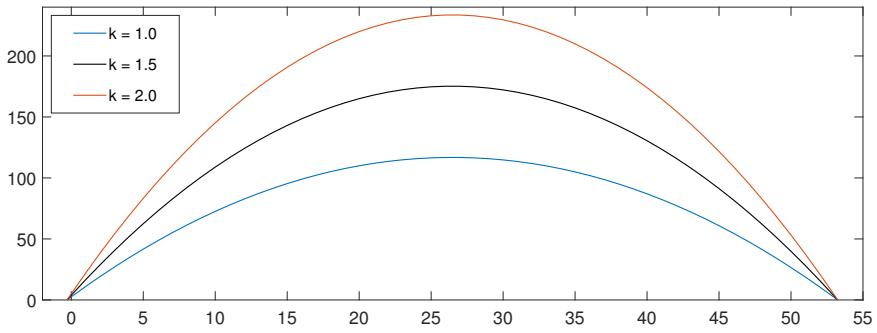

Figure 6.9: Yield surfaces used in calibration.

The results from the yield surface calibration approach are displayed in Figure 6.10. This shows that the method is rather unsuccessful. The increased radius of the yield surface has little to no effect, even though the radius is doubled. In fact, the initial ice material constants give a slightly higher mean force. When the radius is increased, the mean force is not increased, but the peaks are much more significant. This is the opposite of what is desirable. Hence, this calibration method is not be pursued any further.

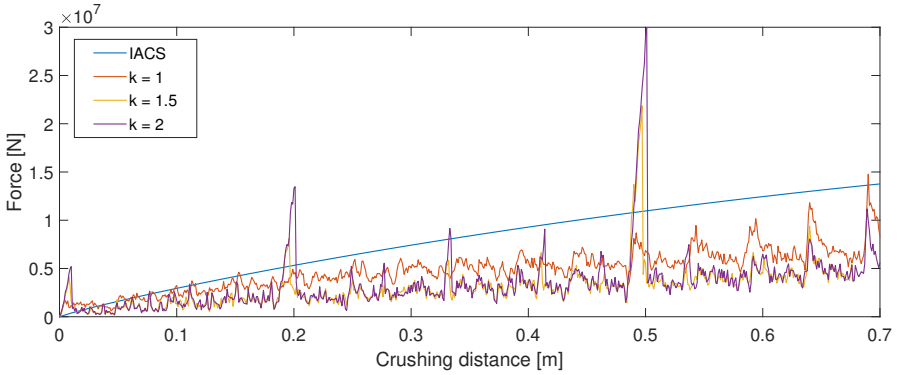

Figure 6.10: Reaction force versus displacement for the calibration runs by adjusting the yield surface.

6.4 Recommended Calibration Parameters

By evaluating the results from the calibration analyses in this chapter, the most reasonable approach to calibrate the material model implemented in this thesis is to manipulate the parameters of the failure criterion. Further, the set of parameters that yield the most promising results are from Run 4 in Table 6.2, which results in the failure criterion in Equation 6.7. These parameters are able to simulate a similar force-displacement curve as IACS PC3. In addition, the force peaks are less significant in this run than in other possible candidates. Figure 6.11 shows the internal energy with the new failure criterin(corresponding to Run 4 in Table 6.2) and the desired energy from PC3. The red curve is a little conservative at the beginning and unconservative towards the end. Still, the energy levels are very close and the new failure criterion is deemed satisfactory in terms of simulating the Polar Class 3 in IACS. Hence, the parameters in Run 4 in Table 6.2 will be used in further analyses in this thesis.

$$\epsilon_f = 0.01 + (\frac{p}{p_2} - 0.75)^2 \tag{6.7}$$

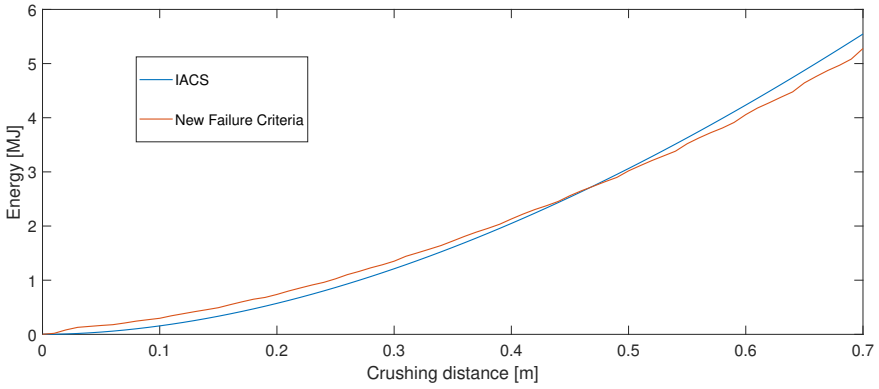

Figure 6.11: Energy comparison between IACS PC3 and numerical analysis with the new failure criterion.

Chapter 7

Integrated Analysis of Iceberg-Structure Impact Interaction

7.1 Background

The Petroleum Safety Authority Norway (Petroleumstilsynet) initiated several studies to increase the insight into the potential impact between glacial ice and offshore structures and how it may threaten structural integrity. The ST19 report by Lu et al. (2018) is one of these studies. In this study, the impact interaction between glacial ice of spheroidal shape with a semi-submersible structure is analysed by the means of non-linear finite element analyses in LS-DYNA. In this chapter, the material model implementation developed is tested in similar analyses and the results are compared across the two studies. The analyses in this thesis are performed in Abaqus.

In the ST19 report by Lu et al. (2018), the shared-energy approach used for ship impacts according to NORSOK N-004 Appendix A (NORSOK, 2017) is adopted. The approach is illustrated in Figure 7.1. In the current problem, the ship in the figure represents the glacial ice. The curve for the iceberg(leftmost curve) is developed by assuming the semi-submersible(installation) is rigid. Similarly, the force-displacement curve for the semi-submersible is established by assuming the iceberg to be rigid. The combined resulting damage of the iceberg and the structure is found when the combined energy dissipation of the two bodies is equal to the required energy dissipation found by external mechanics. The approach disregards the coupled interaction effect from iceberg-structure impact. The method is adopted in the ST19 report since coupled analysis with a continuum mechanics model of glacial ice was found to be associated with too many uncertainties.

In this thesis, two shared-energy design approaches are utilized. Both the approach in NORSOK N-004 and integrated analysis with the newly

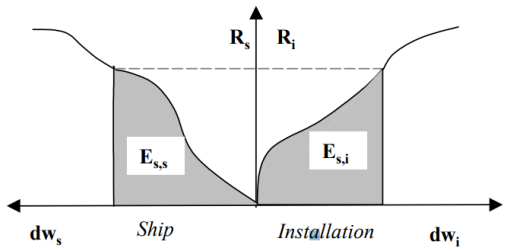

Figure A.3-3 Dissipation of strain energy in ship and platform

Figure 7.1: Strain energy dissipation in ship and platform from NORSOK (2017). In the current case, the ship represents the iceberg.

implemented material model are performed. The latter involves that both the semi-submersible and the and the glacial ice will consist of deformable bodies. The model setup is as identical as possible as the model used in the ST19 report by Lu et al. (2018). These results from both shared-energy design approaches are compared with each other and the results from the ST19 report by (Lu et al., 2018), which is performed in LS-DYNA.

7.2 Model Description

7.2.1 Modelled Bodies

The model of the semi-submersible column used in the ST19 report (Lu et al., 2018) is developed at NTNU. This model is converted from LS-DYNA to Abaqus to make sure that the analyses are comparable across the FE solvers. Only half the column is modelled. Some problems arose during the conversion of the model as some 4-node elements collapsed into triangular elements, causing problems with the surface normal. The problem was solved by dragging the nodes with the "edit mesh" tool in Abaqus. The dimensions of the FE-model is 17.2x31.875x6.1 m(width x height x depth). The FE-model of the column is shown in Figure 7.2. The vertical stiffeners are modelled as 320x50x40x12 mm, 320x50x50x11 mm and 240x40x30x10 mm L-bars. The thickness of the outer plating varies between 16-18 mm. The mesh size in the model is approximately 120 mm and the mesh consists of S4R elements. S4R is a 4-node general-purpose shell with reduced integration and finite membrane strains.

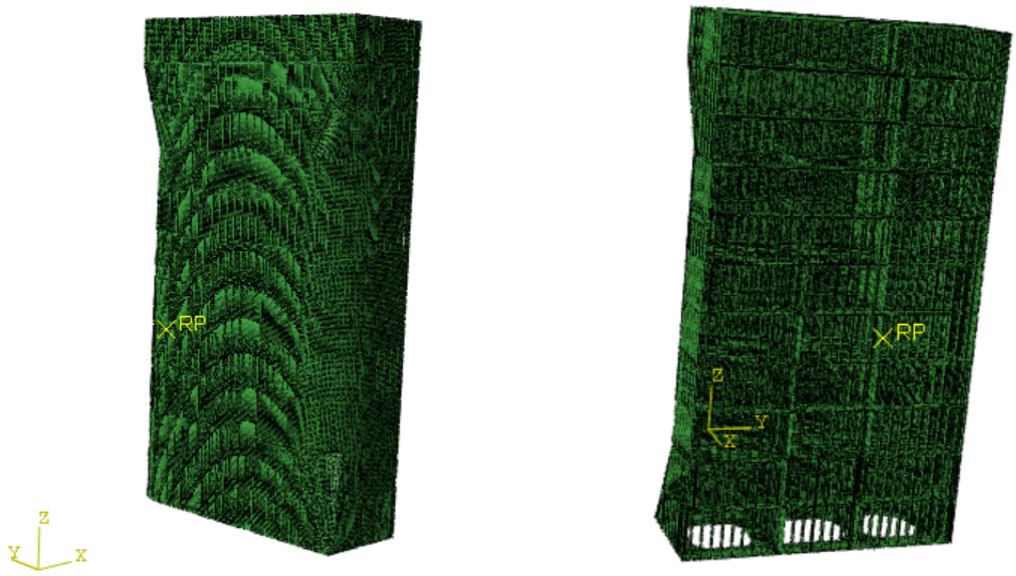

(a) Front (b) Back

Figure 7.2: FE-model of the semi-submersible column.

The iceberg is modelled as a spheroid with a long axis of 15 m and a short axis of 10.4 m. Only one-quarter of the iceberg is modelled due to computational efficiency. The meshed glacial ice feature is displayed in Figure 7.3. A mesh size of 100 mm is applied. This is not the same mesh size which was used in the calibration of the ice material model implementation. It would be optimal to use the same mesh size, but it is chosen to use 100 mm due to limited computational capacity. The iceberg consists of solid cubic C3D8R elements.

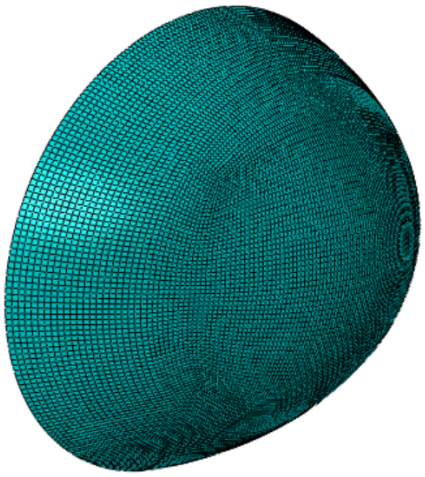

Figure 7.3: Modelled quarter-spheroidal ice model.

7.2.2 Material and Fracture Modelling of the Steel Column

The material modelling in ST19 of the steel column is performed by applying a Holloman-type power law hardening with a yield plateau. The fracture criterion used is the Bressan-William-Hill(BWH) instability criterion and the material behaviour is handled by an implemented subroutine in LS-DYNA. A corresponding subroutine for Abaqus is not available. Hence, this modelling will not be further described here. Instead DNV GL RP-C208 (DNV-GL, 2016) is used to model the material and fracture properties of the steel column. The stress-strain curve consists of three parts, as shown in Figure 7.4. Part 1, 2 and 3 are obtained by applying the plastic strain and corresponding yield stress. These values are found from tables in DNV GL RP-C208. Part 4 represents the power law hardening. This is implemented piece-wise by using Equation 7.1. The parameters are dependent on both the steel grade and the thickness. In the studies in this thesis steel grades S355 and S420 are used, as listed in Table 7.1.

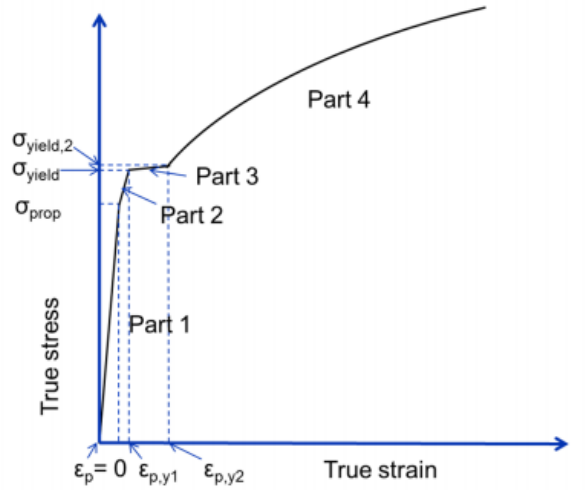

Figure 7.4: Stress strain curve from DNV GL RP-C208.

$$\sigma = K(\epsilon_p + (\frac{\sigma_{yield,2}}{K})^{\frac{1}{n}} - \epsilon_{p,y2})^n, \qquad \epsilon_p > \epsilon_{p,y2} \tag{7.1}$$

Table 7.1: Characteristic material properties of the steel column from DNV GL RP-C208.

	S355		**S420**	
Thickness [mm]	**t $\leq$ 16**	**16 < t $\leq$ 40**	**t $\leq$ 16**	**16 < t $\leq$ 40**
E [MPa]	2060000	206000	206000	206000
Poisson Ratio	0.3	0.3	0.3	0.3
σ_{prop} **[MPa]**	320.0	311.0	378.7	360.6
σ_{yield} **[MPa]**	357.0	346.9	422.5	402.4
$\sigma_{yield,2}$ **[MPa]**	366.1	355.9	426.3	406
$\epsilon_{p,y1}$	0.004	0.004	0.004	0.004
$\epsilon_{p,y1}$	0.015	0.015	0.012	0.012
K [MPa]	740	740	738	703
n	0.166	0.166	0.14	0.14
Density $[kg/m^3]$	7850	7850	7850	7850

For the material failure modelling, the ductile damage and damage evolution options in Abaqus are used. The fracture criteria adopted is based on 1^{st} principle strain. The ductile damage option assumes that the equivalent strain is a function of stress triaxiality. The critical fracture strain is dependent on the mesh size, plate thickness and material quality. It should be noted that the ST19 report (Lu et al., 2018) argues that the fracture criterion in DNV-GL-RP-C208 is overly conservative. The argumentation is based on experimental data from stiffened panel indentations tests (Alsos and Amdahl, 2009). The results show that the DNV-GL-RP-C208 predicts too early fracture. In Figure 7.5 the failure criterion is plotted in terms of fracture strain and stress triaxiality for S355 steel with a thickness of 10 mm for both characteristic and mean values.

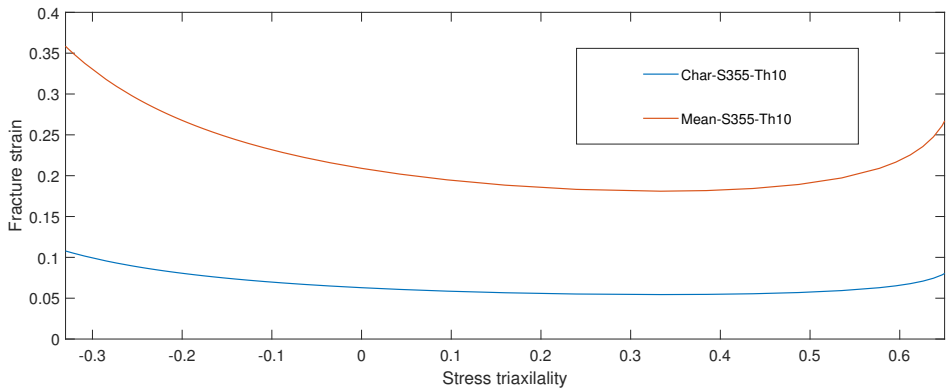

Figure 7.5: Fracture criterion plotted with respect to Fracture strain versus Stress triaxiality.

7.2.3 Setup

Contact

The interaction is modelled by the general contact options. The contact domain is the spheroidal glacial ice, both internal and exterior elements, with the column. Self contact is applied for both the column and the glacial ice. For all contact, the penalty formulation is applied with a friction coefficient of 0.15.

Load and Boundary Conditions

In this quasi-static analysis, the glacial ice represents the load. It is applied a constant velocity of 3 m/s in a straight horizontal direction against the platform column. The velocity is applied with a smooth step in the beginning of the analysis to avoid any significant dynamic effects. The column is held fixed in all degrees of freedom at the back, top and bottom of the structure.

Impact Scenarios

There is many potential areas where the glacial ice might strike the semi-submersible column. The potential areas are dependent on the size and draft of the platform, but also relative motions between the ice and the structure caused by waves. The ST19 report (Lu et al., 2018) included a probabilistic analysis of motions in waves which determined that the potential impact area range from 5.5 m above the waterline to 10 m below the waterline. Based on this probabilistic analysis, it is selected a set of representative impact locations, including column corner, column bulkhead and stiffened panels of the column front. In this thesis, it is chosen to do impact simulation with two different scenarios. The first scenario is that the glacial ice hits the column corner at a stiffened deck at the waterline, i.e. at point (a) in Figure 7.6. The second scenario is that the ice impacts at the cruciform of the stiffened deck at the waterline and a bulkhead, i.e. Point (e) in Figure 7.6.

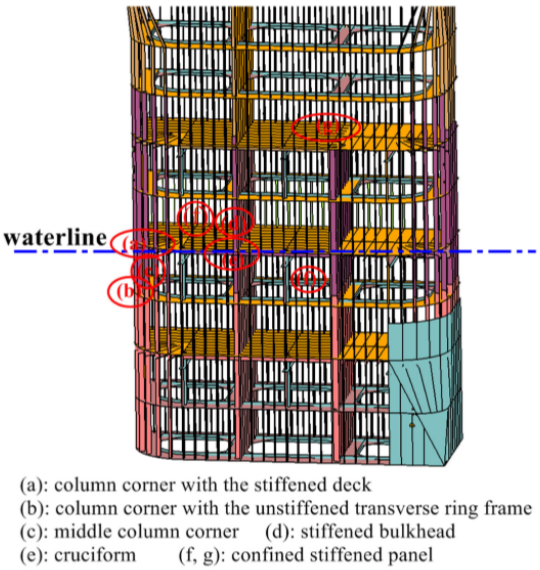

Figure 7.6: Impact location in the ST19 report (Lu et al., 2018).

7.3 Integrated Analysis with the NORSOK N-004 Shared-Energy Design Approach

The impact interaction scenarios are analysed with the shared-energy approach in NORSOK N-004 in this section. That is, the energy dissipation of the bodies included in the impact are studied separately and the coupled effects are disregarded.

7.3.1 Impact Scenario 1 - Column Corner at the Stiffened Deck

The first scenario investigated is the impact between the glacial ice and the stiffened deck at the column corner at waterline level.

Rigid Glacial Ice Analysis

Initially, impact analyses with a rigid iceberg is run. In other words, the iceberg is modelled as a rigid body crushing against the deformable column. This corresponds to the NORSOK N-004 approach to find the force-deformation curve and energy dissipation of the installation. The model is run with both characteristic and mean values from DNVGL-RP-C208 for the material and fracture modelling. The former is considered to be the most conservative choice.

In Figure 7.7 the reaction force is plotted versus the crushing distance. The initial bending stiffness is slightly above 10 MN. At Point 1 in Figure 7.7 the two curves have a change in slope and separate from each other. The curve with characteristic material properties has a drop at this point, while the "Mean" curve continues to increase. For both cases, the stiffened deck and frame buckles, see Figure 7.8a. However, it seems as the frame is loaded to its limit in the analysis with the characteristic value and looses some of it's bearing capacity. Hence, this might explain the separation of the curves at this point. At Point 2 the fracture in the outer plating initiates for characteristic values, see Figure 7.8b. This occur at an indentation of 0.6 m and it is present in the force-displacement plot in the form of a drop in the blue curve. It is noteworthy that the capacity is still considerable after the initiation of the fracture. At Point 3 in Figure 7.7 the outer shell rupture initiates with the mean steel material properties, see Figure 7.8c. It occurs at an indentation of around 1.7 m., i.e. after a much larger indentation than for characteristic values, which shows that the energy dissipation and behaviour of the structure is very dependent on the chosen material and failure modelling of the column.

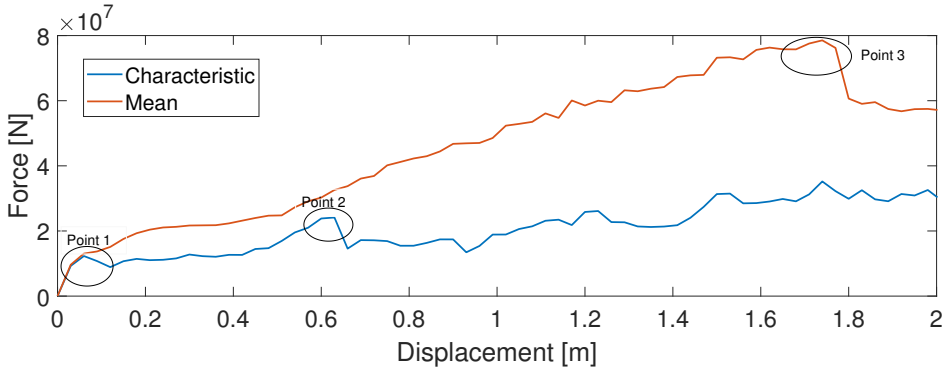

Figure 7.7: Rigid ice crushing resistance versus crushing characteristic and mean values from DNVGL-RP-C208. Impact scenario 1.

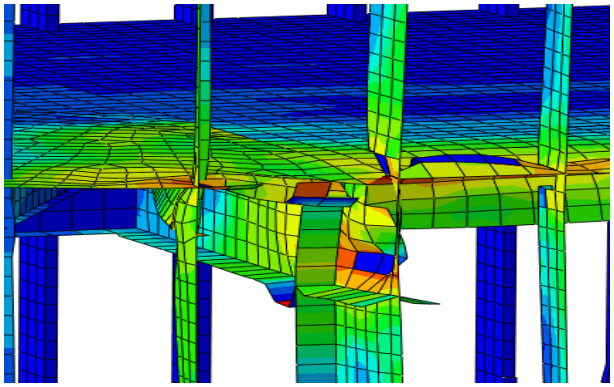

(a) Point 1 in Figure 7.7. Front view with outer plating removed. Characteristic material values.

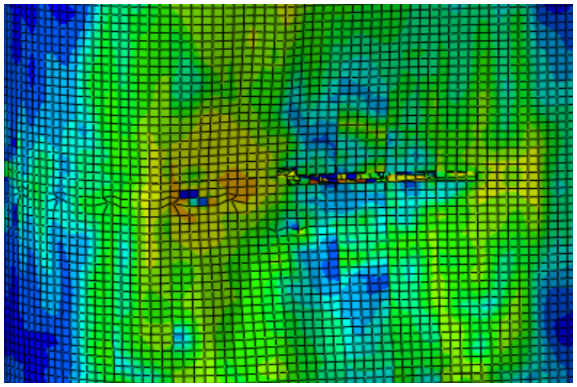

(b) Point 2 in Figure 7.7. View of the outer plating in the impacted area with characteristic material values.

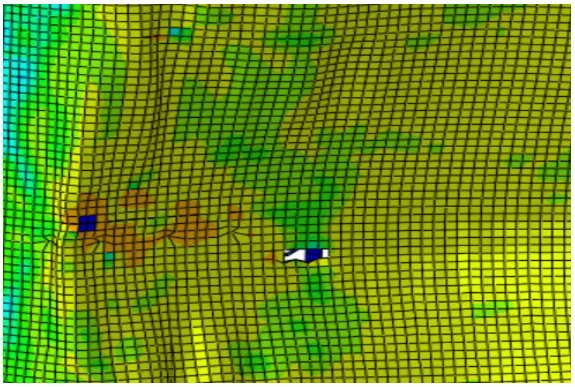

(c) Point 3 in Figure 7.7. View of the outer plating in the impacted area with mean material values.

Figure 7.8: Snapshots of distinctive points in Figure 7.7. Impact scenario 1.

Rigid Structure Analysis

In order to find the force-deformation curve and energy dissipation for the iceberg in the NORSOK N-004 shared-energy design approach, an analysis with deformable ice and rigid structure is run. Figure 7.9 shows the deformation and erosion in the iceberg as it is crushed against the rigid semi-submersible column. It shows an ordered deformation around the corner of the rigid column. The effect of the column corner geometry is clearly visible in the deformation plot as only about half of the iceberg hits the structure. The resulting reaction forces are plotted to the left(blue curve) in Figure 7.10. The initial peak of the force-displacement curve is quite large, about 30 MN. This indicates that the resistance in the structure must be large before the iceberg starts to dissipate a considerably amount of energy.

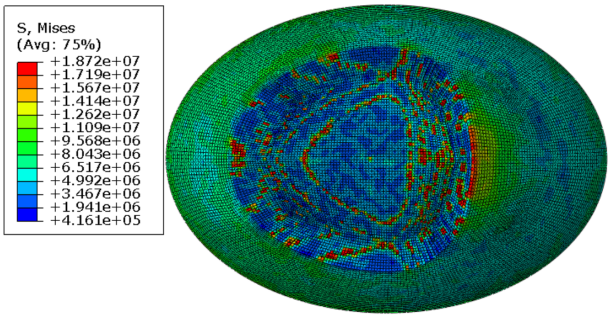

Figure 7.9: Deformation of the iceberg in the rigid structure analysis of impact scenario 1.

Ice-Structure Impact Resistance

In Figure 7.10 the force-displacement curves from the rigid ice and rigid structure analyses are plotted together. In the ST19 report (Lu et al., 2018) it is found that an energy dissipation of 7.5 MJ is critical. If 7.5 MJ are to be dissipated in this impact scenario, the structure must dissipate almost all of the energy. At a force of 20 MN the structure is displaced 0.55 m and it dissipates 7.5 MJ. At the same time, the glacial ice doesn't dissipate any significant amount of energy. The dotted red line represents the energy dissipation of the two involved bodies.

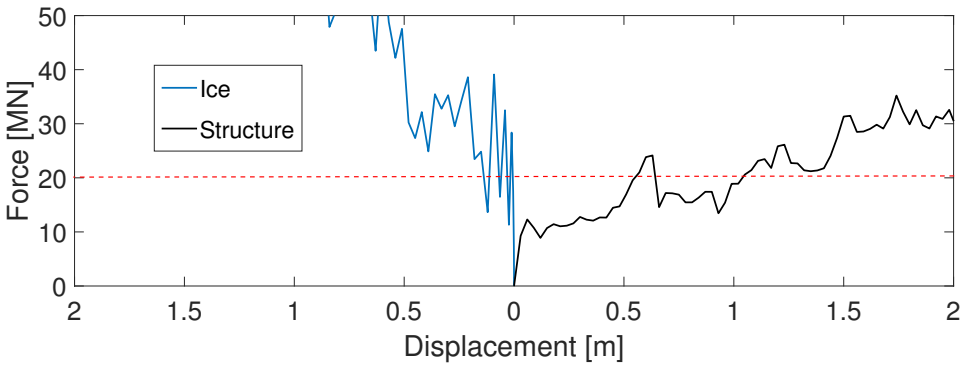

Figure 7.10: The ice-structure impact resistance of impact scenario 1 with the NORSOK approach.

7.3.2 Impact scenario 2 - Intersection of Stiffened Deck and Bulkhead

The impact scenario of the glacial hitting the cruciform of a stiffened deck and a bulkhead(impact location (e) in Figure 7.6) is the second scenario that is

investigated in this thesis.

Rigid Glacial Ice Analysis

A rigid iceberg analysis is run against the deformable column to find the force-deformation curve and energy dissipation for the structure in the NORSOK N-004 approach. The analysis is only run with characteristic material values.

Figure 7.11 shows the resulting force-displacement curve with distinctive points. Point 1 shows that the structure has an initial bending capacity of 25 MN. This is considerably larger than in impact scenario 1, which is to expect due to the direct contribution of the bulkhead. Succeeding this point, the stiffened deck starts to buckle, as Figure 7.12a shows. At point 2 the outer plating fractures at the unstiffened ring frame below the waterline(Figure 7.12b). It is worth to mention that the structure has a significant capacity also past this point.

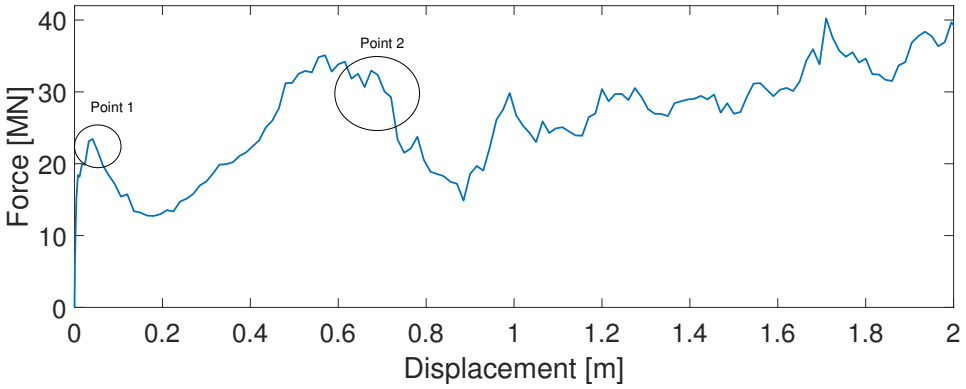

Figure 7.11: Crushing resistance column subjected to rigid ice impact. Impact scenario 2.

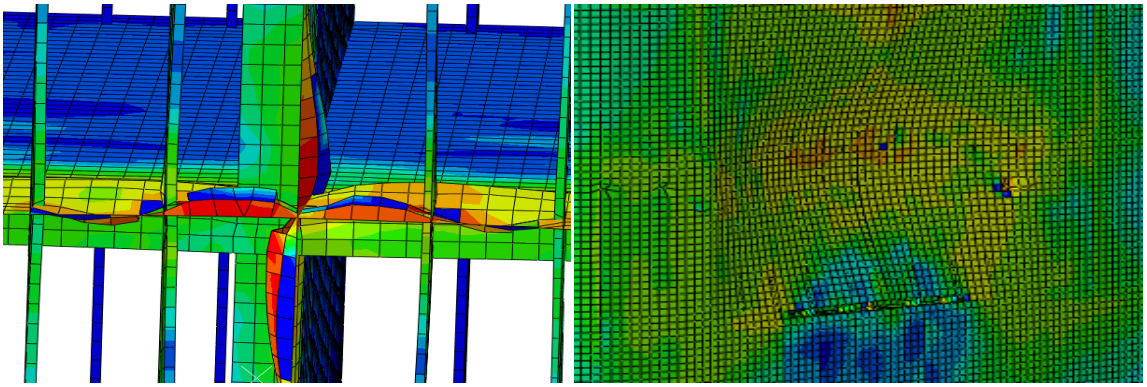

(a) Point 1 in Figure 7.11. Front view with the outer plating removed.

(b) Point 2 in Figure 7.11. View of the outer plating in the impacted area.

Figure 7.12: Snapshots of distinctive points in Figure 7.11. Impact scenario 2.

Rigid Structure Analysis

The force-displacement curve for the glacial ice in the NORSOK-004 approach is found by running analysis with deformable ice and rigid structure. Figure 7.13 shows the deformation and the erosion of the iceberg as it is crushed against the rigid wall of the semi-submersible column. The impact resistance is plotted on the left side in Figure 7.14(blue curve).

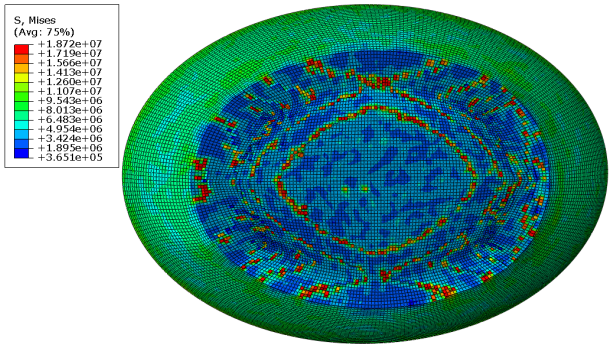

Figure 7.13: Deformation of the iceberg in the rigid structure analysis of impact scenario 2.

Ice-Structure Impact Resistance

The ice-structure impact resistance for impact scenario 2 in the NORSOK N-004 approach is plotted in Figure 7.14. The red dotted line represents the critical energy dissipation found by the Lu et al. (2018)(7.5 MJ). Even though the impact resistance is larger in this scenario, it is not large enough to crush the glacial ice

substantially. Hence, the structure must dissipate the main part of the energy. With an energy dissipation of 7.5 MJ, the structure displaces 0.43 m.

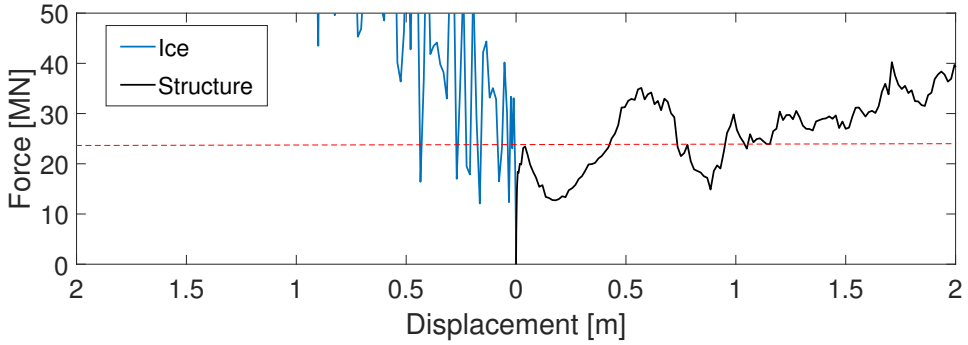

Figure 7.14: The ice-structure impact resistance in impact scenario 2 with the NORSOK approach.

7.4 Coupled Shared-Energy Design Approach

The coupled analysis is performed with the newly implemented material model and the failure criterion emerged from the calibration, i.e. Equation 6.7. The main purpose of this is to see the coupling effect when both the glacial ice and the semi-submersible column are modelled as deformable bodies. Appendix C contains additional plots of the coupled analyses.

7.4.1 Impact Scenario 1 - Column Corner at the Stiffened Deck

Figure 7.15 shows the reaction force versus the crushing distance of the coupled analysis with both characteristic and mean properties of the steel material in the column. Additionally, an analysis is performed by increasing the characteristic stress-strain curve by 25 %. That is, only the stress-strain curve is multiplied with a factor of 1.25, neither the failure modelling or other properties are manipulated. The analysis is performed to see how sensitive the erosion of the ice-elements is to the increase of the stress-strain curve. As Figure 7.15 shows, it has a minor effect; the blue(characteristic) and yellow(characteristic x 1.25) curve are almost identically. However, with mean material properties, the crushing resistance is larger and clearly distinct from the other analyses as the crushing distance increases. This indicates that fracture modelling is a very important aspect of the coupled analysis.

Until Point 1 in Figure 7.15, the force increases rapidly without any significant deformations in all the coupled analyses. This proceeds until the reaction force is about 20 MN, which can be interpreted as the initial bending capacity of the structure. Beyond this point, the force level drops a bit and keeps a more or less constant magnitude. In Figure 7.16a a snapshot inside the column right after Point 1 is displayed. This show that the frame and the associated plating starts to buckle. It may explain the sudden change of the slope of the force-displacement curve at Point 1.

At Point 2 in Figure 7.15 the curves takes separate paths. The slope of the red curve(mean) is considerably higher than the other curves. This can be explained by looking at Figure 7.16b, which is a snapshot of the outer plating of the column in the impacted area at Point 2 in Figure 7.15. It shows that initiation of outer shell rupture at the stiffened deck is occurring at this point. This is valid for both the blue and yellow curve. The figure enlightens the differences in the behaviour of the curves. However, the rupture may not be critical for the capacity of the structure as the force doesn't drop dramatically, but rather continues at a constant level. At Point 3 in Figure 7.15 the analysis with mean material properties experience a drop in force. At this point the outer shell fracture, as seen in Figure 7.16c. Although, this does not take place in the same area as for the other analyses, but rather takes place at the unstiffened ring frame below the waterline. It is noteworthy that at this point the contact area is large and the spheroidal iceberg is in contact with the ring frame.

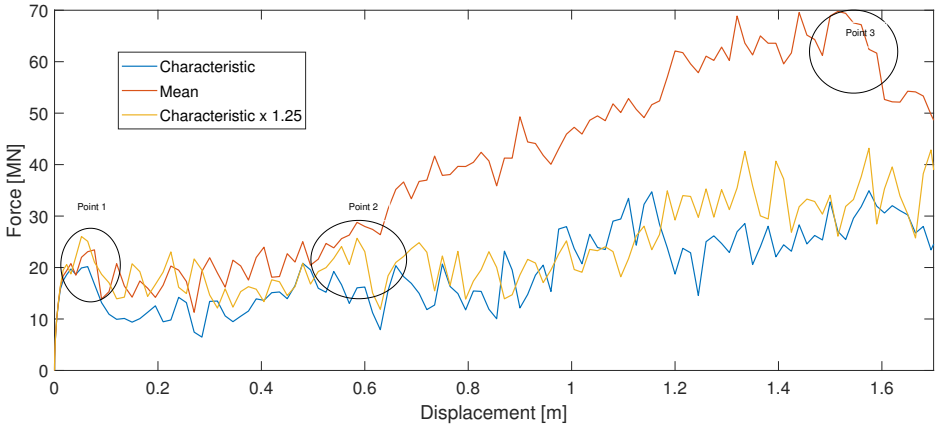

Figure 7.15: Coupled analysis of scenario 1. Crushing resistance versus crushing characteristic, characteristic x 1.25 and mean values from DNVGL-RP-C208. Impact scenario 1.

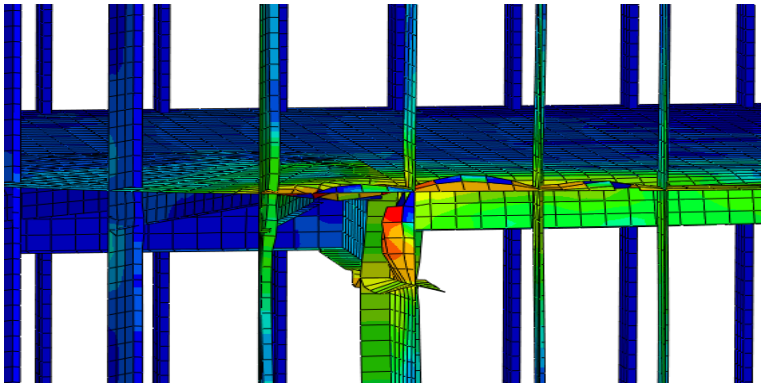

(a) Point 1 in Figure 7.15. Front view with the plating removed. Characteristic material values.

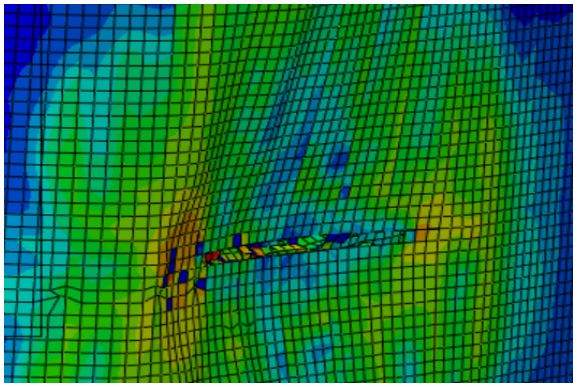

(b) Point 2 in Figure 7.15. View of the outer plating in the impacted area with characteristic material values.

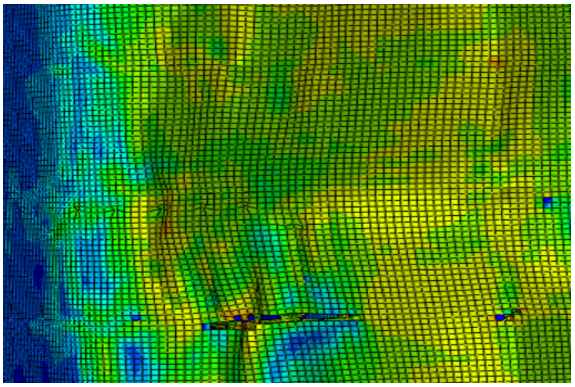

(c) Point 3 in Figure 7.15. View of the outer plating in the impacted area with mean material values.

Figure 7.16: Snapshots of distinctive points in Figure 7.15. Impact scenario 1.

Figure 7.17 shows the deformation of the spheroidal glacial ice in all the three of the coupled analyses at an indentation of 1.5 m. The damage on the ice is rather small in all analyses. There is some erosion towards the left of the figures, which is where the ice hits a bulkhead in the column. The erosion is especially present in the analysis with characteristic material values and the analysis with increased characteristic stress-strain curve, i.e. Figure 7.17a and Figure 7.17c. This is a little surprising since the mean steel properties are less conservative and yield the highest forces and resistance. Thus, one could expect that the column would be able to crush the glacial ice even more than with characteristic values. On the other hand, one plausible explanation of this behaviour is that the steel is more ductile with mean values and is able to handle larger deformations before fracture. It can then, at least to a larger extent, fold around the iceberg causing a pressure that increases the confinement of the ice. Hence, the strength of the glacial ice increases and the erosion is less present.

Another probable explanation of the lack of deformation and erosion in the glacial ice might be that the initial peak that emerges when the failure criterion is adjusted(Run 4 in Figure 6.4) is never surpassed. Hence, the spheroidal glacial ice might not get around to start the erosion properly.

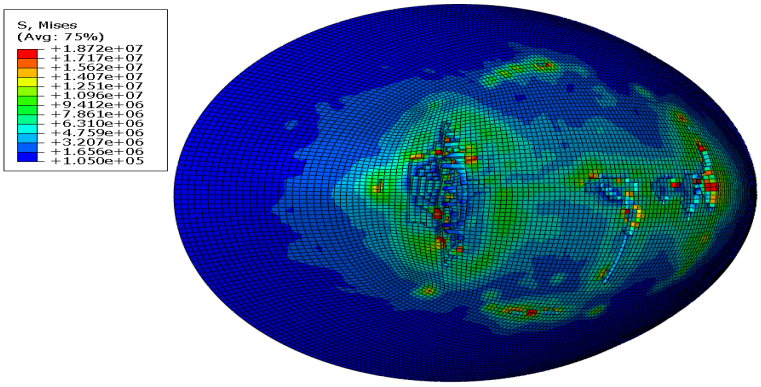

(a) Characteristic steel properties.

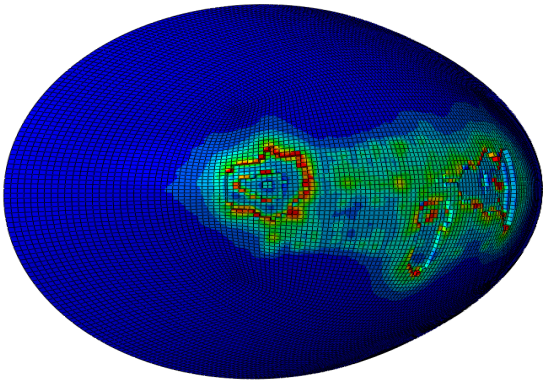

(b) Mean steel properties.

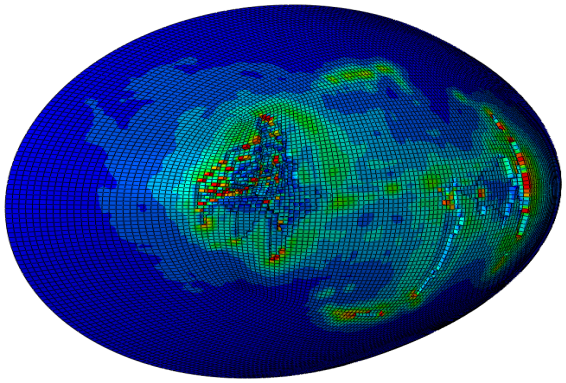

(c) Characteristic x 1.25 steel properties.

Figure 7.17: Deformation of the glacial ice at an indentation of 1.5 m.

Energy Dispersion

The energy in the coupled analysis is dissipated by both the structure and the iceberg. As Figure 7.18 shows, the energy is mainly dissipated by the structure in the coupled analysis with characteristic material properties. The dotted black line represents the amount of energy that is found to be critical in the ST19 report and shows how much each of the involved bodies will dissipate at this energy level. In this scenario, the glacial ice will only dissipate 4 % of the energy. The dissipated energy with mean and characteristic x 1.25 material values are plotted in Appendix C. The energy dissipation is also very low in the ice in these

analyses.

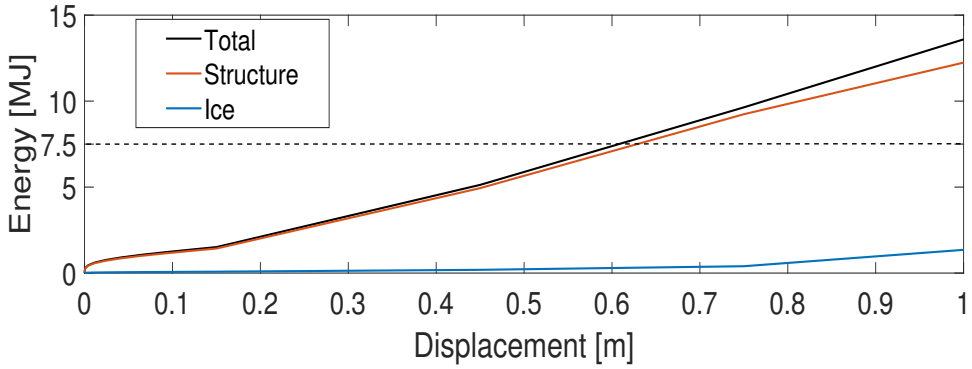

Figure 7.18: Internal energy dissipated by the glacial ice and the structure in the coupled analysis of scenario 1 with characteristic steel properties.

7.4.2 Impact Scenario 2 - Intersection of Stiffened Deck and Bulkhead

The impact scenario of the glacial ice hits the cruciform of the stiffened deck and bulkhead is also subjected to a coupled analysis. The resulting force-displacement curve is plotted in Figure 7.19 with distinctive points marked. The pattern of the curve is very similar to the pattern in impact scenario 1. Point 1 shows the initial bending stiffness, about 20 MN. After this, the stiffened deck starts to buckle, See Figure 7.20a. At Point 2 the outer shell initiates rupture(Figure 7.20b), which affects the structure by a drop in the resistance. At Point 3 the outer shell starts to rupture with mean material values, see Figure 7.20c. As anticipated, the effect of chosen material values is very important in this impact scenario as well(i.e. characteristic or mean values).

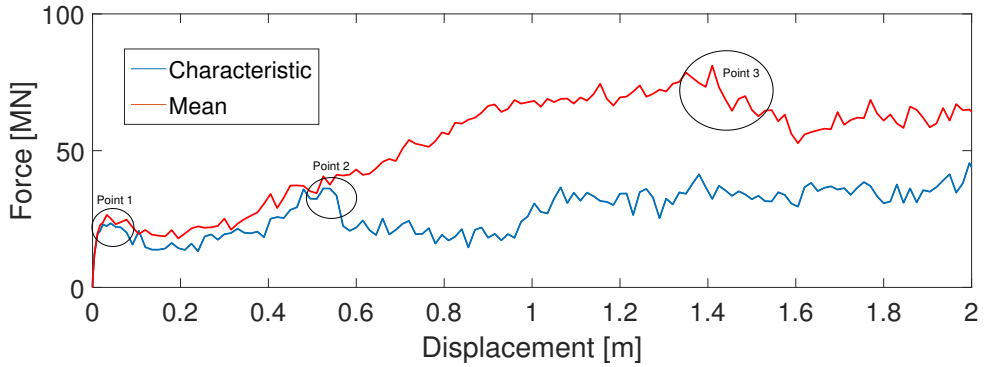

Figure 7.19: Coupled analysis of scenario 2. Crushing resistance versus crushing distance. Characteristic and mean values from DNVGL-RP-C208.

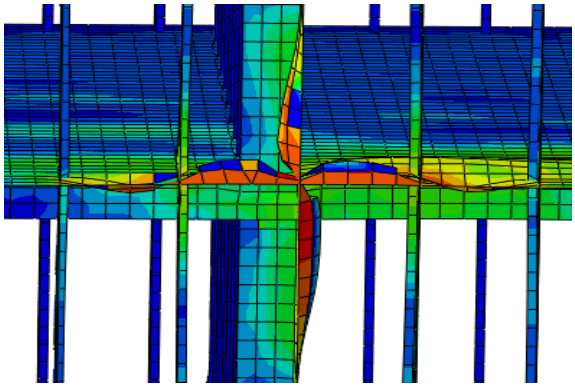

(a) Point 1 in Figure 7.19. Front view with the outer plating removed. Characteristic material values.

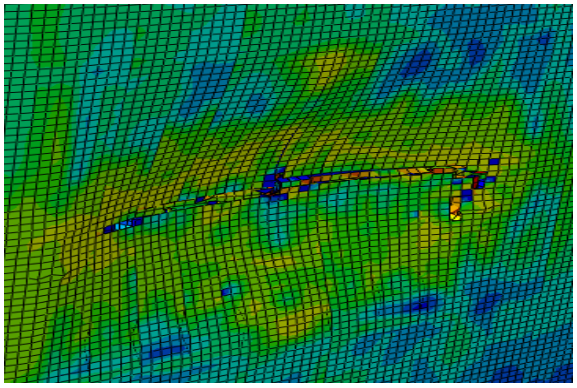

(b) Point 2 in Figure 7.19. View of the outer plating in the impacted area. Characteristic material values.

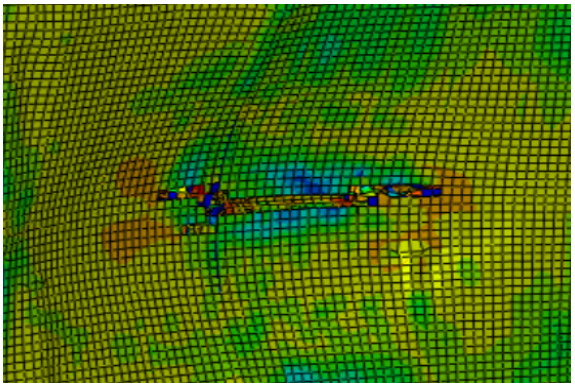

(c) Point 3 in Figure 7.19. View of the outer plating in the impacted area. Mean material values.

Figure 7.20: Snapshot of distinctive points in 7.19.

The deformation of the glacial ice in impact scenario 2 is displayed Figure 7.21. The ice do not appear to be damaged significantly in either of the analyses. The

iceberg almost behave like a rigid body. Hence, it is suspected that it doesn't contribute considerably in the energy dissipation. The iceberg is a little more damaged with characteristic values.

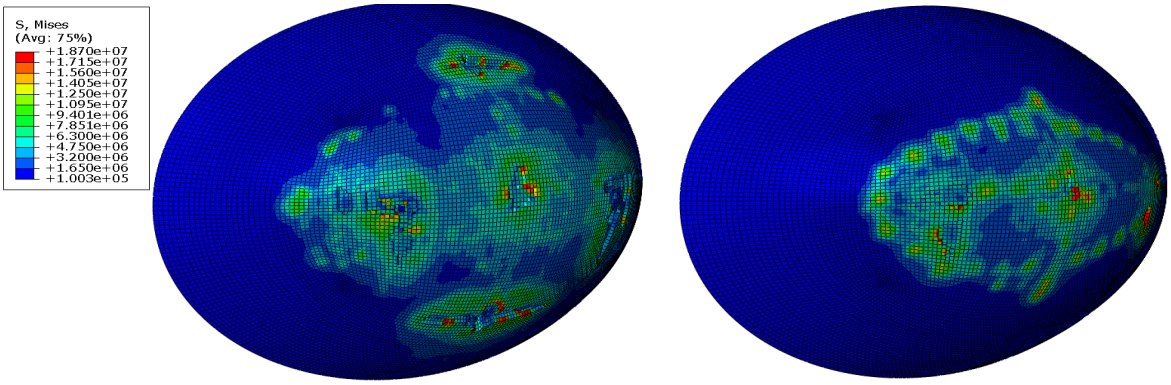

(a) Characteristic steel properties. (b) Mean steel properties.

Figure 7.21: Deformation of the glacial ice in scenario 2 at an indentation of 1.5 m.

Energy Dispersion

In the impact scenario with the ice hitting the cruciform, the glacial ice dissipates even less energy. At a total energy dispersion of 7.5 MJ(dotted black line), the ice only dissipates 1.5 % of the total energy. Hence, the structure must dissipate almost all of the energy. At this location, the structure is stiffer than at the location in impact scenario 1. This results in less displacement when 7.5 MJ is dissipated, about 0.46 m. In the analysis with mean material values, the ice dissipates less than 1 % of the energy, see the plot in Appendix C.

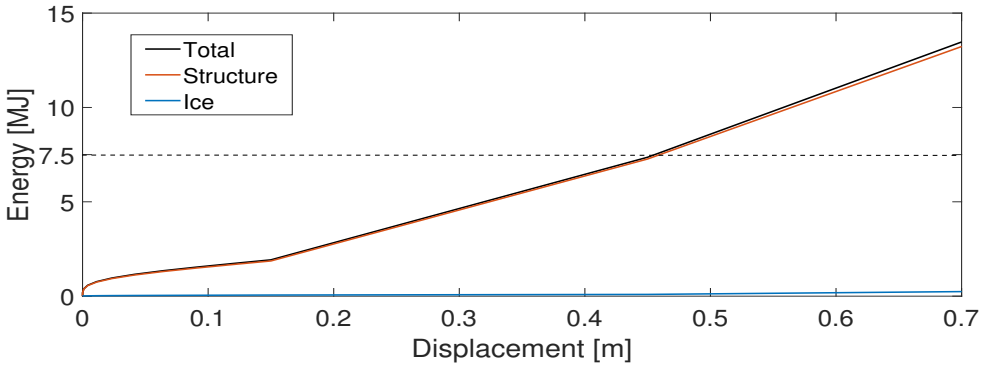

Figure 7.22: Internal energy dissipated by the glacial ice and the structure in the coupled analysis of scenario 2 with characteristic steel properties.

7.5 Discussion

Both the NORSOK N-004 and the coupled shared-energy design approaches yield fairly similar results in terms of energy dissipation. The iceberg is very strong and it is almost not deformed at all. Hence, the structure dissipates all the energy, more or less. The initial peak that is present in the force-displacement curve for the iceberg is very large. The semi-submersible column has to be much stiffer if it shall overcome this peak and start to crush the glacial ice properly. One explanation might be that as the structure deforms around the iceberg and creates high hydrostatic pressure in the ice elements. This will make the ice stronger since it's material behaviour is modelled with the pressure dependent Tsai-Wu yield surface.

Another explanation, which may be more plausible, might be that the calibration of the implemented material model is not perfectly performed. In the calibration process, the initial peak was newer fully eliminated. In addition, the calibration was performed with a spherical iceberg with a radius of 1.5 m and mesh size of 50 mm, while the integrated analysis is run with a spheroidal iceberg with 15 m long axis, 10.4 m short axis and mesh size of 100 mm. Ideally, the iceberg geometry and mesh should be the same in the calibration and the integrated analysis. Hence, the results might be affected..

It is noteworthy that the modelled platform in the impact analysis is not designed with ice-strengthened columns.

7.5.1 Comparison with the ST19 Report

In the rigid ice analysis in the ST19 report (Lu et al., 2018) it was found that the initial bending capacity of the column in impact scenario 1 is 5 MN, which is lower than the capacity of 10 MN found in this thesis. In both analyses, the resistance against indentation increases as the crushing continues and the fracture of the outer plating occurs at approximately 0.6 m. The rigid ice analysis of impact scenario 2 also yield some differences in results between the study in this thesis and ST19. The initial peaks are 15 MN and 25 MN, respectively. However, even though the initial bending capacity is larger in this thesis, the resistance against indentation is larger past this point in ST19.

In the ST19 report (Lu et al., 2018) it is generally found that both the ice and the structure should deform and dissipate the energy in all the investigated impact scenarios. The impact resistance curves of the ice are not found by numerical ice crushing simulations as in this thesis and doesn't contain a severe initial peak. Thus, by applying the NORSOK N-004 shared-energy design approach, it is found that both interacting bodies dissipate energy and the structural displacement is less than found in this thesis.

The differences in results in this thesis and ST19 may be influenced by several factors. Firstly, the analyses are performed in two different NLFEA software, Abaqus and LS-DYNA. The conversion of the model from one software to another may cause differences and the model setup will never be identical since the software function differently. Regardless, it is not expected that this is a major reason for the deviation of results across the studies. The material and fracture modelling of the steel column is a subject where the analyses differ considerably. Due to the lack of available subroutine in Abaqus, the material modelling is performed with characteristic values from DNV GL-RP-C208, which gives conservative results. However, it is suspected that the main reason is the strength of the glacial ice. The glacial ice in this thesis appears to be much stronger than the estimations performed in ST19 of the strength of glacial ice.

7.6 Coupled Analysis with the Original Failure Criterion

In the coupled analysis applying the failure criterion from the calibration, the glacial ice fails to dissipate any significant amount of energy. The iceberg appears to almost behave like a rigid body. Hence, it is performed a simple coupled analysis with the original failure criterion proposed by Liu (2011). As shown in Chapter 6, this failure criterion yield less crushing resistance in the ice.

Impact scenario 2 with characteristic material values from DNV GL RP-C208 are chosen for this analysis.

Figure 7.24 show the development of reaction force versus the crushing distance in the analysis with the original failure criteria. If 7.5 MJ is to be dissipated, the ice will not contribute significantly to the dissipation, see Figure 7.23. However, as the displacement increases, the ice starts to dissipate energy. At a crushing distance of 1.5 m, the glacial ice dissipates 14 % of the total energy. This is more than in the corresponding analysis with the failure criterion emerged from the calibration, where the ice dissipates 6 % at 1.5 m crushing distance. This is also visible in the deformation visualization of the ice in Figure 7.25. The ice has clearly eroded at several spots, especially at the centre where it hits the bulkhead. However, this erosion is very local and only severely present at locations with large resistance, such as at frames and bulkhead.

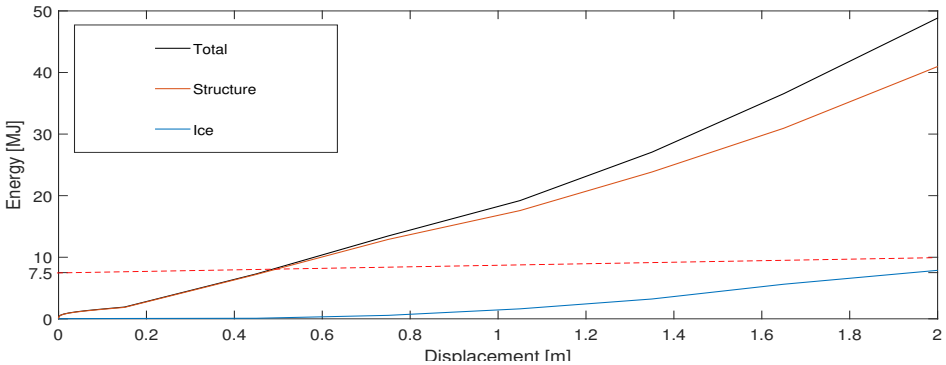

Figure 7.23: Internal energy dissipated by the glacial ice and the structure in the coupled analysis of scenario 2 with characteristic steel properties and original failure criterion.

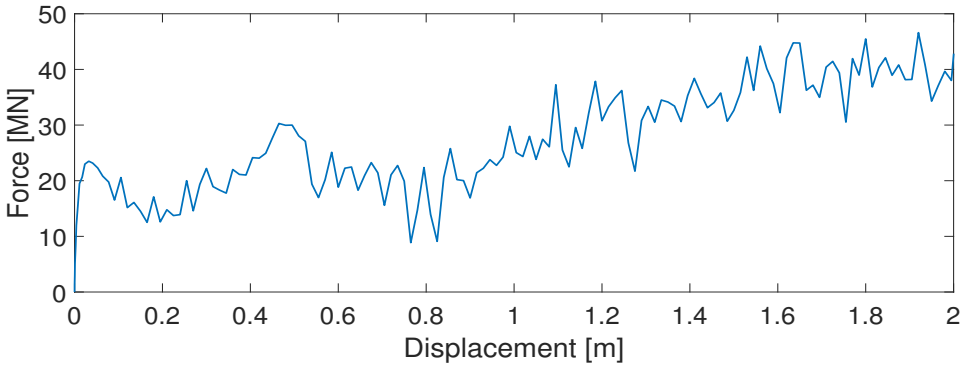

Figure 7.24: Crushing resistance versus crushing distance in the coupled analysis of scenario 2 with characteristic steel properties and original failure criterion.

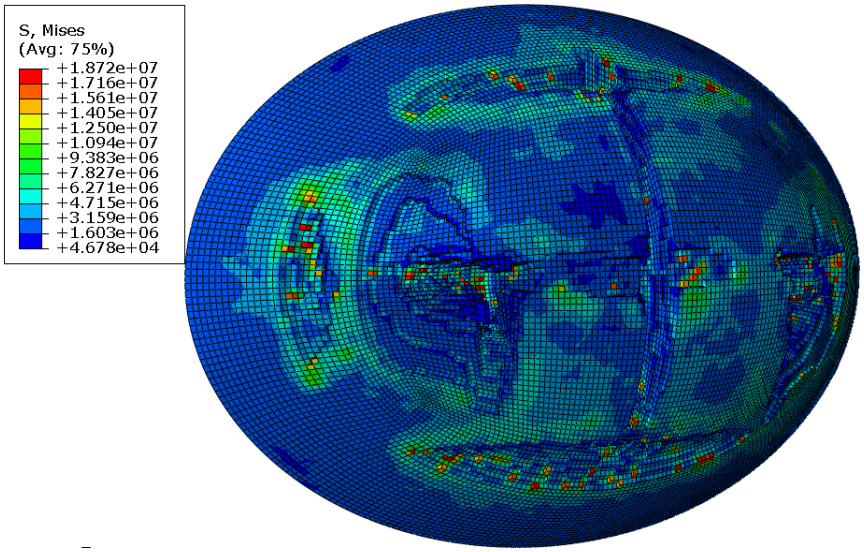

Figure 7.25: Deformation of the glacial ice in scenario 2 at an indentation of 1.5 m with the original failure criterion.

Chapter 8

Conclusion

Glacial ice introduces a great threat to marine structures that operate in the Arctic areas. The consequences of impact interaction between a floating structure and ice may be critical for structural integrity. Henceforth, the demand for trustworthy models of the material behaviour of glacial arises due to the desire to design cost-efficient structures that have the necessary resistance to avoid fatal consequences. This master thesis is a step on the path to the long term goal of being able to estimate, with great confidence, the consequences ice-structure impacts has on the structural integrity of marine structures.

The main objective of this master thesis is to increase the understanding of ice mechanics and the effect various material data has on the performance of the modelled iceberg. A new implementation of the mathematical material model of ice proposed by Liu (2011) is developed as a subroutine in FORTRAN to the FE software Abaqus. The new subroutine is compared with existing subroutines, both in terms of implementation of mathematical operators and with respect to the performance in numerical simulations. It is believed that the new implementation has adopted the optimal numerical methods to solve the mathematical operators. Numerical simulations with a single volume element show that the new implementation behaves as desired with respect to the ability to follow the yield surface and to update the yield surface under reloading. Analyses with larger ice features crushing against a rigid wall show that the model is able to erode elements realistically in an ordered pattern as they are crushed.

However, the implementation inhabits some weaknesses. Firstly, it is very sensitive to the choice of ice constants in the yield surface. If constants are chosen so that the cut-off-pressure is located within the yield surface, the analyses tend to fail. Thus, it is recommended to use ice constants that has a first root larger than the cut-off pressure, such as the constants proposed by Kierkegaard (1993). Another drawaback of the model is the amount of hourglass energy. The attempt to reduce the hourglass energy to acceptable levels in this

thesis was not completely successful, as described in Chapter 5.

In Chapter 6 the newly implemented material model is subjected to calibration against Polar Class 3 in the IACS Unified Requirements for Polar ships. It is attempted to calibrate both by manipulating the yield surface and by manipulating the failure criterion, where the latter gave the most satisfactory results. The new failure criterion is shown in Equation 6.7. With this criterion, the implementation is able to simulate the IACS PC3 force-displacement curve. However, a undesired initial peak is present.

Integrated analyses of ice-structure impact interaction are performed to compare the two methods of shared-energy design, i.e. the NORSOK N-004 approach and coupled analysis. The material model implementation developed in this thesis is used in the analyses. Both approaches yield similar results as the iceberg appear to be much stronger than the structure. As follows, it is not discovered any substantial coupling effects in the impact interaction. The lack of energy dissipation in the ice may be due to confinement of the ice or due to the initial peak in the calibration. The latter was investigated further by applying the original failure criterion proposed by Liu (2011), which gives lower resistance in the ice. Still, the structure must deform severely in order for the ice to dissipate a considerable amount of energy. It is noteworthy that the modelled structure in the integrated analyses is not ice-strengthened and the deformations of the glacial ice only occur at areas of particular stiffness, such as frames and bulkheads. Hence, integrated analysis with a stronger structure would give extra information that may increase the understanding of ice mechanics.

The material modelling of the steel structure in the coupled analyses are performed with both characteristic and mean values from DNV GL RP-C208, where characteristic values is the most conservative choice. However, the analyses yield surprising results. The ice is less deformed and dissipates even less energy with mean values than with characteristic values. It was expected that with mean values, which implies a stiffer structure, the structure inhabits a larger ability to crush the ice. On the other hand, a plausible explanation of this behaviour may be that the steel is more ductile with mean values and allows larger deformations before fracture.

The results in this master thesis are interesting and give valuable insight into the behaviour of ice in numerical simulations. Nevertheless, the new implementation is found to have some drawbacks and the integrated analyses yield less shared energy dissipation in the two colliding bodies than other studies have estimated, such as the ST19 report (Lu et al., 2018). Accordingly, further investigation and validation must be performed to have great confidence in coupled analysis with glacial ice.

Chapter 9

Recommended Further Work

This master thesis addresses the topic of ice mechanics and the implementation of the material behaviour of ice in NLFEA. A new implementation is developed with partial success. Numerical simulations have revealed some areas that need to be investigated in further detail before coupled shared energy analyses are reliable. In the following, the recommended areas of focus are presented.

1. As described in Chapter 4, the numerical analysis tend to fail when the cut-off-pressure is within the yield surface. This limits the choice of ice constants in the yield surface. Consequently, the process of deleting elements when the cut-off-pressure is exceeded should be investigated further.

2. In the implementation of the glacial ice material behaviour, the failure of elements is handled by sudden deletion. This may have unwanted consequences, such as a sudden change of loading on adjacent elements. Thus, the topic of how the material degrades after a damage initiation criteria is met should be addressed.

3. The amount of hourglass energy is above recommended values. Different hourglass controls in Abaqus are applied in order to reduce the artificial energy without satisfactory results. This is a subject that needs to be further studied. It is proposed to start with questioning the physical effect of the displacement scaling factor applied in Abaqus. It is suspected that the hourglass energy might be related to the deletion of elements.

4. Further calibration of the implementation may be performed to avoid the initial peak, which is not desirable if one is to simulate Polar Class 3 in IACS.

5. The thesis has not focused on the effect the geometry of the glacial ice has on the impact. This is an important aspect of ice-structure impacts that should be addressed.

6. In the integrated analyses, the damage on the ice only occur at areas with large stiffness, such as frames and bulkheads. Hence, integrated analysis with a stronger structure would give interesting information that may increase the understanding of ice mechanics.

Bibliography

Abaqus, 2005a. Abaqus analysis users's manual.
URL https://www.sharcnet.ca/Software/Abaqus610/Documentation/docs/v6.10/books/usb/default.htm?startat=pt06ch24s01aus102.html

Abaqus, 2005b. Getting started with abaqus/explicit: Keywords version.
URL https://classes.engineering.wustl.edu/2009/spring/mase5513/abaqus/docs/v6.6/books/gsx/default.htm?startat=ch03s07.html

Alsos, H. S., Amdahl, J., 2009. On the resistance to penetration of stiffened plates, part i–experiments. International Journal of Impact Engineering.

Amdahl, J., 2007. TMR 4205 Buckling and Ultimate Strength of Marine Structures. NTNU.

Bøhlerengen, S., 2013. Probabilistic material modeling of iceberg for analysis of accidental impacts with ships and offshore structures. Master's thesis, NTNU.

Daley, C., 2000. Iacs unified requirements for polar ships - background notes to design ice loads.

Derradji-Aouat, A., 2000. A unified failure envelope for isotropic fresh water ice and iceberg ice. ETCE/OMAE 2000 Joint Conference.

DNV-GL, 2016. DNVGL-RP-C208 - Determination of structural capacity by non-linear finite element analysis methods. DNV GL.

Ferrari, N., 2014. Model for ice material properties in iceberg-ship collisions analyses by finite elements. Master's thesis, University of Genoa.

Hill, B. T., 2006. Ship iceberg collision database v.1.13. National Research Council Canada.

Hopperstad, O. S., Børvik, T., 2018. Impact mechanics part 1: Modelling of plasticity and failure with explicit finite element methods.

Huang, J., Griffiths, D., 2009. Return mapping algorithms and stress predictors for failure analysis in geomechanics. Journal of Engineering Mechanics.

Høyland, K. V., 2017. At-334 arctic marine measurements techniques, operations and transport module i sea ice features and properties.

IACS, 2016. Requirements concerning POLAR CLASS.

ISO, 2007. ISO 19906 Petroleum and natural gas industries — Arctic offshore structures.

Kierkegaard, H., 1993. Ship collisions with icebergs. Ph.D. thesis, Technical University of Denmark.

Kim, E., 2014. Experimental and numerical studies related to the coupled behavior of ice mass and steel structures during accidental collisions. Ph.D. thesis, NTNU.

Krabbenhøft, K., 2002. Basic computational plasticity. Tech. rep., Technical University of Denmark.

Liu, Z., 2011. Analytical and numerical analysis of iceberg collisions with ship structures. Ph.D. thesis, NTNU.

Liu, Z., Amdahl, J., Løset, S., 2010. Plasticity based material modelling of ice and its application to ship-iceberg impacts. Elsier.

LS-DYNA, 2005. Radial return.
URL `https://www.dynasupport.com/tutorial/computational-plasticity/radial-return`

Lu, W., YU, Z., Berg, M. V. D., Lubbad, R., Amdahl, J., Løset, S., Kim, E., 2018. Asessment of structural damage due to glacial ice impact. Tech. rep., ArcIso AS.

Løset, S., 1993. Thermal energy conservation in icebergs and tracking by temperature. Journal of Geophysical Research: Oceans.

NORSOK, 2016. Action and action effects.

NORSOK, 2017. Design of steel structures.

Palmer, A., Croasdale, K., 2013. Arctic Offshore Engineering. World Scientific.

Schulson, E. M., Duval, P., 2009. Creep and Fractire of Ice. Cambridge University Press.

Storheim, M., 2016. Structural response in ship-platform and ship-ice collisions. Ph.D. thesis, NTNU.

Stronge, W., 2000. Impact mechanics. Cambridge University Press.

Appendix A

Single element analyses

The figures in this section shows the results of the single element analysis with the implementation by Woongshik Nam and Ferrari (2014) using the Derradji-Aouat (2000) ice material constants. In the implementation "Ferrari (2014) modified" a restriction against updating the yielding limit is removed.

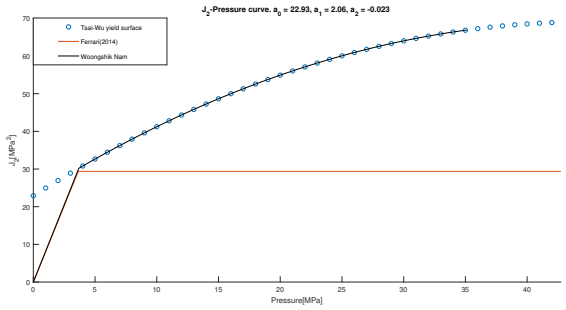

Figure A.1: J2-Pressure plot of the implementation by Woongshik Nam and Ferrari (2014).

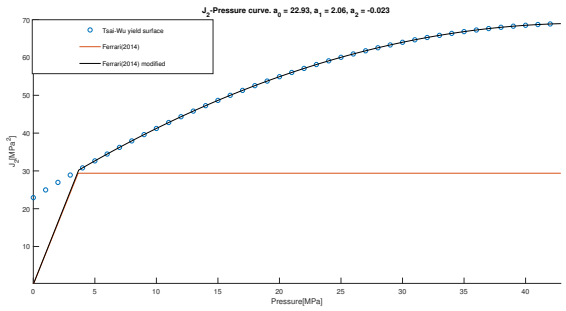

Figure A.2: J2-Pressure plot of the original and modified implementation by Ferrari (2014).

Appendix B

Ice Crushing Analysis from the Project Thesis

In the project thesis prior to this master thesis, ice crushing analyses was performed in order to check the performance of the various implemented material models. The resulting forces and deformations of these simulations are shown in Figure B.2 and Figure B.1. The simulations are performed with the ice material constants proposed by Derradji-Aouat (2000). The model used is not the same as in the analyses the master thesis, were a new model is established in MSC PATRAN to ensure as identical setup between the FEA softwares LS-DYNA and Abaqus. The implementations by Woongshik Nam used in the project thesis and master thesis are not identical. The latter is an updated version of the former.

In due time, it has been discovered that the analyses in the project thesis are not run on identical premises across the softwares. Thus, the comparison of the implementations are not fully reliable. In addition, the implementation by Ferrari (2014) are suspected to not successfully implement the mathematical model of the material behaviour, which is the reason the implementation isn't further investigated in this thesis.

Figure B.1: Comparison of the force versus displacement of the material models in the project thesis.

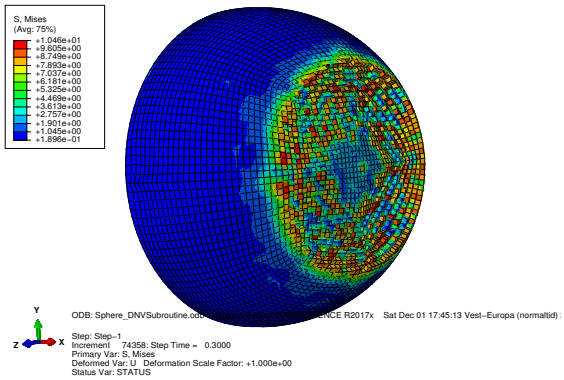

(a) von Mises stress(MPa) on spherical ice model against a rigid wall with the material model by Ferrari (2014).

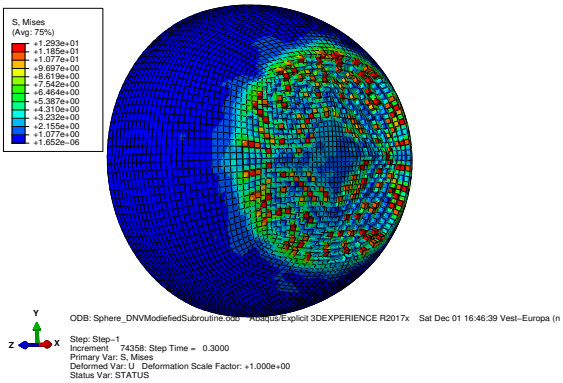

(b) von Mises stress(MPa) on spherical ice model against a rigid wall with the modified version of the material model by Ferrari (2014).

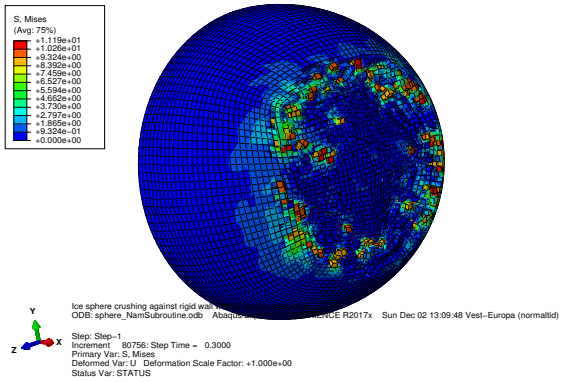

(c) von Mises stress(MPa) on spherical ice model against a rigid wall with the old material model by Woongshik Nam

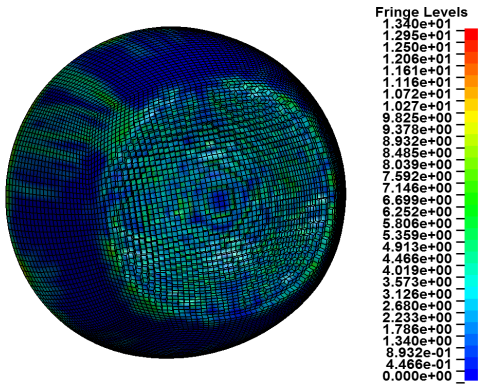

(d) von Mises stress(MPa) on spherical ice model against a rigid wall with the material model implemented in LS-DYNA.

Figure B.2: Deformation of the glacial ice from the project thesis.

Appendix C

Coupled Analysis

In this section some additional plots of the coupled analyses are shown.

C.1 Impact scenario 1 - Corner of stiffened deck

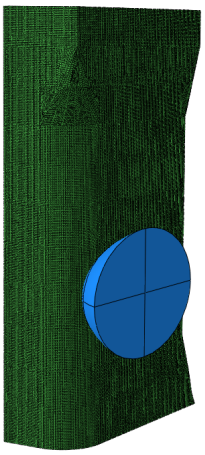

Figure C.1: Ice impact at corner of stiffened deck.

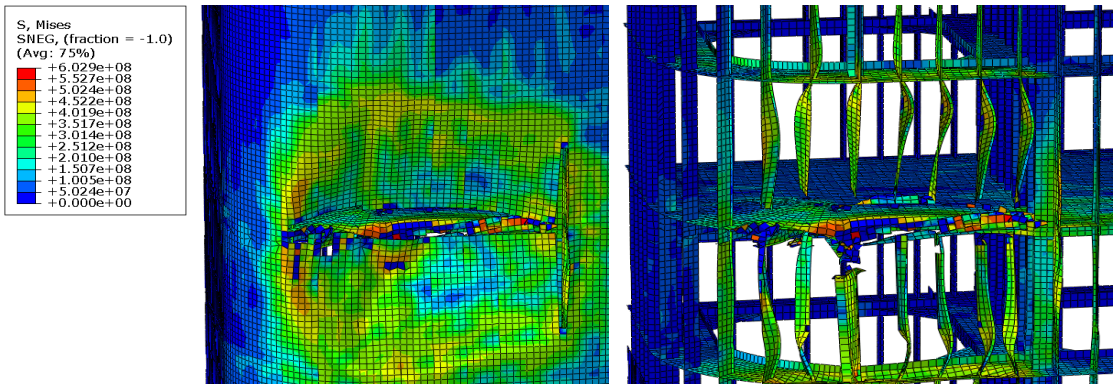

(a) Deformation of the column outer plating at an indentation of 1 m. Characteristic values.

(b) Deformation of the column without the outer plating at an indentation of 1 m. Characteristic values.

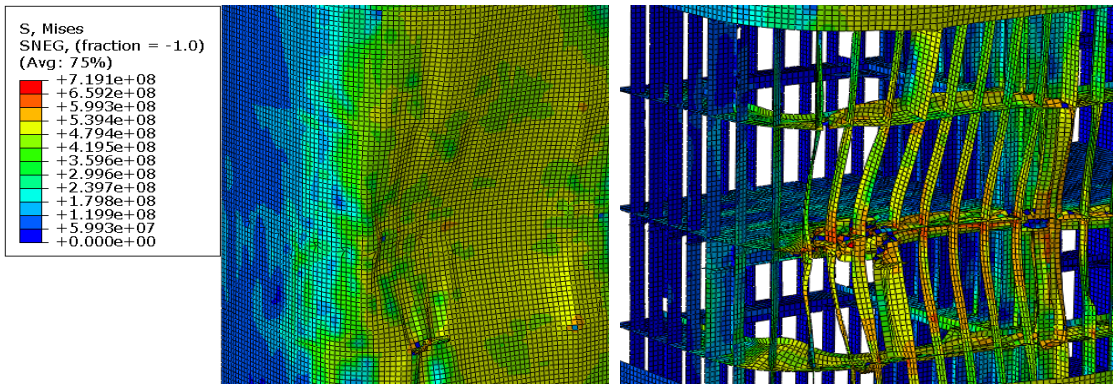

(c) Deformation of the column outer plating at an indentation of 1 m. Mean values.

(d) Deformation of the column without the outer plating at an indentation of 1 m. Mean values values.

Figure C.2: Deformation of the column in the coupled analysis of impact scenario 1.

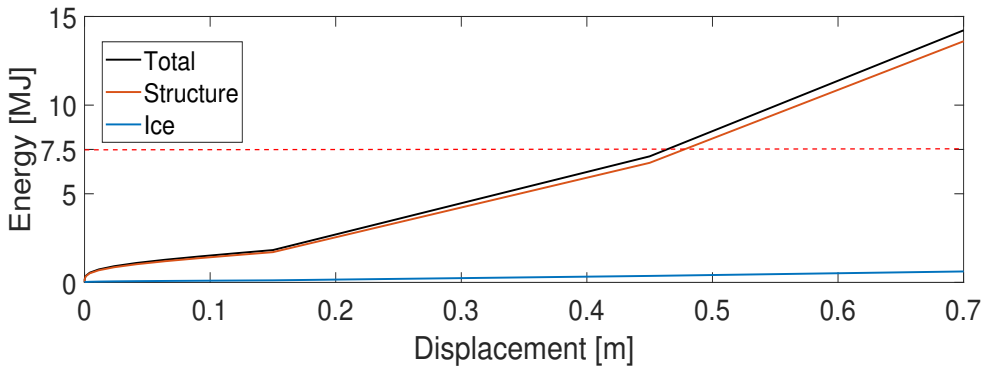

Figure C.3: Internal energy dissipated by the glacial ice and the structure in the coupled analysis of scenario 1 with Mean steel properties.

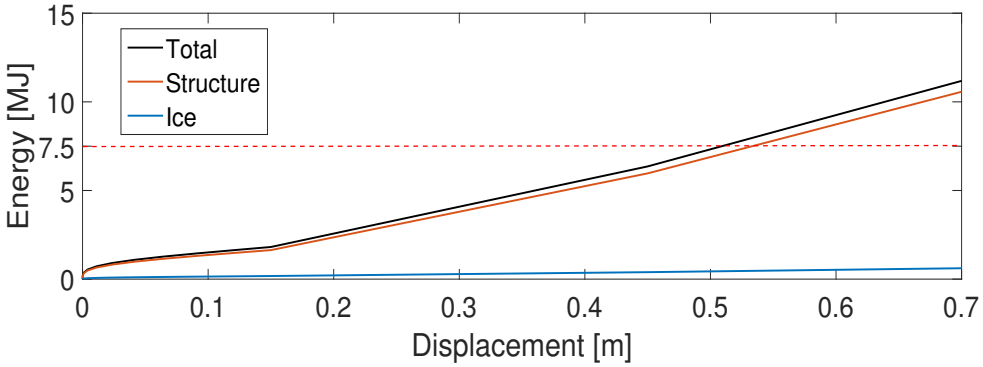

Figure C.4: Internal energy dissipated by the glacial ice and the structure in the coupled analysis of scenario 1 with characteristic x1.25 steel properties.

C.2 Impact scenario 2 - Intersection of stiffened deck and bulkhead

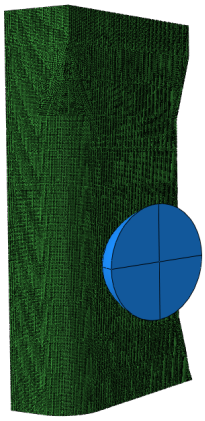

Figure C.5: Ice impact at intersection of stiffened deck and bulkhead.

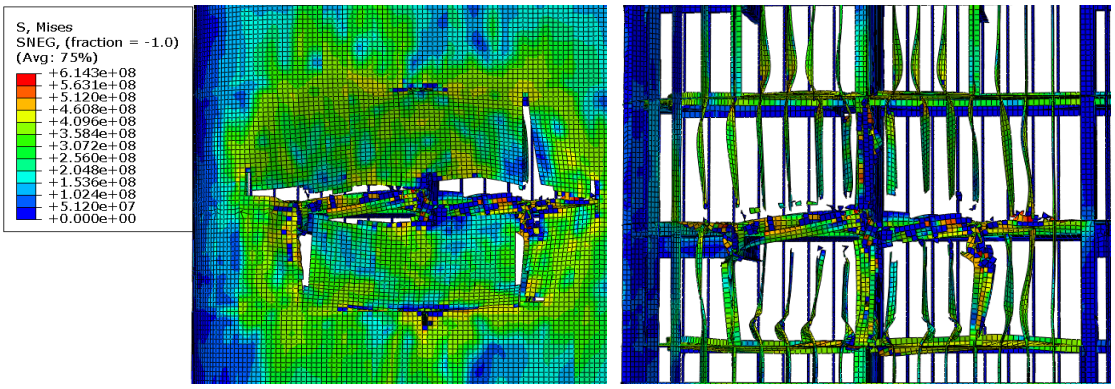

(a) Deformation of the column outer plating at an indentation of 1 m. Characteristic values.

(b) Deformation of the column without the outer plating at an indentation of 1 m. Characteristic values.

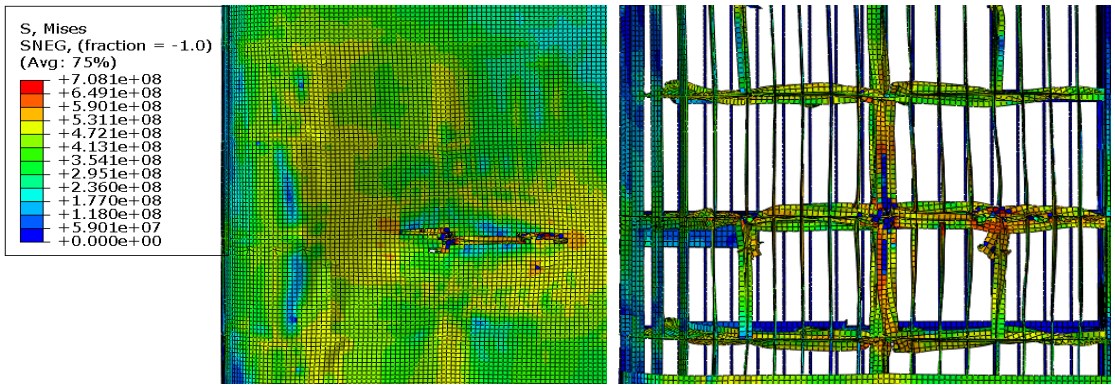

(c) Deformation of the column outer plating at an indentation of 1 m. Mean values.

(d) Deformation of the column without the outer plating at an indentation of 1 m. Mean values values.

Figure C.6: Deformation of the column in the coupled analysis of impact scenario 2.

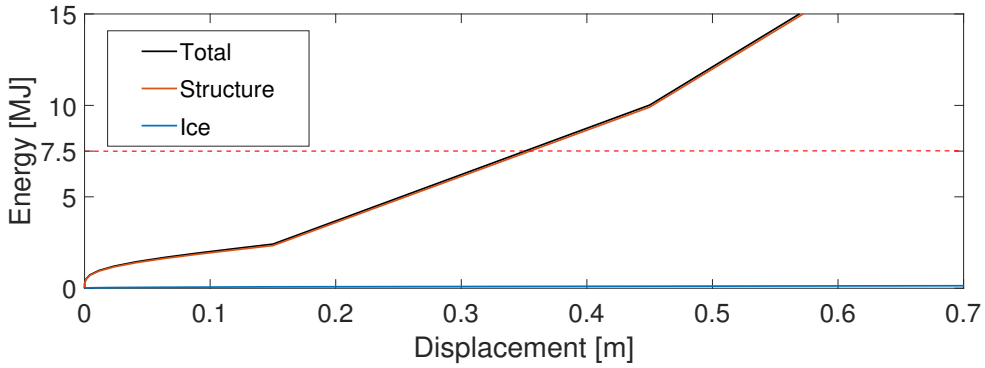

Figure C.7: Internal energy dissipated by the glacial ice and the structure in the coupled analysis of scenario 2 with mean steel properties.

Vebjørn Kjerstad

Modelling of Iceberg Impact Interaction with Floating Structures

NTNU
Norwegian University of
Science and Technology